

## ABSTRACT

QUINLIVAN, PATRICIA ANN. Effects of Activated Carbon Surface Chemistry and Pore Structure on the Adsorption of Methyl Tertiary-Butyl Ether and Trichloroethene from Natural Water. (Under the direction of Detlef R.U. Knappe.)

Activated carbon adsorption is the best available treatment technology for the control of many objectionable trace organic compounds. Activated carbons are frequently characterized by the iodine number and BET surface area, but these parameters do not correlate well with trace organic compound removal from natural water. Therefore, the objective of this research was to develop activated carbon selection criteria that assure the effective removal of trace organic contaminants from natural water and to base the selection criteria on the adsorbent's pore structure and surface chemistry. To systematically evaluate pore structure and surface chemistry effects, a matrix of activated carbon fibers (ACFs) with three activation levels and four surface chemistry levels was studied. To evaluate whether adsorption trends established for ACFs were also valid for granular activated carbon (GAC), ACF results were compared with those obtained for three commercially available GACs. Adsorption capacities were determined for natural organic matter (NOM), for relatively hydrophilic methyl tertiary-butyl ether (MTBE) and relatively hydrophobic trichloroethene (TCE) in organic-free water, and for MTBE and TCE in the presence of NOM. NOM isotherms showed that DOC adsorption occurred primarily in pores with diameters in the 11 to 500 Å range and that electrostatic interactions between NOM and the carbon surface played a role in NOM adsorption. According to both single-solute isotherms and micropollutant isotherms in the presence

of NOM, hydrophobic adsorbents more effectively removed TCE and MTBE than hydrophilic adsorbents. Effective adsorbents for drinking water treatment should therefore contain little oxygen and nitrogen whose presence increases the polarity of the adsorbent surface. Based on the elemental composition of the low-ash carbons evaluated in this study, activated carbons should have oxygen and nitrogen contents that sum to no more than 2 to 3 mmol/g to assure sufficient hydrophobicity. In addition, both single-solute isotherms and isotherms in the presence of NOM indicated that adsorbents should exhibit a large pore volume in micropores with widths that are about 1.5 times larger than the kinetic diameter of the target adsorbate. Furthermore, based on the micropollutant isotherms in the presence of NOM, an effective adsorbent should possess a micropore size distribution that extends to widths that are approximately twice the kinetic diameter of the target adsorbate to prevent pore blockage or restriction as a result of NOM adsorption.

**EFFECTS OF ACTIVATED CARBON SURFACE CHEMISTRY AND PORE  
STRUCTURE ON THE ADSORPTION OF METHYL TERTIARY-BUTYL  
ETHER AND TRICHLOROETHENE FROM NATURAL WATER**

By

**PATRICIA ANN QUINLIVAN**

A thesis submitted to the Graduate Faculty of  
North Carolina State University  
in partial fulfillment of the  
requirements for the  
Degree of Master of Science

**DEPARTMENT OF CIVIL ENGINEERING**

**Water Resources and Environmental Engineering**

Raleigh

2001

APPROVED BY:

---

---

Chair of Advisory Committee

*Dedicated in loving memory of my niece, Shannon Tamul*

*“Many people will walk in and out of your life,  
but only true friends will leave footprints in your heart.”*

*-Eleanor Roosevelt*

## **BIOGRAPHY**

Patty Quinlivan was born on October 13, 1976 in Buffalo, NY. She received her BS in Civil Engineering from North Carolina State University, where she graduated summa cum laude and was valedictorian of her college. She then decided to pursue her MS degree in Civil Engineering from North Carolina State University, where she worked with Dr. Detlef Knappe and Ph.D. candidate Lei Li. Her work was supported through an NSF fellowship and AWWARF. She received the 2000 Holly Cornell Scholarship and is a member of AWWA.

## ACKNOWLEDGEMENTS

First, I would like to thank my advisor and the chair of my committee, Dr Detlef Knappe, whose constant support and guidance were instrumental in the completion of this thesis. Thank you to Dr Robert Borden and Dr Francis de los Reyes for joining my committee and providing their input and ideas. Furthermore, I would like to acknowledge David Black, Beverly Taylor, and Sharon Shoup for their assistance with GC and elemental analyses. I would like to extend my gratitude to Lei Li for the chemical modification and characterization of the carbons used in this research, to Travis Wagner for his assistance with the NOM isotherms, and to Steve Wade and Tom Dismukes for their assistance with the repair and maintenance of the rotary tumbler. I would also like to thank the AWWA Research Foundation for funding the project on which I worked as well as the NSF, who helped fund my research through a graduate research fellowship and the AWWA, who awarded me with the Holly A Cornell Scholarship. Additionally, I would like to thank the Contra Costa Water District for donating the water used in the natural water isotherms and Nippon Kynol for donating the ACFs used in this research. Finally, many, many thanks are extended to my family and friends who were there through the good and bad times of the past two years. There are too many of you to name, but you know who you are, and I could not have done it without your love and support.

# TABLE OF CONTENTS

**LIST OF TABLES ..... vii**

**LIST OF FIGURES ..... x**

## **CHAPTER 1. EFFECTS OF ACTIVATED CARBON PORE STRUCTURE AND SURFACE CHEMISTRY ON THE ADSORPTION OF TRICHLOROETHENE AND METHYL TERTIARY-BUTYL ETHER – SINGLE SOLUTE**

**ISOTHERMS..... 1**

- 1.1. INTRODUCTION ..... 1
- 1.2. BACKGROUND ..... 2
  - 1.2.1 Activated Carbon Pore Structure ..... 2
  - 1.2.2 Activated Carbon Surface Chemistry ..... 4
- 1.3. EXPERIMENTAL..... 7
  - 1.3.1 Solvents..... 7
  - 1.3.2 Adsorbates ..... 8
  - 1.3.3 Adsorbents ..... 10
  - 1.3.4 Adsorbent characterization ..... 12
  - 1.3.5 Isotherms..... 13
- 1.4. RESULTS AND DISCUSSION ..... 14
  - 1.4.1 Adsorbent Characterization ..... 14
  - 1.4.2. TCE and MTBE Adsorption ..... 20
- 1.5. CONCLUSIONS ..... 32

## **CHAPTER 2. EFFECTS OF ACTIVATED CARBON SURFACE CHEMISTRY AND PORE STRUCTURE ON THE ADSORPTION OF ORGANIC CONTAMINANTS – ISOTHERMS IN THE PRESENCE OF NATURAL ORGANIC MATTER..... 34**

- 2.1 INTRODUCTION ..... 34
- 2.2 BACKGROUND ..... 35
  - 2.2.1 NOM Adsorption ..... 35
  - 2.2.2 Micropollutant Adsorption in the presence of NOM..... 39
  - 2.2.3 Modeling of Adsorption ..... 42
  - 2.2.4 Research Objective ..... 46
- 2.3 MATERIALS AND METHODS ..... 47
  - 2.3.1 Solvents..... 47
  - 2.3.2. Adsorbates (Micropollutant probes) ..... 47

2.3.3 Adsorbents .....	48
2.3.4 Isotherms.....	48
2.3.5 Mathematical Modeling.....	49
2.4 RESULTS AND DISCUSSION.....	50
2.4.1 NOM adsorption .....	50
2.4.2 Micropollutant adsorption in the presence of NOM.....	56
2.5 CONCLUSIONS .....	73
<b>LIST OF REFERENCES .....</b>	<b>75</b>
<b>APPENDICES .....</b>	<b>82</b>
Appendix A. Raw Data.....	83
Appendix B. Isotherm Plots.....	135

## LIST OF TABLES

Table 1.1	Nomenclature for ACF matrix.....	11
Table 1.2	BET surface areas and pore volumes of ACFs and pulverized GACs. ....	16
Table 1.3	Elemental analysis and $pH_{PZC}$ results for ACF matrix .....	19
Table 1.4	Elemental analysis, ash content, and $pH_{PZC}$ results for pulverized GACs <sup>a</sup> ...	20
Table 1.5	Freundlich parameters for single-solute TCE and MTBE isotherms. ....	22
Table 2.1	Pore structure effects on Freundlich parameters for dose-normalized DOC isotherms on acid-washed ACFs. ....	53
Table 2.2	Freundlich parameters for dose-normalized DOC isotherms on GACs. ....	56
Table 2.3	Adsorbent performance rankings in the presence of NOM. ....	70
Table 2.4	Adsorbent performance rankings in ultrapure water. ....	71
Table A.1	DOC isotherms for AW10.....	83
Table A.2	DOC isotherms for AW15.....	84
Table A.3	DOC isotherms for AW20.....	84
Table A.4	DOC isotherms for F600.....	85
Table A.5	DOC isotherms for G219.....	86
Table A.6	DOC isotherms for Picazine.....	86
Table A.7	Single-solute TCE isotherm data for AW10.....	87
Table A.8	Single-solute TCE isotherm data for AW15.....	87
Table A.9	Single-solute TCE isotherm data for AW20.....	88
Table A.10	Single-solute TCE isotherm data for OAW10 – Run 1.....	89
Table A.11	Single-solute TCE isotherm data for OAW10 – Run 2.....	89
Table A.12	Single-solute TCE isotherm data for OAW15 – Run 1.....	90
Table A.13	Single-solute TCE isotherm data for OAW15 – Run 2.....	90
Table A.14	Single-solute TCE isotherm data for OAW20 – Run 1.....	91
Table A.15	Single-solute TCE isotherm data for OAW20 – Run 2.....	91
Table A.16	Single-solute TCE isotherm data for HAW10.....	92
Table A.17	Single-solute TCE isotherm data for HAW15.....	92
Table A.18	Single-solute TCE isotherm data for HAW20.....	93
Table A.19	Single-solute TCE isotherm data for AAW10.....	93
Table A.20	Single-solute TCE isotherm data for AAW15.....	94
Table A.21	Single-solute TCE isotherm data for AAW20.....	94
Table A.22	Single-solute TCE isotherm data for F600.....	95
Table A.23	Single-solute TCE isotherm data for G219 – Run 1.....	96
Table A.24	Single-solute TCE isotherm data for G219 – Run 2.....	96
Table A.25	Single-solute TCE isotherm data for Picazine – Run 1.....	97
Table A.26	Single-solute TCE isotherm data for Picazine – Run 2.....	97
Table A.27	Single-solute MTBE isotherm data for AW10 – Run 1.....	98
Table A.28	Single-solute MTBE isotherm data for AW10 – Run 2.....	98
Table A.29	Single-solute MTBE isotherm data for AW10 – Run 3.....	99
Table A.30	Single-solute MTBE isotherm data for AW15.....	99
Table A.31	Single-solute MTBE isotherm data for AW20.....	100
Table A.32	Single-solute MTBE isotherm data for OAW10 – Run 1.....	101

Table A.33	Single-solute MTBE isotherm data for OAW10 – Run 2.....	101
Table A.34	Single-solute MTBE isotherm data for OAW15 – Run 1.....	102
Table A.35	Single-solute MTBE isotherm data for OAW15 – Run 2.....	102
Table A.36	Single-solute MTBE isotherm data for OAW20 – Run 1.....	103
Table A.37	Single-solute MTBE isotherm data for OAW20 – Run 2.....	103
Table A.38	Single-solute MTBE isotherm data for HAW10 .....	104
Table A.39	Single-solute MTBE isotherm data for HAW15 .....	104
Table A.40	Single-solute MTBE isotherm data for HAW20 .....	105
Table A.41	Single-solute MTBE isotherm data for AAW10 – Run 1.....	105
Table A.42	Single-solute MTBE isotherm data for AAW10 – Run 2.....	106
Table A.43	Single-solute MTBE isotherm data for AAW15 – Run 1.....	106
Table A.44	Single-solute MTBE isotherm data for AAW15 – Run 2.....	107
Table A.45	Single-solute MTBE isotherm data for AAW20 – Run 1.....	107
Table A.46	Single-solute MTBE isotherm data for AAW20 – Run 2.....	108
Table A.47	Single-solute MTBE isotherm data for F600.....	108
Table A.48	Single-solute MTBE isotherm data for G219.....	109
Table A.49	Single-solute MTBE isotherm data for Picazine – Run 1.....	109
Table A.50	Single-solute MTBE isotherm data for Picazine – Run 2.....	110
Table A.51	Data from TCE isotherms in the presence of NOM for AW10 – Run 1.....	110
Table A.52	Data from TCE isotherms in the presence of NOM for AW10 – Run 2.....	111
Table A.53	Data from TCE isotherms in the presence of NOM for AW15 – Run 1.....	111
Table A.54	Data from TCE isotherms in the presence of NOM for AW15 – Run 2.....	112
Table A.55	Data from TCE isotherms in the presence of NOM for AW20.....	112
Table A.56	Data from TCE isotherms in the presence of NOM for OAW10.....	113
Table A.57	Data from TCE isotherms in the presence of NOM for OAW15 – Run 1.....	113
Table A.58	Data from TCE isotherms in the presence of NOM for OAW15 – Run 2.....	114
Table A.59	Data from TCE isotherms in the presence of NOM for OAW20.....	114
Table A.60	Data from TCE isotherms in the presence of NOM for HAW10 – Run 1.....	115
Table A.61	Data from TCE isotherms in the presence of NOM for HAW10 – Run 2.....	115
Table A.62	Data from TCE isotherms in the presence of NOM for HAW10 – Run 3.....	116
Table A.63	Data from TCE isotherms in the presence of NOM for HAW15 – Run 1.....	116
Table A.64	Data from TCE isotherms in the presence of NOM for HAW15 – Run 2.....	117

Table A.65 Data from TCE isotherms in the presence of NOM for HAW20 – Run 1.....	117
Table A.66 Data from TCE isotherms in the presence of NOM for HAW20 – Run 2.....	118
Table A.67 Data from TCE isotherms in the presence of NOM for AAW10.....	118
Table A.68 Data from TCE isotherms in the presence of NOM for AAW15.....	119
Table A.69 Data from TCE isotherms in the presence of NOM for AAW20.....	119
Table A.70 Data from TCE isotherms in the presence of NOM for F600.....	120
Table A.71 Data from TCE isotherms in the presence of NOM for G219.....	120
Table A.72 Data from TCE isotherms in the presence of NOM for Picazine.....	121
Table A.73 Data from MTBE isotherms in the presence of NOM for AW10 – Run 1.....	121
Table A.74 Data from MTBE isotherms in the presence of NOM for AW10 – Run 2.....	122
Table A.75 Data from MTBE isotherms in the presence of NOM for AW15.....	122
Table A.76 Data from MTBE isotherms in the presence of NOM for AW20.....	123
Table A.77 Data from MTBE isotherms in the presence of NOM for OAW10 – Run 1.....	123
Table A.78 Data from MTBE isotherms in the presence of NOM for OAW10 – Run 2.....	124
Table A.79 Data from MTBE isotherms in the presence of NOM for OAW15.....	124
Table A.80 Data from MTBE isotherms in the presence of NOM for OAW20.....	125
Table A.81 Data from MTBE isotherms in the presence of NOM for HAW10 – Run 1.....	125
Table A.82 Data from MTBE isotherms in the presence of NOM for HAW10 – Run 2.....	126
Table A.83 Data from MTBE isotherms in the presence of NOM for HAW15.....	127
Table A.84 Data from MTBE isotherms in the presence of NOM for HAW20.....	128
Table A.85 Data from MTBE isotherms in the presence of NOM for AAW10 – Run 1.....	129
Table A.86 Data from MTBE isotherms in the presence of NOM for AAW10 – Run 2.....	130
Table A.87 Data from MTBE isotherms in the presence of NOM for AAW15.....	131
Table A.88 Data from MTBE isotherms in the presence of NOM for AAW20.....	131
Table A.89 Data from MTBE isotherms in the presence of NOM for F600 – Run 1.....	132
Table A.90 Data from MTBE isotherms in the presence of NOM for F600 – Run 2.....	132
Table A.91 Data from MTBE isotherms in the presence of NOM for G219 – Run 1.....	133
Table A.92 Data from MTBE isotherms in the presence of NOM for G219 – Run 2.....	133
Table A.93 Data from MTBE isotherms in the presence of NOM for Picazine.....	134

## LIST OF FIGURES

Figure 1.1	Molecular structures and dimensions for trichloroethene and methyl tertiary-butyl ether.....	9
Figure 1.2	Micropore size distributions of acid-washed ACF samples.....	17
Figure 1.3	Effects of surface chemistry modifications on micropore size distributions of ACFs 10 and 20. ....	17
Figure 1.4	Micropore size distributions of pulverized GAC samples .....	18
Figure 1.5	TCE and MTBE isotherms on hydrogen-treated ACFs .....	23
Figure 1.6	Effect of pore volume on TCE adsorption .....	26
Figure 1.7	Effect of chemical treatments on MTBE adsorption from cyclohexane.....	29
Figure 1.8	Effect of chemical treatments on TCE adsorption from cyclohexane. ....	29
Figure 1.9	Effect of adsorbent hydrophobicity on TCE adsorption capacity.....	31
Figure 1.10	Effect of adsorbent hydrophobicity on MTBE adsorption capacity .....	31
Figure 2.1	DOC isotherms on acid-washed ACF samples. ....	51
Figure 2.2	Dose-normalized DOC isotherms on acid-washed ACF samples.....	52
Figure 2.3.	Correlation between DOC adsorption capacity and pore volume in the 11-500 Å width range.....	54
Figure 2.4.	Dose-normalized DOC isotherms on GACs. ....	55
Figure 2.5.	Effect of NOM on TCE adsorption by AW20. ....	57
Figure 2.6.	Effect of ACF pore structure on TCE adsorption from SJDW (acid-washed ACFs). ....	58
Figure 2.7.	Effect of ACF pore structure on MTBE adsorption from SJDW (acid-washed ACFs). ....	60
Figure 2.8.	Effect of ACF surface chemistry modification on MTBE adsorption from SJDW (ACF10). ....	60
Figure 2.9.	Correlation between adsorption capacity and pore volume in the appropriate size range—TCE. ....	62
Figure 2.10.	Correlation between adsorption capacity and pore volume in the appropriate size range—MTBE.....	64
Figure 2.11.	Effect of ACF surface chemistry modifications on TCE adsorption from SJDW (ACF20). ....	65
Figure 2.12.	Effect of ACF surface chemistry modifications on MTBE adsorption from SJDW (ACF20). ....	66
Figure 2.13.	Effect of ACF surface chemistry modifications on MTBE adsorption from SJDW (AW10 vs. OAW10). ....	67
Figure 2.14.	Effect of adsorbent hydrophobicity on TCE adsorption capacity in the presence of NOM ( $C_{0, TCE} = 100 \mu\text{g/L}$ ). ....	68
Figure 2.15.	Effect of adsorbent hydrophobicity on MTBE adsorption capacity in the presence of NOM ( $C_{0, MTBE} = 100 \mu\text{g/L}$ ). ....	68
Figure B.1	Effect of NOM on MTBE Adsorption by AW10.....	135
Figure B.2	Effect of NOM on TCE adsorption by AW10 .....	135
Figure B.3	Effect of NOM on MTBE Adsorption by AW15.....	136

Figure B. 4	Effect of NOM on TCE Adsorption by AW15 .....	136
Figure B.5	Effect of NOM on MTBE Adsorption by AW20.....	137
Figure B.6	Effect of NOM on TCE Adsorption by AW20 .....	137
Figure B.7	Effect of NOM on MTBE Adsorption by OAW10.....	138
Figure B.8	Effect of NOM on TCE Adsorption by OAW10 .....	138
Figure B. 9	Effect of NOM on MTBE Adsorption by OAW15.....	139
Figure B.10	Effect of NOM on TCE Adsorption by OAW15 .....	139
Figure B.11	Effect of NOM on MTBE Adsorption by OAW20.....	140
Figure B.12	Effect of NOM on TCE Adsorption by OAW20 .....	140
Figure B.13	Effect of NOM on MTBE Adsorption by HAW10.....	141
Figure B.14	Effect of NOM on TCE Adsorption by HAW10 .....	141
Figure B.15	Effect of NOM on MTBE Adsorption by HAW15.....	142
Figure B.16	Effect of NOM on TCE Adsorption by HAW15 .....	142
Figure B.17	Effect of NOM on MTBE Adsorption by HAW20.....	143
Figure B.18	Effect of NOM on TCE Adsorption by HAW20 .....	143
Figure B.19	Effect of NOM on MTBE Adsorption by AAW10.....	144
Figure B.20	Effect of NOM on TCE Adsorption by AAW10 .....	144
Figure B.21	Effect of NOM on MTBE Adsorption by AAW15.....	145
Figure B.22	Effect of NOM on TCE Adsorption by AAW15 .....	145
Figure B.23	Effect of NOM on MTBE Adsorption by AAW20.....	146
Figure B.24	Effect of NOM on TCE Adsorption by AAW20 .....	146
Figure B.25	Effect of NOM on MTBE Adsorption by F600 .....	147
Figure B.26	Effect of NOM on TCE Adsorption by F600.....	147
Figure B.27	Effect of NOM on MTBE Adsorption by G219 .....	148
Figure B.28	Effect of NOM on TCE Adsorption by G219 .....	148
Figure B.29	Effect of NOM on MTBE Adsorption by Picazine.....	149
Figure B.30	Effect of NOM on TCE Adsorption by Picazine .....	149

# **CHAPTER 1. EFFECTS OF ACTIVATED CARBON PORE STRUCTURE AND SURFACE CHEMISTRY ON THE ADSORPTION OF TRICHLOROETHENE AND METHYL TERTIARY-BUTYL ETHER – SINGLE SOLUTE ISOTHERMS**

## **1.1. INTRODUCTION**

Activated carbon is widely used for the control of synthetic and naturally occurring organic chemicals in drinking water. Both powdered and granular activated carbons are employed, and the quality of activated carbons is typically assessed by the iodine number or the Brunauer, Emmett, and Teller (BET) surface area obtained from nitrogen adsorption at 77 K. However, the carbon usage rate and thus the cost of activated carbon adsorption processes is frequently unrelated to these parameters because the molecular dimensions and chemical characteristics of iodine and nitrogen are not representative of typical organic contaminants in aqueous solution. Consequently, these parameters do not recognize the importance of molecular sieving, i.e. the exclusion of larger organic contaminants from adsorbent pores that are accessible to nitrogen or iodine (Kasaoka et al. 1989a, Kasaoka et al. 1989b). Furthermore, effects of pore surface chemistry on adsorbate/adsorbent and solvent/adsorbent interactions (Kaneko et al. 1989, Pendleton et al. 1997, Franz et al. 2000, Considine et al. 2001) are not accounted for. To develop a rational framework for the selection of activated carbons an improved understanding of the effects of pore size and pore surface chemistry on organic contaminant adsorption from aqueous solution is required. Therefore, the first objective of this study was to systematically evaluate the effects of activated carbon pore structure and surface chemistry on the adsorption of two common drinking water contaminants: the relatively polar fuel oxygenate methyl tertiary-butyl ether (MTBE) and the relatively nonpolar

solvent trichloroethene (TCE). The second objective was to develop simple descriptors of activated carbon characteristics that facilitate the selection of suitable adsorbents for the removal of organic contaminants from aqueous solution.

## **1.2. BACKGROUND**

Powdered and granular activated carbons are typically manufactured from relatively heterogeneous base materials such as bituminous coal, lignite, coconut-shells, or wood while more recently developed activated carbon fibers (ACFs) are prepared from homogeneous polymeric base materials such as polyacrylonitrile, cellulose or phenolic resin (Kasaoka et al. 1989a). Following carbonization of the base material, creation of the internal pore structure is typically achieved by thermal oxidation using steam and CO<sub>2</sub> or chemical oxidation using phosphoric acid. Both the base material and activation conditions affect activated carbon pore structure and surface chemistry (Smisek et al. 1970).

### *1.2.1 Activated Carbon Pore Structure*

Activated carbon is a highly porous material with an internal surface area of about 500-2500 m<sup>2</sup>/g (Derbyshire et al. 2001). The pores that give rise to this large surface area can be envisioned as spaces between irregularly arranged graphite-like platelets (Leon y Leon et al. 1992) or condensed, polyaromatic sheets (Banal et al. 1988), the fundamental building blocks of activated carbons. To classify pores according to size, the International Union of Pure and Applied Chemistry differentiates between (1) micropores (<2 nm

width), (2) mesopores (2 - 50 nm width), and (3) macropores (> 50 nm width) (Sing et al. 1985). Powdered and granular activated carbons for water treatment typically exhibit a heterogeneous pore structure, in which micropores, mesopores and macropores are present (Kasaoka et al. 1989a). In contrast, ACFs exhibit monodispersed pore size distributions (Kasaoka et al 1989a), an observation that was confirmed by scanning tunneling microscopy (Daley et al. 1996). The latter study showed that ACF preparation could be controlled such that only ellipsoidal micropores were present in the bulk fiber. At the ACF surface, both mesopores and micropores were observed; however, the mesopores were oriented parallel to the fiber axis and thus did not penetrate the bulk fiber to a depth greater than about 60 nm. Because of their narrower pore size distribution, ACFs are particularly suitable to elucidate pore size effects on organic compound adsorption from aqueous solution (Kasaoka et al. 1989b, Pelekani and Snoeyink 1999, Pelekani and Snoeyink 2000, Pelekani and Snoeyink 2001).

The size of adsorbent pores affects the adsorption of organic contaminants in two ways. First, adsorption strength increases with decreasing pore size because (1) contact points between the adsorbate and the adsorbent surface increase (Newcombe et al. 1997) and (2) adsorption potentials between opposing pore walls begin to overlap once the micropore width is less than twice the adsorbate diameter (Matsumoto et al. 1997). Second, size exclusion limits the adsorption of contaminants of a given size and shape if pores are too small. In aqueous systems, size exclusion is observed when the pore width is smaller than about 1.7 times the second largest dimension of the adsorbate (Kasaoka et al. 1989b).

Given that many organic contaminants are small (i.e. total surface areas of about 100-300 Å<sup>2</sup> (Okouchi et al. 1992), which corresponds to spherical diameters of about 5.5-10 Å), the above observations suggest that the presence of small micropores is important for their removal from aqueous solution. For example, Newcombe (2001) observed that the adsorption capacity for the naturally occurring taste and odor compound 2-methylisoborneol (MIB) correlated well with the volume of micropores with a diameter of about 10 Å.

### *1.2.2 Activated Carbon Surface Chemistry*

At the edges of the condensed, polyaromatic sheets that constitute the building blocks of activated carbons, heteroatoms, i.e. atoms other than carbon, are encountered that define the chemical characteristics of activated carbon surfaces. Oxygen is an important heteroatom that commonly occurs in the form of carboxylic acid groups, phenolic or enolic hydroxyl groups, and quinone carbonyl groups (Boehm et al. 1964, Puri 1970, Mattson and Mark 1971, Snoeyink and Weber 1972). Activated carbons assume an acidic character when exposed to oxygen between 200 and 700°C or to oxidants such as hydrogen peroxide, nitric acid, or nitric and sulfuric acid mixtures in aqueous solution (Puri 1970, Puri 1983). The increased activated carbon acidity is primarily explained by the formation of carboxylic acid and (ph)enolic hydroxyl groups (Boehm et al. 1964, Mattson and Mark 1971), and X-ray photoelectron spectroscopy (XPS) data showed that the above oxidation techniques non-selectively increased the surface concentrations of both groups (Polovina et al. 1997, Mangun et al. 1999). While the majority of the

oxidation conditions employed by Mangun et al. (1999) also increased the surface concentration of quinone carbonyl groups, the opposite trend was observed by Polovina et al. (1997).

The presence of basic oxygen-containing functionalities such as chromene- and pyrone-type structures has also been postulated (Garten and Weiss 1957, Boehm 1970). However, a consensus is developing that the basic character of activated carbons arises primarily from delocalized  $\pi$ -electrons on the condensed polyaromatic sheets (Leon y Leon et al. 1992, Barton et al. 1997). These electron-rich Lewis base sites develop as oxygen is removed from the activated carbon surface, e.g. by heat treatment in an inert atmosphere. This treatment does not only remove inherently acidic groups, but also other oxygen-containing functionalities that decrease the basicity of activated carbons by attracting and thus localizing  $\pi$ -electrons of the condensed, polyaromatic sheets (Coughlin and Ezra 1968). The removal of oxygen not only renders an activated carbon surface more basic but also less polar, a desirable trait when the adsorption of organic contaminants from aqueous solution is the primary treatment objective. While heat treatment in an inert atmosphere effectively removes oxygen-containing functional groups from the activated carbon surface, it produces highly reactive sites such as free-radical edge sites and dangling carbon atoms (Coulson 1960, Menendez et al. 1996a). As a result, re-exposure of such carbons to the atmosphere results in oxygen adsorption and the consequent loss of basic and hydrophobic properties. However, Menendez et al. (1996a, 1996b) recently showed that heat treatment in a hydrogen-atmosphere produces

relatively stable carbon atoms at the edges of the graphitic platelets that no longer contain unpaired electrons (Coulson 1960, Menendez 1996a). Consequently, oxygen readsorption on carbons heat-treated in H<sub>2</sub> was greatly reduced compared to carbons heat-treated in N<sub>2</sub>. The use of ammonia (NH<sub>3</sub>) has also been explored for the preparation of basic activated carbons (Jansen and van Bekkum 1994, Biniak et al. 1997). Apart from the removal of oxygen-containing functional groups during heat-treatment in a NH<sub>3</sub> atmosphere, the incorporation of basic nitrogen moieties such as pyridine-type structures can explain the enhanced basicity of ammonia-treated carbons (Biniak et al. 1997, Jansen and van Bekkum 1995).

Numerous studies have shown that increases in the oxygen or acidic functional group contents of activated carbons impair the adsorption of organic compounds from aqueous solution (Kaneko et al. 1989, Pendleton et al. 1997, Franz et al. 2000, Considine et al. 2001, Karanfil and Kilduff et al. 1999). Although oxidation of activated carbons enhanced the removal of polar organic compounds from the gaseous phase (Mangun et al. 1999, Dimotakis et al. 1995), Kaneko et al. (1989) showed that the *removal* of acidic functional groups enhanced the adsorption of both relatively polar and relatively nonpolar organic compounds from aqueous solution. This observation was explained by the preferential adsorption of water on carbon surfaces containing oxygen groups (Kaneko et al. 1989). Water can adsorb by means of hydrogen bonds on oxygen-containing functional groups, and clustering of additional water molecules occurs around water molecules adsorbed at these sites (Puri 1970, Dubinin et al. 1955, Barton et al. 1984, Pan

and Jaroniec 1996, Müller et al. 1996, Müller et al. 1998, McCallum et al. 1999, Müller et al. 2000). Such water clusters can prevent pollutant access to hydrophobic regions on the activated carbon surface, reduce the interaction energy between the pollutant and the adsorbent surface, and/or effectively block pollutant access to micropores (Kaneko et al. 1989, Pendleton et al. 1997, Franz et al. 2000, Coughlin and Ezra 1968, Müller et al. 2000, Mahajan et al. 1980). Pendleton et al. (1997) also remarked that organic contaminant adsorption from aqueous solution necessitates the displacement of water from the activated carbon surface. Enthalpy measurements showed that water displacement by MIB became increasingly difficult with an increase in the hydrophilic site concentration on the activated carbon surface. Consequently, water adsorption explains why polar activated carbons exhibit a smaller adsorption capacity for trace organic compounds than less polar activated carbons with similar micropore volumes (Pendleton et al. 1997, Newcombe et al. 1997). Overall, the detrimental effects of water adsorption illustrate that adsorbents with stable hydrophobic surfaces bear the greatest promise for the removal of trace organic contaminants from drinking water sources. Nonetheless, adsorbents need to be sufficiently hydrophilic so that they are wetted by water to be useful for water treatment applications (Davis and Powers 2000).

### **1.3. EXPERIMENTAL**

#### *1.3.1 Solvents*

Isotherm experiments were conducted in ultrapure laboratory water (tap water treated by reverse osmosis, ion exchange, and granular activated carbon adsorption, resistance  $\geq$

14.85 M $\Omega$ /cm). Ultrapure water was amended with a 1 mM phosphate buffer (0.5 mM Na<sub>2</sub>HPO<sub>4</sub>•H<sub>2</sub>O and 0.5 mM NaH<sub>2</sub>PO<sub>4</sub>) to maintain a pH of 7.2. Furthermore, 100 mg/L sodium azide were added to eliminate aerobic biological activity. To evaluate solvent effects, adsorption experiments were also conducted in nonpolar cyclohexane (HPLC-grade, Sigma-Aldrich, St. Louis, MO).

### *1.3.2 Adsorbates*

TCE and MTBE, two common drinking water contaminants, served as probe molecules for the assessment of adsorbate polarity effects. TCE is a relatively hydrophobic adsorbate (aqueous solubility at 25°C = 1,198 mg/L (Schwarzenbach et al. 1993)) while MTBE is relatively hydrophilic (aqueous solubility  $\approx$  50,000 mg/L (Nichols et al. 2000)). In addition, TCE and MTBE differ in molecular size and shape (Figure 1.1); TCE is a planar molecule while MTBE approximates a tetrahedron. Kinetic diameters for TCE and MTBE are 5.6 Å (Chintawar and Greene 1997) and 6.2 Å (Sano et al. 1995), respectively.

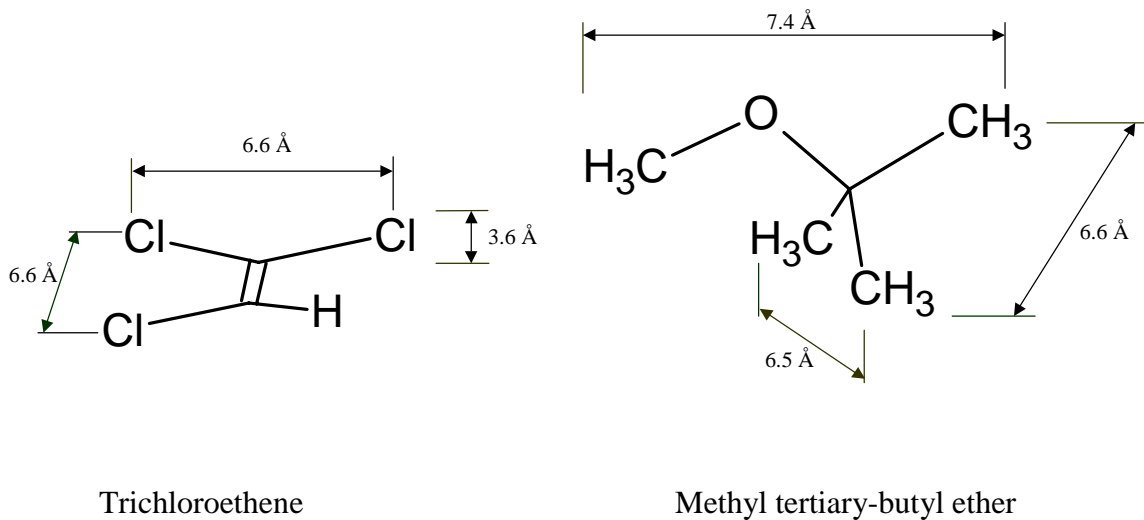


**Figure 1.1 Molecular structures and dimensions for trichloroethene and methyl tertiary-butyl ether. Molecular dimensions were calculated from the Cambridge Structural Database and the van der Waals radii for methyl groups and chlorine (2.0 and 1.8 Å, respectively (Pauling 1960)).**

MTBE stock solutions were prepared in ultrapure water at a concentration of approximately 1,500 mg/L, and TCE stock solutions were prepared in methanol at a concentration of about 3,400 mg/L. The latter concentration assured that methanol concentrations in isotherm tests remained below 0.1%, a level at which no co-solvent effects were observed in prior studies (Kilduff et al. 1998).

### *1.3.3 Adsorbents*

Three commercially available ACF samples (ACF-10, ACF-15, and ACF-20) were obtained from Nippon Kynol. The phenolic-resin fibers were pyrolyzed and subsequently oxidized in a steam and CO<sub>2</sub> atmosphere to obtain three activation levels. Upon receipt, all ACF samples were acid-washed by soaking the ACF overnight in 2 N HCl and subsequently boiling the ACF for 1 hour in 2 N HCl. The samples were then rinsed with ultrapure water until no chloride was detected by AgNO<sub>3</sub> addition to the rinse water. Acid-washed ACF samples were dried in an oven at 130°C and served as the base material for subsequent surface chemistry modifications.

Acid-washed activated carbon fibers were oxidized by contacting 5 g of ACF with 200 mL of 30% H<sub>2</sub>O<sub>2</sub> for 16 hours at room temperature. Following oxidation, the ACF was dried in an oven at 130°C. Heat treatment in a hydrogen atmosphere followed a procedure similar to that described by Menendez et al. (1996b). A 1.5-g sample of acid-washed ACF was mixed with 1 g of platinum-impregnated GAC (Alfa Aesar, Ward Hill, MA), and the mixture was placed into a 3-zone tube furnace (Lindberg/Blue M, Asheville, NC) equipped with an alumina tube (7.62-cm O.D., Vesuvius McDanel, Beaver Falls, PA). The furnace temperature was raised to 900°C, held at this temperature for 2 hours and then cooled to 500°C, all in a N<sub>2</sub> atmosphere. At 500°C, the gas supply was switched to H<sub>2</sub> for 3 hours. Finally, ACF samples were cooled to room temperature in the tube furnace under N<sub>2</sub>. For ammonia-treatments, a 1.5-g sample of acid-washed ACF was placed into the tube furnace without catalyst. The furnace temperature was

raised to 900°C, held at this temperature for 2 hours and then cooled to 700°C, all in a N<sub>2</sub> atmosphere. At 700°C, the gas supply was switched to NH<sub>3</sub> for 1 hour. Finally, ACF samples were cooled to room temperature in the tube furnace under N<sub>2</sub>. All gases were ultrahigh purity (UHP) or research grade, and gas streams passed through oxygen, carbon dioxide, and water traps prior to entering the reaction tube. All gas flow rates were 200 mL/min. Tube ends were sealed with stainless steel plates, PTFE-lined gaskets, and high temperature grease to prevent leakage of H<sub>2</sub> and NH<sub>3</sub> or intrusion of atmospheric oxygen, CO<sub>2</sub>, and water. Upon heat treatment, samples were stored in a desiccator at room temperature. To facilitate comparisons among modified ACFs, the abbreviations shown in Table 1.1 will be used throughout this thesis.

**Table 1.1 Nomenclature for ACF matrix**

<b>Treatment</b>	<b>Abbreviation</b>		
	<b>ACF-10</b>	<b>ACF-15</b>	<b>ACF-20</b>
Acid-washed	AW10	AW15	AW20
Oxidized after acid-washing	OAW10	OAW15	OAW20
Hydrogen-treated after acid-washing	HAW10	HAW 15	HAW 20
Ammonia-treated after acid-washing	AAW10	AAW15	AAW20

To verify whether correlations developed for the ACF matrix are also valid for commercially available granular activated carbons (GACs), tests were conducted with bituminous coal-based F-600 GAC (Calgon Carbon Corporation, Pittsburgh, PA), coconut shell-based G-219 GAC (PicaUSA, Columbus, OH), and chemically activated wood-based Picazine GAC (PicaUSA, Columbus, OH). To enhance adsorption rates,

GACs were pulverized with a mortar and pestil until 95% by mass passed a 45- $\mu$ m sieve (325 U.S. mesh). Upon sieving, the portion remaining on the sieve was recombined with the portion that passed through the sieve, dried at 130°C, and stored in a desiccator.

#### *1.3.4 Adsorbent characterization*

BET surface areas, micropore volumes and pore size distributions were determined from N<sub>2</sub> isotherm data collected at 77 K (Autosorb-1-MP, Quantachrome Corporation, Boynton Beach, FL). Prior to analysis, ACF samples were outgassed overnight at 473 K. BET surface areas were determined from 11-point adsorption isotherms that were completed with a 0.1-g sample in the 0.01-0.1 relative pressure range. Subsequently, N<sub>2</sub> isotherms were obtained over a relative pressure range from 10<sup>-6</sup> to 1 with 0.01-g sample sizes. The ACF sample mass for the latter N<sub>2</sub> isotherm was adjusted such that the BET surface area matched the value obtained with the larger sample mass. The micropore volumes and pore size distributions were subsequently calculated from the adsorption data using the density functional theory (Vulcan kernel, PC software version 1.19, Quantachrome, Boynton Beach, FL).

The point of zero charge for activated carbon surfaces was assessed by mass titrations as described by Noh and Schwarz (1989) and Barton et al. (1997). Using carbon doses up to 5% (wt/wt), mass titrations were performed in 25-mL crimp-cap culture tubes containing 20 mL of 0.1 N NaCl solution. To eliminate interferences from dissolved and atmospheric CO<sub>2</sub>, the NaCl solution was sparged with N<sub>2</sub> for four hours, and culture

tubes were filled and capped in an anaerobic hood. Changes in solution pH as a result of the activated carbon additions were measured in an anaerobic hood after tumbling suspensions for 48 hours. The  $\text{pH}_{\text{PZC}}$  was taken as the average plateau value that was obtained for the largest carbon doses.

Carbon, hydrogen, and nitrogen contents were determined with a CHN Elemental Analyzer (Perkin-Elmer Corp., Norwath, CT). The phosphorous content of Picazine GAC was determined with an ICP Optical Emission Spectrometer (Perkin-Elmer Corp., Norwath, CT). Prior to analysis, the samples were dried overnight at 105°C and cooled in a desiccator. Oxygen contents were measured directly according to ASTM D5622 (Huffman Laboratories, Golden, CO). Ash contents of GACs were determined by combusting about 5 g of adsorbent in a muffle furnace at 550°C for 2 hours.

### *1.3.5 Isotherms*

For isotherms in ultrapure water, adsorbent doses between 10 and 7500 mg/L were utilized. Adsorbents were placed into brown glass bottles that were subsequently filled to the neck with the amended ultrapure water. TCE or MTBE stock solutions were added with a constant rate syringe (CR-700, Hamilton, Reno, NV) to yield an initial concentration of about 1000 µg/L (some MTBE isotherm experiments were conducted at an initial concentration of approximately 100 µg/L to reduce the amount of carbon required to complete the tests). Once the micropollutant was added to a bottle, it was topped off immediately with ultrapure water to create headspace-free conditions and

capped using PTFE-faced silicon septa and open-top closures. A mixing time of 2 weeks in a rotary tumbler was sufficient to reach adsorption equilibrium, as established in screening tests, and micropollutant losses were not observed in triplicate blanks containing no carbon over that time period. Upon equilibration, adsorbents were separated from the liquid by sedimentation (ACFs) or filtration through 0.45  $\mu\text{m}$  filters (pulverized GACs). Remaining liquid-phase TCE and MTBE concentrations were measured by purge and trap preconcentration, gas chromatographic (GC) separation and flame ionization detection (FID).

For adsorption tests in cyclohexane, ACF doses of 10 and 15 g/L were tested in 40-mL EPA vials. TCE or MTBE were spiked into cyclohexane to yield an initial concentration of 100 mg/L. Thirty-mL aliquots of this solution were pipetted into the vials, which were capped with PTFE-faced silicon septa and open-top closures. The samples were tumbled for one week, and remaining liquid phase concentrations were analyzed by direct injection GC/FID. Blanks containing no carbon showed no adsorbate losses over the equilibration time.

## **1.4. RESULTS AND DISCUSSION**

### *1.4.1 Adsorbent Characterization*

To elucidate pore structure and surface chemistry effects on the adsorption of TCE and MTBE from aqueous solution, a matrix of twelve ACFs was prepared and characterized. To test whether the trends established with the ACFs were also valid for GACs, three

commercially available GACs were characterized and tested in pulverized form. Table 1.2 summarizes BET surface areas as well as micropore and mesopore volumes of the studied adsorbents. The results illustrate that the BET surface areas of the ACFs increased with increasing level of activation, i.e. from ACF 10 to ACF 20. Increases in BET surface area were primarily attributable to increases in micropore volume although the mesopore volumes of the ACFs also increased somewhat with increasing activation level. Figure 1.2 depicts micropore size distributions for acid-washed ACFs. Micropores of AW10 were concentrated in the 7 to 11 Å width range while those of AW15 and 20 were concentrated in the 9 to 13 Å width range. The micropore size distributions obtained in the current study are in close agreement with prior results for as-received ACFs with the same designations Daley et al. 1996, Pelekani and Snoeyink 1999, Pelekani and Snoeyink 2000, Pelekani and Snoeyink 2001). As shown in Table 1.2, the employed chemical modification techniques changed BET surface areas by less than 10% compared to the corresponding acid-washed ACFs. Oxidative treatments reduced the micropore volumes of the activated carbons by about 12 to 23% while heat treatments in H<sub>2</sub> or NH<sub>3</sub> atmospheres had little effect on micropore volumes (4% decrease to 7% increase). With the exception of OAW15, mesopore volume changes were in the ±20% range and were relatively small (in terms of cm<sup>3</sup>/g) given the microporous nature of the ACFs. Although surface chemistry modifications had small effects on BET surface areas and pore volumes, they had no noticeable effects on pore size distributions as illustrated in Figure 1.3. Therefore, the developed ACF matrix permitted the evaluation of surface chemistry effects on TCE and MTBE adsorption in the absence of pore size effects. For the

commercially available GACs, Figure 1.4 shows that both F600 and G219 exhibited pore size distributions that were broader and less uniform than those of the ACFs. Micropores of F600 were concentrated in the 7 to 12 Å width range while those of G219 were concentrated in the 7 to 13 Å width range. The micropores of Picazine were largest among the commercially available GACs and were concentrated in the 9 to 15 Å width range.

**Table 1.2 BET surface areas and pore volumes of ACFs and pulverized GACs. Micropore and mesopore volumes were obtained from DFT calculations.**

<b>Sample</b>	<b>BET surface area (m<sup>2</sup>/g)</b>	<b>Micropore volume (cm<sup>3</sup>/g)</b>	<b>Mesopore volume (cm<sup>3</sup>/g)</b>
AW10	760	0.387	0.075
OAW10	750	0.340	0.089
HAW10	830	0.414	0.074
AAW10	720	0.371	0.061
AW15	1480	0.567	0.099
OAW15	1350	0.439	0.154
HAW15	1530	0.593	0.085
AAW15	1510	0.573	0.098
AW20	1670	0.594	0.120
OAW20	1530	0.504	0.144
HAW20	1710	0.622	0.096
AAW20	1700	0.599	0.130
F600	1290	0.353	0.085
G219	1460	0.438	0.118
Picazine	1680	0.377	0.252

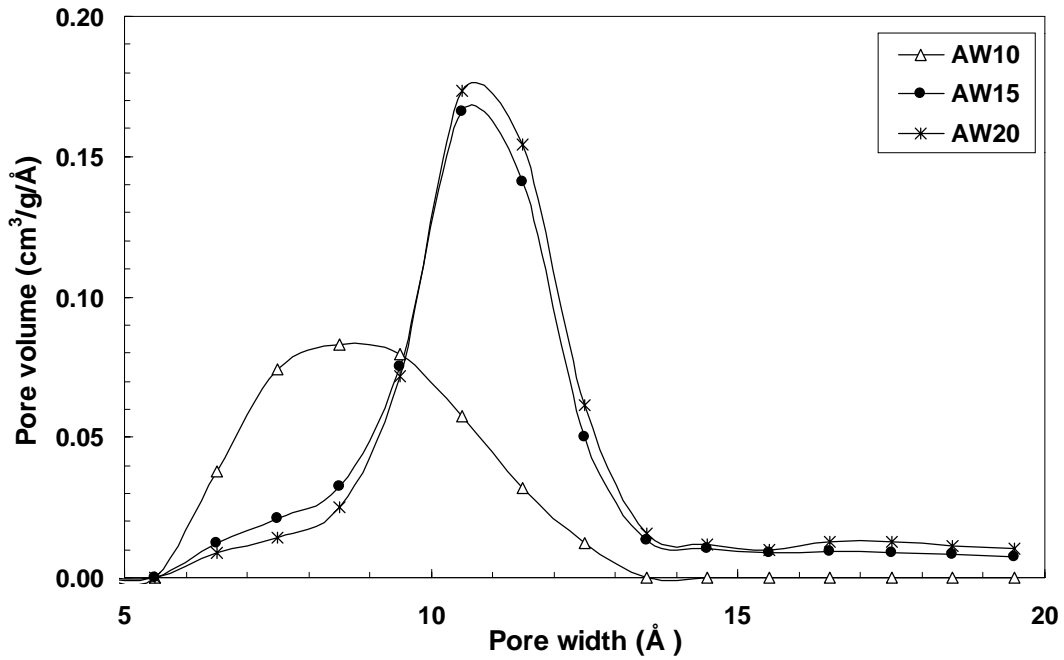


Figure 1.2 Micropore size distributions of acid-washed ACF samples

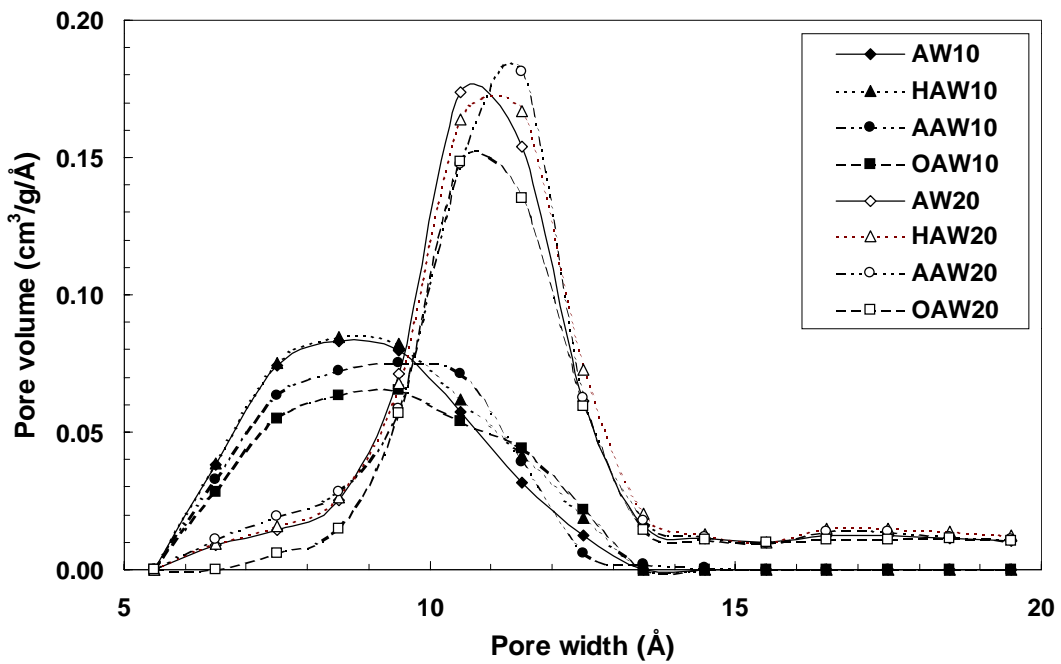
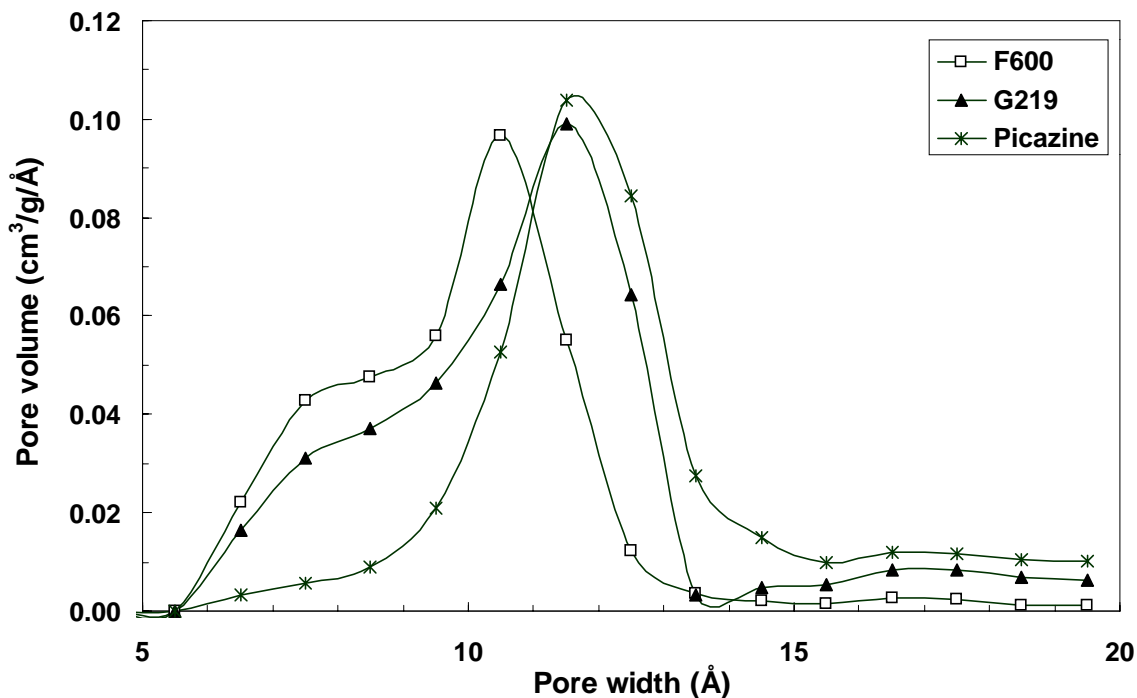


Figure 1.3 Effects of surface chemistry modifications on micropore size distributions of ACFs 10 and 20. Trends for ACF 15 were similar to those observed for ACF 20 (data for ACF 15 not shown for clarity of figure).



**Figure 1.4 Micropore size distributions of pulverized GAC samples**

Elemental analysis and  $pH_{PZC}$  data for the ACF matrix are summarized in Table 1.3. The sum of the C, H, N, and O contents represented approximately 94-99% of the total adsorbent mass, confirming that the ash content of the phenolic resin-based ACFs was small. Table 1.3 further illustrates that oxidation of acid-washed ACFs increased the oxygen content to about 10% while heat treatments of acid-washed ACFs in hydrogen and ammonia atmospheres decreased oxygen contents to about 2% or less. Using  $H_2O_2$  to oxidize ACF 15, Mangun et al. (1999) also obtained an oxygen content of about 10%, and XPS analyses showed that this treatment increased the surface concentrations of carboxylic acid, phenolic hydroxyl, and carbonyl groups. As observed in prior studies (Barton et al. 1997), the incorporation of oxygen-containing functionalities as a result of surface oxidation rendered the adsorbents more acidic while the removal of oxygen-

containing functionalities through heat-treatment rendered the adsorbents more basic. Ammonia-treatment increased nitrogen contents of the ACFs to about 1.5 to 1.9%. Consistent with the incorporation of basic pyridine-type structures, which was expected based on the chosen treatment conditions (Janssen and van Bekkum 1994, Biniak et al. 1997, Janssen and van Bekkum 1995), the  $\text{pH}_{\text{PZC}}$  data illustrate that the ammonia-treatment yielded the most basic ACFs of the adsorbent matrix. The results of the elemental analyses and mass titrations indicate that a given chemical treatment yielded ACFs with similar polarity and surface acidity/basicity, which permitted the study of pore structure effects on TCE and MTBE adsorption in the absence of surface chemistry effects.

**Table 1.3 Elemental analysis and  $\text{pH}_{\text{PZC}}$  results for ACF matrix<sup>a</sup>**

ACF	C (Wt. %)	H (Wt. %)	N (Wt. %)	O (Wt. %)	Total (%)	$\text{pH}_{\text{PZC}}$
<b>AW10</b>	90.18 ± 0.31	0.34 ± 0.02	0.17 ± 0.02	4.57	95.26	4.8
<b>AW15</b>	92.73 ± 0.29	0.40 ± 0.17	0.18 ± 0.01	3.62	96.93	5.4
<b>AW20</b>	92.33 ± 0.15	0.27 ± 0.01	0.15 ± 0.01	3.58	96.33	4.4
<b>OAW10</b>	82.21 ± 1.17	0.54 ± 0.04	0.14 ± 0.01	10.78	93.68	3.0
<b>OAW15</b>	82.37 ± 0.84	0.36 ± 0.02	0.19 ± 0.02	11.34 ± 0.54	94.25	2.9
<b>OAW20</b>	86.30 ± 0.48	< 0.04	<0.04	9.58 ± 0.06	97.63	3.2
<b>HAW10</b>	93.14 ± 0.92	0.36 ± 0.17	0.11 ± 0.03	2.32 ± 0.19	95.92	6.4
<b>HAW15</b>	96.00 ± 0.60	0.27 ± 0.03	0.09 ± 0.01	1.39	97.74	6.5
<b>HAW20</b>	95.68 ± 0.23	0.24 ± 0.02	0.09 ± 0.02	1.66	97.68	6.7
<b>AAW10</b>	92.22 ± 0.81	0.38 ± 0.08	1.80 ± 0.63	2.08 ± 0.17	96.47	8.7
<b>AAW15</b>	95.26 ± 0.55	0.73 ± 0.06	1.89 ± 0.23	1.45 ± 0.16	99.33	8.7
<b>AAW20</b>	93.50 ± 0.53	0.29 ± 0.04	1.52 ± 0.66	1.23 ± 0.45	96.54	8.7

<sup>a</sup> Values represent means ± one standard deviation

Table 1.4 summarizes the elemental composition, ash content, and  $\text{pH}_{\text{PZC}}$  data for pulverized GACs. The results showed that the low-ash GACs exhibited a wide range of oxygen contents. F600 and G219, the GACs with the lower oxygen contents, exhibited a basic character while Picazine with an oxygen content of nearly 16% was strongly acidic. Because Picazine is chemically activated using phosphoric acid, one could argue that a fraction of the measured oxygen content was associated with phosphates instead of the carbon surface. A phosphorous content of approximately 1% (wt/wt) was measured for Picazine, suggesting that no more than approximately 2% (wt/wt) oxygen was associated with phosphates. Consequently, the largest fraction of the measured oxygen content of Picazine (Table 1.4) was associated with the carbon surface, which explains its acidic character.

**Table 1.4 Elemental analysis, ash content, and  $\text{pH}_{\text{PZC}}$  results for pulverized GACs<sup>a</sup>**

<b>Carbon</b>	<b>C (Wt. %)</b>	<b>H (Wt. %)</b>	<b>N (Wt. %)</b>	<b>O (Wt. %)</b>	<b>Ash (Wt. %)</b>	<b>Total (%)</b>	<b><math>\text{pH}_{\text{PZC}}</math></b>
<b>F600</b>	92.50 ± 1.68	< 0.04	0.33 ± 0.04	2.60	1.84 ± 0.01	97.27	8.3
<b>G219</b>	90.61 ± 0.45	< 0.04	0.05 ± 0.04	4.90	2.82 ± 0.04	98.37	9.7
<b>Picazine</b>	76.92 ± 0.53	0.40 ± 0.03	0.03 ± 0.03	15.88	3.37 ± 0.11	96.59	2.1

<sup>a</sup> Values represent means ± one standard deviation

#### *1.4.2. TCE and MTBE Adsorption*

To elucidate the effects of adsorbent surface chemistry and pore structure on the adsorption of organic pollutants from aqueous solution, single-solute TCE and MTBE isotherms experiments were conducted with each member of the ACF matrix. To

compare single-solute isotherm results in a quantitative manner, isotherms were described by the Freundlich model [ $q_e = K (C_e)^{1/n}$ ], where  $q_e$  and  $C_e$  are the equilibrium solid-phase and liquid-phase concentrations, respectively, and  $K$  and  $1/n$  are fitting parameters. A larger  $K$  value represents a larger adsorption capacity while a larger  $1/n$  value represents a more homogeneous adsorbent with a narrower site energy distribution (Derylo-Marczewska et al. 1984, Carter et al. 1995). Figure 1.5 summarizes TCE and MTBE isotherm data along with Freundlich isotherm model fits for hydrogen-treated ACFs, and Table 1.5 summarizes TCE and MTBE Freundlich isotherm parameters for all studied adsorbents. As indicated in Figure 1.5 and by the  $K$  values in Table 1.5, TCE adsorbed to a greater extent on activated carbon surfaces than MTBE. Given the greater aqueous solubility of MTBE, primarily because its ether oxygen can serve as a hydrogen bond acceptor in water, MTBE adsorption on activated carbon surfaces requires the disruption of relatively strong solute/solvent interactions. Consequently, adsorption of MTBE is energetically less favored than adsorption of TCE, for which solute/solvent interactions are weaker. These results are consistent with adsorbate solubility or polarity effects on adsorption that have been well established in the literature [e.g. Lundelius 1920, Weber 1972, McGuire et al. 1978, Belfort 1979, Crittenden et al. 1999].

**Table 1.5 Freundlich parameters for single-solute TCE and MTBE isotherms. The 95% confidence intervals for each parameter are shown in parentheses.**

Carbon	TCE		MTBE	
	K Average (Lower; Upper)	1/n Average (Lower; Upper)	K Average (Lower; Upper)	1/n Average (Lower; Upper)
<b>AW10</b>	5.23 (3.95; 6.92)	0.487 (0.403; 0.570)	0.0886 (0.0785; 0.1000)	0.603 (0.572; 0.633)
<b>AW15</b>	2.11 (1.82; 2.43)	0.554 (0.511; 0.596)	0.141 (0.128; 0.155)	0.634 (0.608; 0.660)
<b>AW20</b>	1.56 (1.35; 1.81)	0.593 (0.545; 0.641)	0.103 (0.0947; 0.112)	0.672 (0.646; 0.697)
<b>OAW10</b>	1.19 (1.04; 1.35)	0.604 (0.572; 0.637)	0.0451 (0.0413; 0.0493)	0.589 (0.571; 0.606)
<b>OAW15</b>	0.627 (0.494; 0.798)	0.591 (0.534; 0.649)	0.0376 (0.0342; 0.0412)	0.630 (0.611; 0.648)
<b>OAW20</b>	0.677 (0.584; 0.786)	0.595 (0.559; 0.632)	0.0301 (0.0241; 0.0375)	0.664 (0.610; 0.718)
<b>HAW10</b>	6.75 (5.67; 8.05)	0.426 (0.374; 0.479)	0.190 (0.152; 0.238)	0.532 (0.471; 0.594)
<b>HAW15</b>	2.85 (2.10; 3.86)	0.482 (0.393; 0.570)	0.206 (0.183; 0.232)	0.597 (0.566; 0.627)
<b>HAW20</b>	2.51 (1.95; 3.23)	0.514 (0.436; 0.592)	0.168 (0.132; 0.214)	0.624 (0.553; 0.695)
<b>AAW10</b>	4.61 (3.77; 5.64)	0.485 (0.426; 0.544)	0.164 (0.145; 0.185)	0.562 (0.531; 0.592)
<b>AAW15</b>	1.98 (1.53; 2.55)	0.567 (0.483; 0.651)	0.197 (0.170; 0.229)	0.546 (0.510; 0.582)
<b>AAW20</b>	2.05 (1.77; 2.38)	0.512 (0.467; 0.556)	0.115 (0.0986; 0.134)	0.631 (0.589; 0.674)
<b>F600</b>	4.05 (3.50; 4.69)	0.462 (0.422; 0.502)	0.150 (0.142; 0.159)	0.486 (0.475; 0.498)
<b>G219</b>	2.63 (2.08; 3.32)	0.484 (0.426; 0.543)	0.127 (0.112; 0.143)	0.540 (0.515; 0.564)
<b>Picazine</b>	0.099 (0.081; 0.121)	0.616 (0.563; 0.668)	0.00193 (0.00150, 0.00248)	0.841 (0.797, 0.884)

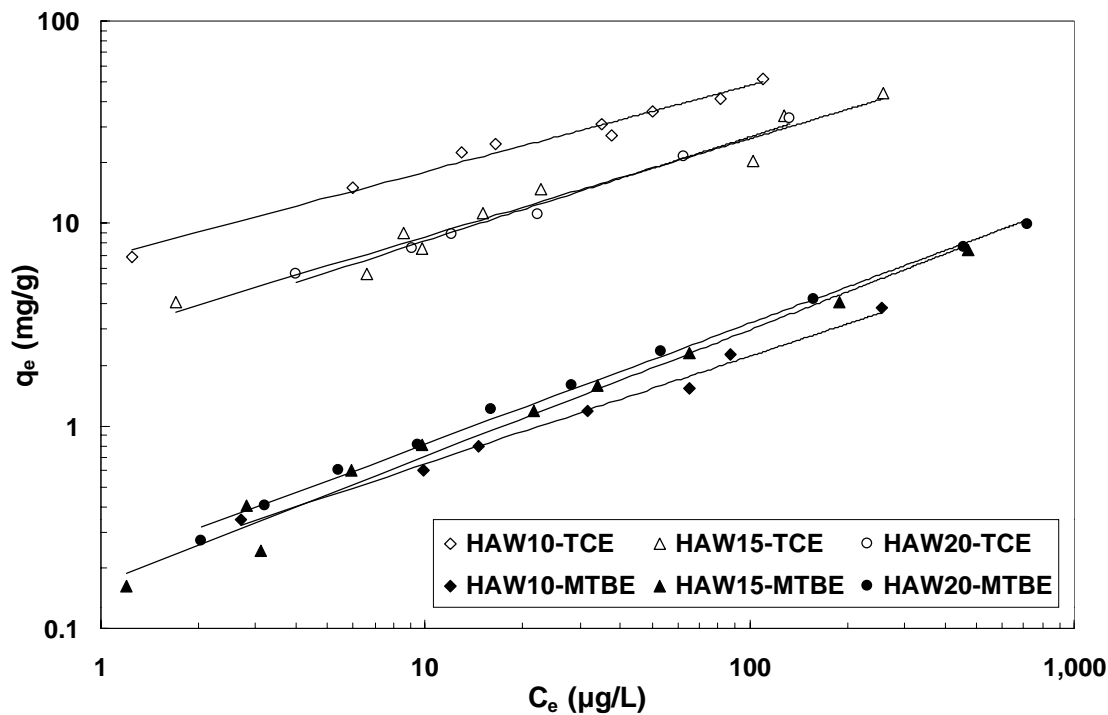


**Figure 1.5 TCE and MTBE isotherms on hydrogen-treated ACFs**

With respect to pore structure, the results in Figure 1.5 show that the ranking of the ACFs in terms of adsorption capacity differed for the two solutes. For TCE, HAW10 exhibited the largest adsorption capacity even though it had the smallest BET surface area of the hydrogen-treated ACFs. The same trend was observed for all other surface chemistry modifications as indicated by the Freundlich K-values in Table 1.5. In comparison, MTBE adsorption capacities were relatively similar at all three ACF activation levels (Figure 1.5). The TCE isotherm data therefore suggest that ACF10 had a larger pore volume in a size range suitable for TCE adsorption than ACFs 15 and 20. Similarly, the MTBE isotherm data suggest that ACFs at all three activation levels had similar pore volumes in a size range suitable for MTBE adsorption. Both TCE and MTBE isotherm

data clearly illustrate that adsorption capacities cannot be predicted from the BET surface areas or total micropore volumes (Table 1.2).

To assess in which pore sizes TCE and MTBE adsorb preferentially, adsorption capacities at an equilibrium liquid-phase concentration of 50  $\mu\text{g/L}$  ( $q_{e, 50}$ ) were correlated with ACF pore volumes in a given size range for each surface chemistry modification. Following a trial-and-error approach similar to that described by Ebie et al. (1995), the results showed that TCE adsorption was controlled by pores in the 7-10 Å width range while MTBE adsorption was controlled by pores in the 8-11 Å width range. These results suggest that both TCE and MTBE adsorb primarily in pores with widths that are 1.3 to 1.8 times larger than their kinetic diameters. Considering that the second-largest dimension of both adsorbates is similar (Figure 1.1), the results of the current study do not fully substantiate that adsorption of organic compounds from aqueous solutions is controlled by the second-largest adsorbate dimension as suggested by Kasaoka et al. (1989b). Given that pores of the studied ACFs are elliptical (Daley et al. 1996), it appears reasonable that the flat TCE molecule is able to access smaller pores than the MTBE molecule, which approximates a tetrahedron.

For TCE, Figure 1.6 illustrates that the available pore volume in the 7-10 Å diameter range primarily controlled TCE adsorption on the more hydrophobic ACFs (AW, HAW, AAW) even though the oxygen contents of these carbons varied by a factor of about three (~1.5 - 4.5%). A comparison among Freundlich K-values (Table 1.5), representing TCE

adsorption capacities at an equilibrium liquid-phase concentration of 1  $\mu\text{g/L}$ , substantiated that pore structure effects dominated over surface chemistry effects for the more hydrophobic ACFs; i.e., 95% confidence intervals generally overlapped for AW, HAW, and AAW at a given activation level while ACF 10 always exhibited the largest K-value for a given surface chemistry modification. Figure 1.6 also shows that the correlation established by the more hydrophobic ACFs predicted the adsorption capacity of the relatively hydrophobic F600 and G219 GACs reasonably well. For the oxidized ACFs, a separate correlation indicated that surface chemistry effects in addition to the availability of a suitable pore volume controlled TCE adsorption for ACFs with larger oxygen contents ( $\sim 10\%$ ). The correlation established by the oxidized ACFs appropriately predicted the adsorption capacity of Picazine GAC with an oxygen content of about 16%. A plot of MTBE adsorption capacity versus micropore volume in the 8-11  $\text{\AA}$  diameter range showed a trend similar to that depicted in Figure 1.6 for TCE (figure not shown). However, surface chemistry effects were of some importance even among the more hydrophobic ACFs. A comparison of the Freundlich K-values in Table 1.5 also shows that the hydrogen-treated ACFs, i.e. the most hydrophobic ACFs of the matrix, exhibited the largest MTBE adsorption capacities at a given activation level. Nonetheless, differences among the more hydrophobic ACFs at a given activation level were small compared to the decrease in MTBE adsorption capacity that was observed upon oxidation (Table 1.5).

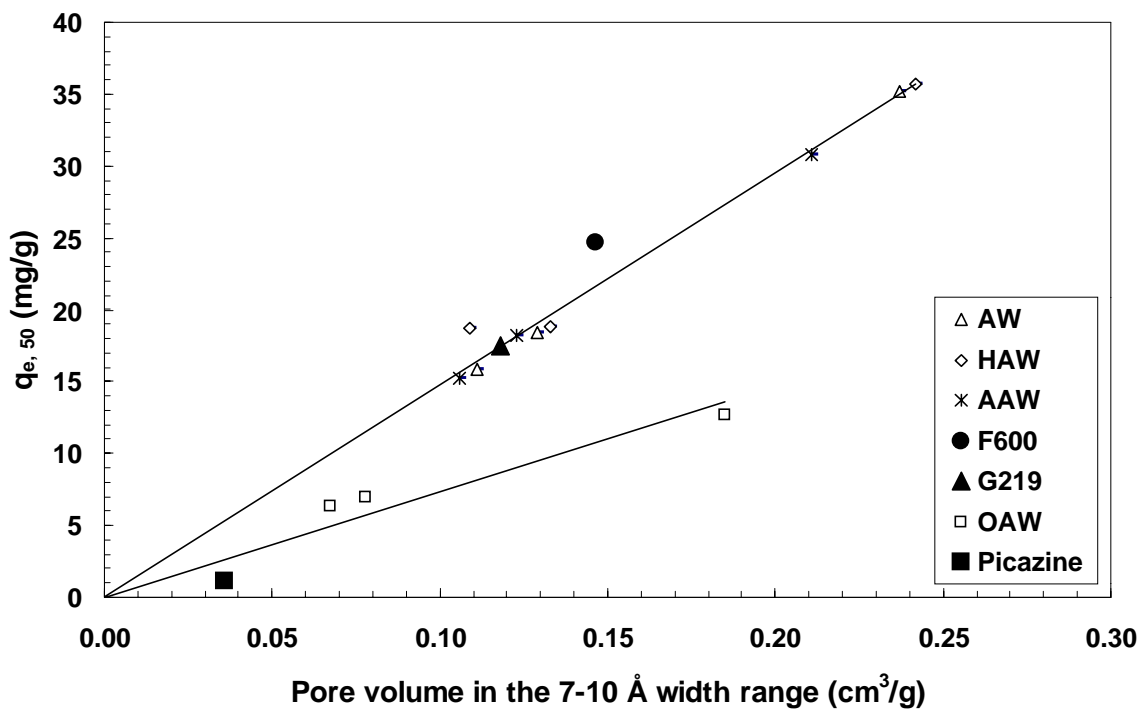


**Figure 1.6 Effect of pore volume on TCE adsorption**

Overall, the isotherm data showed that the adsorption of both relatively hydrophobic (TCE) and relatively hydrophilic (MTBE) organic pollutants from aqueous solution is adversely affected by the introduction of surface oxygen groups (see Freundlich K-values in Table 1.5). Prior studies have shown that the adsorption of polar organics such as acetone (Mangun et al. 1999, Dimotakis et al. 1995) or acetaldehyde (Mangun et al. 1999) from the gas-phase is enhanced upon surface oxidation because of dipole-dipole interactions (Mangun et al. 1999) or hydrogen bonding, and a similar result may be anticipated for MTBE vapor. However, in aqueous solution, MTBE has to compete with water for polar adsorption sites. Given that the concentration of MTBE is small compared

to that of water, water adsorption should be favored over MTBE adsorption at polar surface sites.

To verify the importance of solvent/adsorbent interactions, MTBE and TCE adsorption was also studied from cyclohexane, a nonpolar solvent. In contrast to the results obtained in aqueous solution, Figure 1.7 shows that the oxidized ACF exhibited the largest MTBE adsorption capacity (by a factor of about 5 to 6) when the solvent was cyclohexane, and the observation was reproducible for the two tested adsorbent doses. The improved performance of the oxidized ACF in cyclohexane can be explained by the preferential adsorption of MTBE on oxygen-containing functional groups that can serve as a hydrogen-bond donor such as carboxylic acid and (ph)enolic hydroxyl groups. In that case, hydrogen bonds can form between the hydrogen atoms of these surface groups and the ether-oxygen of MTBE. However, in the presence of water, hydrogen bonds will preferentially form between water and these surface groups. Consequently, the availability of specific adsorption sites, i.e. hydrogen-bond donor sites, for MTBE will decrease greatly in aqueous solution. However, the loss of such sites to water adsorption alone cannot explain why the MTBE adsorption capacity of oxidized ACFs in aqueous solution is lower than that of more hydrophobic ACFs with a smaller surface concentration of hydrogen-bond donor sites. It is plausible that hydrogen-bond donor sites become essentially unavailable to MTBE in aqueous solution and that MTBE adsorption therefore shifts from a site-specific hydrogen-bonding mechanism in cyclohexane to a non-specific dispersive mechanism in aqueous solution, where MTBE

adsorbs instead on the graphitic basal planes of the adsorbent. Hence, the lower MTBE adsorption capacity of oxidized adsorbents with a larger concentration of surface-oxygen groups results from the increased formation of water clusters that reduce access to the graphitic basal planes, reduce the interaction energy between MTBE and the adsorbent surface, and/or block pore entrances (Kaneko et al. 1989, Pendleton et al. 1997, Franz et al. 2000, Coughlin and Ezra 1968, Müller et al. 2000, Mahajan et al. 1980). Results for TCE adsorption from cyclohexane showed that surface chemistry effects were negligible (Figure 1.8), a result that suggests that TCE adsorption occurs by a non-specific dispersive mechanism. In aqueous solution, however, the TCE adsorption capacity of oxidized adsorbents was compromised because of the enhanced formation of water clusters as explained above for MTBE. The results and interpretations of the current study are consistent with those of a recent study by Franz et al. (2000) who investigated the adsorption of phenol, aniline, nitrobenzene, and benzoic acid from both water and cyclohexane. Overall, the above results as well as those by Franz et al. (2000) show that enhanced water adsorption on polar adsorbents negates the benefits of providing specific adsorption sites capable of forming hydrogen-bonds with a targeted adsorbate such as MTBE (this study), phenol, aniline, or benzoic acid (Franz et al. 2000).

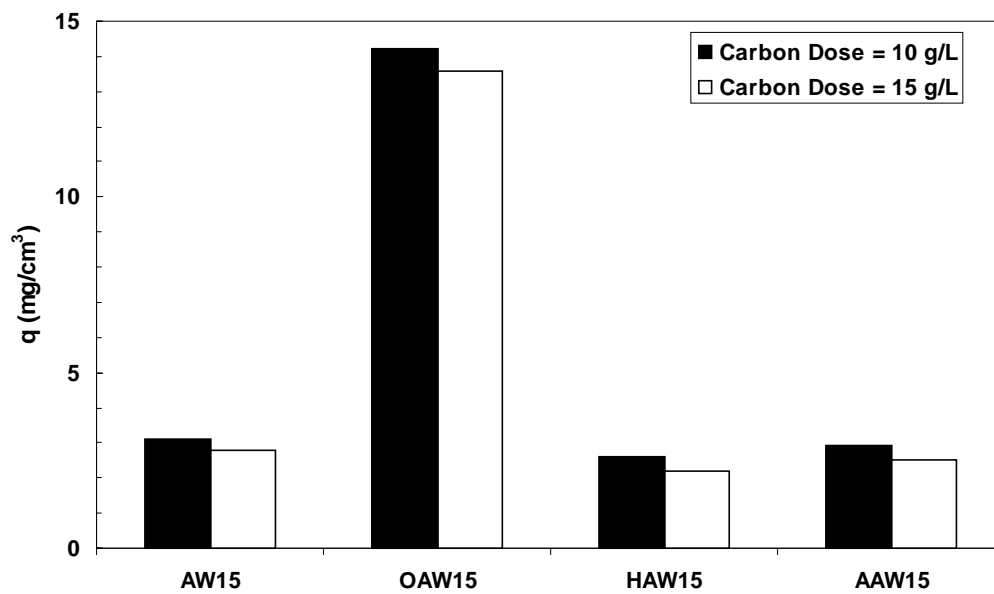


**Figure 1.7 Effect of chemical treatments on MTBE adsorption from cyclohexane. Solid-phase MTBE concentrations were normalized by the pore volume in the 8-11 Å width range.**

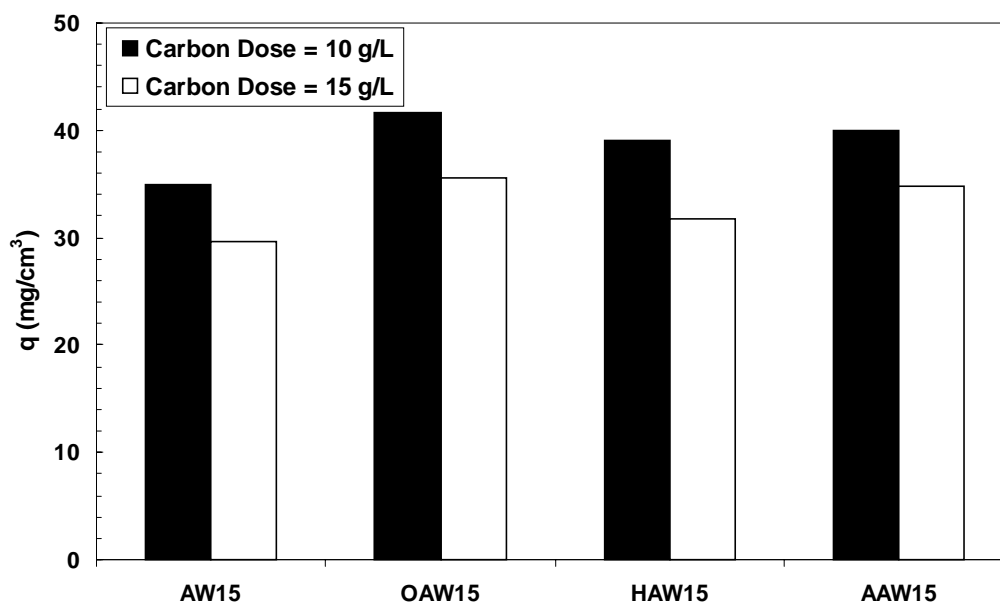


**Figure 1.8 Effect of chemical treatments on TCE adsorption from cyclohexane. Solid-phase TCE concentrations were normalized by the pore volume in the 7-10 Å width range.**

To determine the effects of adsorbent polarity on TCE and MTBE adsorption, micropollutant adsorption capacities were plotted against the sum of the oxygen and nitrogen contents (mmol/g) of each adsorbent as shown in Figures 1.9 and 1.10 for TCE and MTBE, respectively. To eliminate pore structure effects, equilibrium solid-phase concentrations at an equilibrium liquid-phase concentration of 50  $\mu\text{g/L}$  were normalized by the pore volume in the pore width range that controlled the adsorption of the targeted micropollutant (i.e. 7-10  $\text{\AA}$  for TCE, 8-11  $\text{\AA}$  for MTBE). Figure 1.9 illustrates that the TCE adsorption capacity decreased with increasing adsorbent polarity, and a similar trend was observed for MTBE (Figure 1.10). These results reiterate that hydrophobic adsorbents, i.e. activated carbons with a low oxygen and nitrogen content ( $< 2$  to  $3$  mmol/g), are most effective for the removal of both hydrophobic and hydrophilic adsorbates from aqueous solution. Figures 1.9 and 1.10 further illustrate that the trends established by the ACF matrix successfully predicted the adsorption behavior of the commercially available GACs.

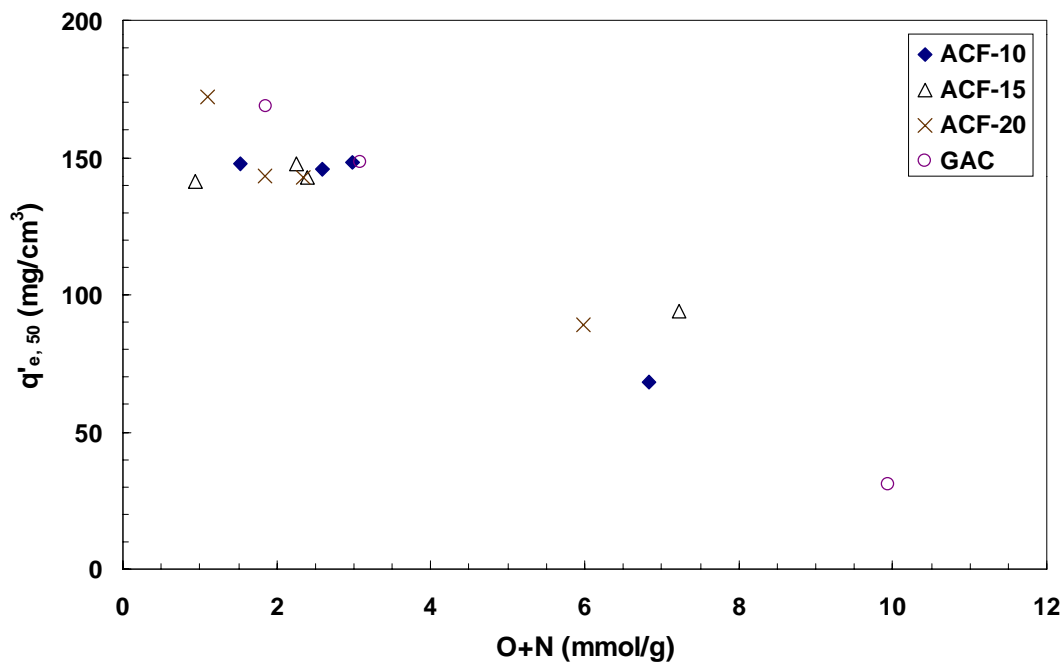


Figure 1.9 Effect of adsorbent hydrophobicity on TCE adsorption capacity

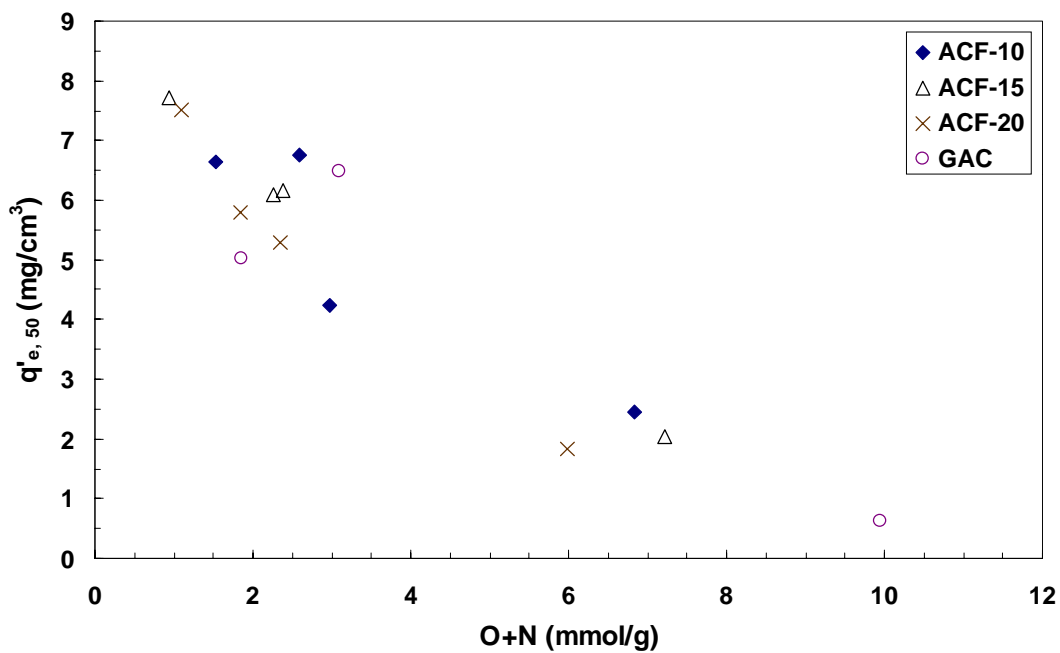


Figure 1.10 Effect of adsorbent hydrophobicity on MTBE adsorption capacity

## 1.5. CONCLUSIONS

To evaluate pore structure and surface chemistry effects on the adsorption of TCE and MTBE from aqueous solution, a matrix of activated carbon fibers (ACFs) with three activation levels and four surface chemistry levels was studied along with three commercially available GACs. From the relationships observed between the adsorbent characteristics and the micropollutant adsorption isotherm data in ultrapure water, the following conclusions were drawn:

- Regardless of the pore structure or surface chemistry, adsorbents always exhibited a larger adsorptive capacity for TCE than for MTBE, a result that is consistent with the greater aqueous solubility of MTBE.
- For carbons with similar surface chemistry, the pore volume of micropores with widths corresponding to about 1.3 to 1.8 times the kinetic diameter of the targeted adsorbate controlled the adsorption capacity. Consequently, relatively small changes in the micropore size distribution of an adsorbent (e.g. 7-11 Å widths in ACF 10 versus 9-13 Å widths in ACFs 15 and 20) can alter the effectiveness of an adsorbent for a given micropollutant. Similarly, small differences in the kinetic diameters among individual target adsorbates (e.g. 5.6 Å for TCE vs. 6.2 Å for MTBE) affect the choice of the most effective adsorbent.
- Adsorbent polarity, as expressed by the sum of the oxygen and nitrogen contents (mmol/g) has the potential to serve as a useful activated carbon selection criterion. As the polarity of a carbon increases, or the O+N content increases, the

micropollutant adsorption capacity decreases. This result is consistent with enhanced water adsorption on polar, oxygen-containing surface functional groups, which leads to the formation of water clusters that block micropollutant access to adsorption sites. Based on the results of this study, an effective adsorbent for the removal of organic contaminants from aqueous solution should have an O+N content of less than 2 to 3 mmol/g.

## **CHAPTER 2. EFFECTS OF ACTIVATED CARBON SURFACE CHEMISTRY AND PORE STRUCTURE ON THE ADSORPTION OF ORGANIC CONTAMINANTS – ISOTHERMS IN THE PRESENCE OF NATURAL ORGANIC MATTER**

### **2.1 INTRODUCTION**

Activated carbon is frequently used for the control of objectionable chemicals from drinking water including taste and odor causing compounds and trace organic contaminants. However, the optimization of activated carbon adsorption processes remains challenging because natural organic matter (NOM) in drinking water sources competes with the targeted micropollutants for adsorption sites. NOM is formed as animal and vegetable material breaks down, and its character varies both seasonally and geographically. The components that make up a particular NOM vary in molecular size and weight as well as in hydrophobicity and charge, and all of these factors affect NOM adsorbability on activated carbon. Furthermore, adsorbent pore structure and surface chemistry control the adsorption of both micropollutants and NOM. A better understanding of the adsorbent and adsorbate characteristics that affect the competition between NOM and organic micropollutants is therefore needed to aid drinking water treatment professionals in selecting the most appropriate adsorbent for a given treatment objective.

## **2.2 BACKGROUND**

### *2.2.1 NOM Adsorption*

NOM, which is ubiquitous in drinking water sources, is formed from the breakdown of animal and vegetable material. The molecular weight of NOM can vary from <500 to >30,000 Daltons. However, high performance size exclusion chromatography (HPSEC) results show that aquatic NOM has a relatively low molecular weight of around 1,000–3,000 Daltons (Pelekani and Snoeyink 1999, Pelekani et al. 1999, Ebie et al. 2001). According to Schlautmann and Morgan (1994), the radius of gyration of Suwannee River fulvic acid was 0.7 nm and the radius of gyration of Suwannee River humic acid was 1.1 nm. At the pH of most natural waters, NOM carries a negative charge that arises from the presence of carboxylic acid and phenolic groups (Perdue et al. 1980, Perdue et al. 1983, Perdue et al. 1984).

Numerous researchers have correlated the adsorption of NOM with the pore structure of activated carbons (e.g. Lee et al. 1981, Summers and Roberts 1988, Ebie et al. 1995, Newcombe et al. 1997, Pelekani and Snoeyink 1999, Ebie et al. 2001). In general, the results of these studies showed that humic substances adsorb in mesopores and large micropores. Pelekani and Snoeyink (1999) showed that the adsorption of humic substances in a non-fractionated groundwater (MW<3000) was negligible on ACFs that contained pores that were primarily smaller than 0.8 nm in width. In contrast, all size ranges of the same NOM adsorbed on an ACF that contained pores in the entire micropore range. Newcombe et al. (1997) showed that the adsorption of the 500-3000

MW fraction of NOM correlated best with the cumulative volume of pores with pore widths ranging from 0.8 to 50 nm, while the adsorption of the >3000 MW fraction correlated well with the mesopore volume. Ebie et al. (1995) showed that the adsorption of non-fractionated humic and fulvic acids with molecular weights between about 500 and 50,000 daltons correlated best with the volume of pores with pore widths in the 3 to 10 nm range.

Given that NOM carries a negative surface charge at neutral pH, electrostatic interactions can play an important role in the adsorption of NOM. If the carbon surface has a positive charge, attractive electrostatic forces arise between the NOM and the carbon surface. Repulsive electrostatic forces can occur in the following situations: (1) when the carbon surface is negatively charged, (2) when NOM molecules interact at high surface concentrations, and/or (3) when adsorbed NOM rendered the surface negatively charged (Newcombe et al. 1999). At pH values typically encountered in drinking water treatment, activated carbon surfaces can be positively or negatively charged or neutral depending on the base material and activation process. In aqueous suspensions, acidic activated carbons, i.e. carbons containing carboxylic acid and phenolic groups, carry a negative surface charge at neutral pH (Mattson and Mark 1971) while basic carbons carry a positive surface charge. In general, chemically activated wood-based carbons have acidic or neutral surfaces while coconut-based and coal-based carbons tend to have neutral or basic surfaces (Newcombe and Drikas 1997, Bjelopavic et al. 1999). Furthermore, the charge of the carbon surface becomes more negative as NOM adsorbs (Newcombe et al.

1993, Morris and Newcombe 1993). Furthermore, the type of electrostatic interaction depends on the surface concentration. At low surface concentrations, electrostatic interactions mainly take place between the surface and the adsorbate (Muller et al. 1985). As the surface concentration increases, the results of Muller et al. (1985) suggest that the charge of the NOM begins to control the surface charge and interactions occur between adsorbed NOM as well as between adsorbed NOM and NOM in solution.

Newcombe and Drikas (1997) studied the electrostatic and non-electrostatic effects on adsorption of NOM onto two activated carbons. One carbon was an almost neutral coal-based carbon with the majority of its pores in the micropore range. The other carbon was an acidic wood-based carbon with both micropores and mesopores. At pH 3, electrostatic effects were minimized because acidic functional groups on the adsorbent surface and the NOM were protonated. In that case, the mesoporous wood-based carbon adsorbed more NOM. Once NOM adsorption was normalized by the volume of pores in the secondary micropore and mesopore range, the two carbons performed comparably. As the pH was increased, the coal-based carbon performed better when the two carbons were compared on the basis of mass adsorbed per  $\text{cm}^3$  of available pore volume, a result that was explained by more favorable electrostatic interactions between NOM and the less acidic coal-based carbon surface. However, the wood-based carbon performed better when the two carbons were compared on the basis of mass adsorbed per gram of activated carbon. Therefore, pore size distribution effects outweighed electrostatic effects for the carbons and NOM evaluated by Newcombe and Drikas (1997).

Karanfil et al. (1999) studied the adsorption of NOM on surface-modified and as-received carbons. The carbons that underwent chemical modification were a chemically activated wood-based carbon and a thermally activated coal-based carbon. The carbons were acid-washed with 2N acid to remove ash components and alkaline impurities. Subsequently, the carbons were heat-treated to remove oxygen-containing functionalities. Upon heating, oxygen is released from carbon surfaces in the form of CO<sub>2</sub>, CO, and H<sub>2</sub>O (Puri and Bansal 1964). Puri (1966) showed that the evolution of CO<sub>2</sub> corresponded to a reduction in surface acidity that is most commonly attributed to carboxyl functional groups (Bansal et al. 1988). Next, the heat-treated carbons were oxidized at 70°C for either 2 hours or 9 hours to increase surface acidity. Finally, a portion of the oxidized carbons were again heat treated to remove strongly acidic and other CO<sub>2</sub> evolving groups. NOM adsorption was dependent on raw material type, activation conditions, and surface treatment. For example, NOM uptake decreased upon oxidation of the coal-based carbon. Given that surface oxidation increased the acidity of the carbon, but had a negligible effect on pore structure, repulsive electrostatic interactions between the negatively charged activated carbon surface and the negatively charged NOM may have explained the decreased NOM adsorption upon surface oxidation. Furthermore, water adsorption on polar surface groups may have decreased the accessible pore volume for NOM. Subsequent heat treatment restored some of the NOM adsorption capacity. For the wood-based carbon, however, similar surface treatments had no effect on NOM uptake. Karanfil et al. (1999) suggested that differences in the surface chemistry may have

existed among the adsorbents that were not characterized by the methods used in their research.

### *2.2.2 Micropollutant Adsorption in the presence of NOM*

It has been widely observed that the capacity of activated carbons for organic micropollutants is lowered in the presence of NOM (Najm et al. 1991a, Qi et al. 1994, Narbaitz and Benedek 1994, Chen et al. 1997, Newcombe et al. 1997, Knappe et al. 1998, Pelekani and Snoeyink 1999, Ebie et al. 2001). The concentration of NOM in drinking water is about 3 to 6 orders of magnitude larger than the concentration of most micropollutants, and the degree of competition is dependent on the initial concentration of the micropollutant (Najm et al. 1991a, Narbaitz and Benedek 1994, Knappe et al. 1998, Pelekani and Snoeyink 1999). The nature of the NOM (e.g. chemical composition, adsorbability) also affects the extent of competition (Bernazeau et al. 1996, Müller et al. 1996). Several studies have explored the effects of activated carbon pore structure on the adsorption of micropollutants in the presence of competing organic matter (Newcombe et al. 1997, Pelekani and Snoeyink 2000, Pelekani and Snoeyink 2001, Ebie et al. 2001). However, to date, the effect of activated carbon surface chemistry on the adsorption of micropollutants in the presence of NOM remains largely unexplored.

Newcombe et al. (1997) studied the adsorption of 2-methylisoborneol (MIB) in the presence of NOM. Experiments with NOM fractions showed that the smallest size fraction ( $MW < 500$ ) resulted in a greater reduction in MIB adsorption than larger size

fractions, indicating that NOM molecules in a size range similar to that of the target compound directly compete with the target compound for adsorption sites. This observation is consistent with the findings of other researchers who determined that smaller NOM molecules are adsorbed preferentially on activated carbons because a large percentage of internal surface area of activated carbon is located in the micropore region that cannot be accessed by larger NOM molecules (Summers and Roberts 1988, Kilduff et al. 1996).

Pelekani and Snoeyink (1999) examined the role of pore size in the adsorption of atrazine from natural water using a series of ACFs. From these experiments, the two main mechanisms in competitive adsorption were determined to be pore blockage and direct competition, and the dominating mechanism was dependent on the pore size distribution. If pores were large enough to admit the micropollutant but not large enough to admit NOM, then pore blockage was the dominant competition mechanism. However, if pores were large enough to admit both NOM and the micropollutant, then direct competition became the dominant competition mechanism. Furthermore, the data showed that pore blockage by NOM as a result of size exclusion more severely reduced the micropollutant capacity than direct competition between NOM and atrazine for adsorption sites. Pelekani and Snoeyink (1999) therefore suggested that adsorbents with a broader pore size distribution in the micropore range reduce pore blockage effects and thus the negative impact of NOM on micropollutant adsorption. In a study looking at the adsorption of four different micropollutants from natural water by three activated carbons, Ebie et al. (2001)

also concluded that the extent of competition was lessened when the pore size distribution was broadened and there was a larger volume percentage of pores greater than 30 Å.

To better understand the role of pore size distribution on competitive adsorption, Pelekani and Snoeyink (2000) performed a series of experiments that examined the adsorption of atrazine in the presence of methylene blue (MB), a dye with a molecular size similar to that of atrazine. Again, ACFs were used to elucidate pore size effects. Because the adsorbates were similar in size, direct competition was observed. By increasing the pore volume and shifting the pore size distribution from the primary micropores ( $< 8$  Å) to the secondary micropores (8–20 Å), the effect of competition on atrazine adsorption was lessened because more adsorption sites were available in the pore size region accessible to both atrazine and MB. Furthermore, atrazine could more easily displace MB in the secondary micropores because the adsorption potential was smaller. A similar study was performed by Pelekani and Snoeyink (2001) in which MB was replaced with congo red (CR), a dye that is larger in size than atrazine. For an ACF that contained principally primary micropores ( $< 8$  Å), both pore blockage and pore constriction occurred, the former lowering the atrazine adsorption capacity and the latter slowing the kinetics of adsorption. Once again, by increasing the pore volume and by shifting the micropore distribution towards the secondary micropores, the effect of NOM competition was lessened. As the pore volume shifted to small secondary micropores, the CR competition mechanism was primarily one of pore constriction that reduced adsorption kinetics but

not adsorption capacity. In the presence of a significant secondary micropore volume (8-20 Å), atrazine capacity reductions as a result of direct site competition between atrazine and CR started to become important while reductions in adsorption kinetics as a result of pore constriction were no longer observed. Pelekani and Snoeyink (2001) also proposed that further activation of ACFs yielded a branched pore structure, in which small micropores branch off from mesopores or larger micropores. In this case, both direct competition in mesopores and large micropores and pore blockage at the entrance of small micropores were observed.

### *2.2.3 Modeling of Adsorption*

Over the last few decades, many useful design tools involving bench-scale tests and mathematical models have been developed to predict the removal of a target compound in a given natural water by a given activated carbon (Najm et al. 1991a, Knappe et al. 1998, Kilduff and Wigton 1999, Ebie et al. 2001). These design tools are based, at least in part, on the ideal adsorbed solution theory (IAST). This theory is capable of modeling adsorption in a multi-solute system given the single-solute isotherm parameters, such as the Freundlich parameters ( $K$  and  $1/n$ ) of each solute, as well as the initial solute concentrations ( $C_0$ ). Underlying assumptions of the IAST include that adsorption sites are equally accessible to all solutes and that adsorption is reversible. While the IAST successfully describes competitive adsorption equilibria in multi-solute systems containing uniquely identifiable compounds such as SOCs, the main difficulty enters when heterogeneous NOM is included as a competing adsorbate.

Kilduff and Wigton (1999) attempted to model the adsorption of TCE in the presence of humic acid. Single-solute TCE adsorption isotherms were modeled using the Langmuir-Freundlich model, and NOM isotherms were modeled by using the Freundlich parameters describing the DOC isotherm for the low-molecular weight humic fraction (< 3000 Daltons). However, the IAST prediction overestimated the solid-phase TCE concentration at high liquid-phase concentrations and underestimated the solid-phase TCE concentration at low liquid-phase concentrations. Kilduff and Wigton (1999) suggested that the inaccurate predictions were caused by the assumption that all sites are equally accessible. The model was therefore adjusted to account for (1) adsorption sites that were accessible to TCE molecules but not to humic molecules and (2) a reduction in effective surface area as a result of NOM adsorption that may have led to pore blockage. These adjustments led to a model that described the data sets well.

Ebie et al. (2001) attempted to model the adsorption of four agricultural chemicals in the presence of NOM. The Freundlich fits of the bulk DOC isotherms were used to model the competing NOM. However, the IAST predictions did not describe the experimental data well. By adding a component to the model to account for the change in capacity due to pore blockage, the SOC isotherms in the presence of NOM could be successfully predicted.

However, pore blockage may not be the only reason why parameters obtained from bulk DOC isotherms do not appropriately describe the competing NOM in the IAST. Studies have shown that the low molecular weight fraction of NOM is preferably adsorbed (Newcombe 1997, Kilduff et al. 1996). Newcombe et al. (1997) proposed that only a very low concentration of low molecular weight (<500 Daltons) NOM is necessary to lower the MIB adsorption capacity via direct competition. Therefore, it is possible that a small fraction of the NOM directly competes with SOCs for adsorption sites, and that the initial concentration and isotherm parameters of this NOM fraction differ greatly from those describing the bulk DOC. Furthermore, current fractionation and analytical techniques for NOM characterization have not been able to identify that fraction of the NOM that competes directly with micropollutants for adsorption sites. For example, a study of three natural waters by Bolto et al. (1999) showed that a DOC fraction always existed that did not absorb light in the UV range. Therefore, a fraction of the low molecular weight NOM may not be detected by UV detectors used to conduct HPSEC.

Another approach for modeling the competing NOM is to approximate it with several fictive components of varying initial concentrations and  $K$  and  $1/n$  values (Sontheimer, Crittenden, and Summers 1988). For this approach, one isotherm with the target organic compound in organic-free water and one isotherm with the target organic compound in the natural water must be conducted. The resulting data along with the IAST were used to determine the  $C_0$ ,  $K$ , and  $1/n$  for each of the fictive components. However, the

determination of the fictive component parameters was difficult and required substantial computer programming skills.

Alternatively, Najm et al. (1991a) proposed that the NOM be modeled as a single component, the equivalent background compound (EBC). This approach also requires one isotherm with the target organic compound in organic-free water and one isotherm with the target organic compound in the natural water. However, substantially less computer programming is required since the competing NOM is modeled as one compound. Several studies found this approach to be successful (Najm et al. 1991a, Knappe et al. 1998, Pelekani and Snoeyink 1999, Graham et al. 2000). Graham et al. (2000) used the EBC approach to model the adsorption of MIB and geosmin from four natural waters. When the  $K$ ,  $1/n$ , and molecular weight of the EBC were kept constant and the initial concentration was allowed to vary for each water, they were able to model all four waters using a single EBC. Furthermore, for three of the waters, the initial concentration of the EBC was approximately 0.45% of the total initial TOC concentration. This result supports the theory that only a small portion of the NOM directly competes with the target compound for adsorption sites.

For trace organic contaminant adsorption in the presence of NOM, Knappe et al. (1998) observed a direct proportionality between the PAC adsorption capacity and the initial micropollutant concentration at a given carbon dose. Using the EBC modeling approach, Knappe et al. (1998) showed that this observation was consistent with the IAST, provided

that the SOC was present in trace amounts. Consequently, mathematical models are not needed to predict the initial concentration dependence of micropollutant isotherms in natural water, provided that a micropollutant isotherm experiment was conducted at a sufficiently low initial concentration in the natural water of interest.

#### *2.2.4 Research Objective*

The overall purpose of the study described in this chapter was to determine the effects of activated carbon surface chemistry and pore size distribution on the adsorption of MTBE and TCE in the presence of NOM. To systematically study the effects of activated carbon pore structure and surface chemistry on adsorption, a matrix of activated carbon fibers (ACFs) was examined. The ACF matrix contained three activation levels and four surface chemistry levels (acid-washed, oxidized, hydrogen-treated, and ammonia-treated). In addition, three commercially available GACs were examined: bituminous coal-based F-600 (Calgon), coconut shell-based G-219 (Pica), and wood-based Picazine (Pica). The target adsorbates chosen were the relatively polar methyl tertiary-butyl ether (MTBE) and the relatively nonpolar trichloroethene (TCE). Physical and chemical adsorbent characterization included pore structure and surface area determinations by ultra-low pressure N<sub>2</sub> adsorption, point of zero charge (PZC) determinations by mass titrations, and elemental analyses. Adsorption capacities were determined from single-solute MTBE and TCE isotherms, NOM isotherms, and MTBE and TCE isotherms in the presence of NOM. All isotherms involving NOM were conducted with Sacramento-San Joaquin Delta Water (Concord, CA).

## 2.3 MATERIALS AND METHODS

### 2.3.1 Solvents

Single-solute isotherm experiments were conducted in ultrapure laboratory water (tap water treated by reverse osmosis, ion exchange, and granular activated carbon adsorption, resistance  $\geq 14.85$  M $\Omega$ /cm). Ultrapure water was amended with a 1 mM phosphate buffer (0.5mM Na<sub>2</sub>HPO<sub>4</sub>•H<sub>2</sub>O and 0.5 mM NaH<sub>2</sub>PO<sub>4</sub>) to maintain a pH of 7.2. Furthermore, 100 mg/L sodium azide were added to eliminate aerobic biological activity. NOM adsorption and micropollutant adsorption in the presence of NOM were evaluated with Sacramento-San Joaquin Delta Water (SJDW). The water was sampled at the intake of the Concord, CA, water treatment plant (Contra Costa Water District), filled into 55-gallon stainless steel drums, and immediately shipped by 3-day freight service to the Environmental Engineering Laboratory at NCSU. Upon arrival, the water was preserved with 100 mg/L sodium azide. Prior to use in isotherm experiments, the water was vacuum filtered through a 0.45- $\mu$ m nylon membrane filter (Magna-R, MSI, Westboro, MA) that was placed in a 47 mm glass microanalysis filter holder (Fisher Scientific, Pittsburgh, PA). The DOC of SJDW was 4.0 mg/L, the pH was 7.9, the total alkalinity was 53 mg/L as CaCO<sub>3</sub>, and the total hardness was 72 mg/L as CaCO<sub>3</sub>.

### 2.3.2. Adsorbates (*Micropollutant probes*)

TCE and MTBE, two common drinking water contaminants, served as probe molecules for the assessment of adsorbate polarity effects. Adsorbate properties have been described in Chapter 1. MTBE and TCE stock solutions were prepared at a concentration

of approximately 265 mg/L. The MTBE solution was prepared in ultrapure water and the TCE stock solution was prepared in methanol. The concentration of the TCE stock solution assured that methanol concentrations in isotherm tests remained below 0.1%, a level at which no co-solvent effects were observed in prior studies (Kilduff et al. 1998).

### *2.3.3 Adsorbents*

Three activated carbon fiber samples (ACF-10, ACF-15, and ACF-20) were chemically modified by acid-washing (AW), oxidation (OAW), hydrogen treatment (HAW), and ammonia treatment (AAW) as described in Chapter 1. In addition, tests were conducted with three commercially available GACs: coal-based F-600 (Calgon), coconut-based G-219 (Pica), and wood-based Picazine (Pica). Physical and chemical adsorbent characteristics were summarized in Chapter 1.

### *2.3.4 Isotherms*

Isotherms in ultrapure water were carried out as described in Chapter 1. For NOM isotherms, adsorbent doses between 10 and 2000 mg/L were utilized. Adsorbents were transferred into 4 oz, 8 oz, or 16 oz amber glass bottles depending on the carbon dose. The bottles were subsequently filled with 100 mL (4 oz bottles), 200 mL (8 oz bottles), or 400 mL (16 oz bottles) of SJDW and capped. A mixing time of 2 weeks in a rotary tumbler was sufficient to reach adsorption equilibrium as determined by kinetic tests. Upon equilibration, samples were filtered through 0.22  $\mu\text{m}$  nylon membrane filters (Magna-R, MSI, Westboro, MA) that were placed in a 25 mm stainless steel syringe filter

holder (Fisher, Pittsburgh, PA). The filters were soaked overnight in organic-free water prior to use. DOC samples were analyzed using a Shimadzu TOC-5000A TOC analyzer (Columbia, MD). All samples were acidified with 1.0 N HCl and sparged with air for 4 minutes to measure non-purgeable organic carbon (NPOC).

For micropollutant isotherms in natural water, adsorbent doses between 2 and 5500 mg/L were utilized. Adsorbents were placed into brown glass bottles that were subsequently filled to the neck with SJDW. Immediately after the addition of SJDW, TCE or MTBE stock solution was added with a constant rate syringe (CR-700, Hamilton, Reno, NV) to yield an initial concentration of approximately 100 µg/L. Once the micropollutant was added, the bottle was topped off immediately with SJDW to create headspace-free conditions and capped using PTFE-faced silicon septa and open-top closures. A mixing time of 4 weeks in a rotary tumbler was sufficient to reach adsorption equilibrium, and micropollutant losses were not observed in blanks containing no carbon over that time period. Upon equilibration, adsorbents were separated from the liquid by sedimentation (ACFs) or filtration through 0.45 µm filters (pulverized GACs), and remaining liquid phase concentrations were measured by purge and trap gas chromatography (GC) and flame ionization detection (FID).

### *2.3.5 Mathematical Modeling*

To model the DOC isotherms, dose-normalized isotherms were described by the Freundlich equation [ $q_e = K(C_e/D)^{1/n}$ ], where  $q_e$  and  $C_e$  are the equilibrium solid-phase and

liquid-phase concentrations, respectively, and  $D$  is the carbon dose.  $K$  and  $1/n$  are the Freundlich isotherm parameters, which were determined by performing a linear regression on the log-transformed experimental data. Competitive adsorption isotherms were modeled as a bi-solute system using the ideal adsorbed solution theory (IAST), where the two adsorbates were TCE or MTBE and a hypothetical equivalent background compound (EBC) that described the competing fraction of the NOM (Najm et al. 1991). The  $K$  and  $1/n$  values for single-solute TCE and MTBE isotherms are shown in Chapter 1. The initial concentration and Freundlich parameters,  $K$  and  $1/n$ , for the EBC were determined by minimization of error between the experimental micropollutant isotherm data in the presence of NOM and the values predicted by the IAST.

## **2.4 RESULTS AND DISCUSSION**

### *2.4.1 NOM adsorption*

Figure 2.1 depicts DOC isotherms for acid-washed ACF samples. As shown in Figure 2.1, AW10 adsorbed negligible quantities of DOC. Given the narrow pore sizes of AW10 (primarily 7-11 Å), size exclusion effects can explain the lack of DOC adsorption. In contrast, AW15 and AW20 exhibited larger DOC adsorption capacities, a result that is consistent with the presence of larger pores (dominant pore widths of AW15 and AW20: 9-13 Å). Figure 2.2 shows the dose-normalized isotherms for the acid-washed ACF samples as well as the best fits of the Freundlich model to the experimental data. Figure 2.2 shows that the dose-normalized data are well described by the Freundlich model. Consequently, Freundlich  $K$ -values can be used to compare DOC adsorption capacities of

the ACFs. As summarized in Table 2.1, AW10 had a significantly lower DOC adsorption capacity than AW15 and AW20.

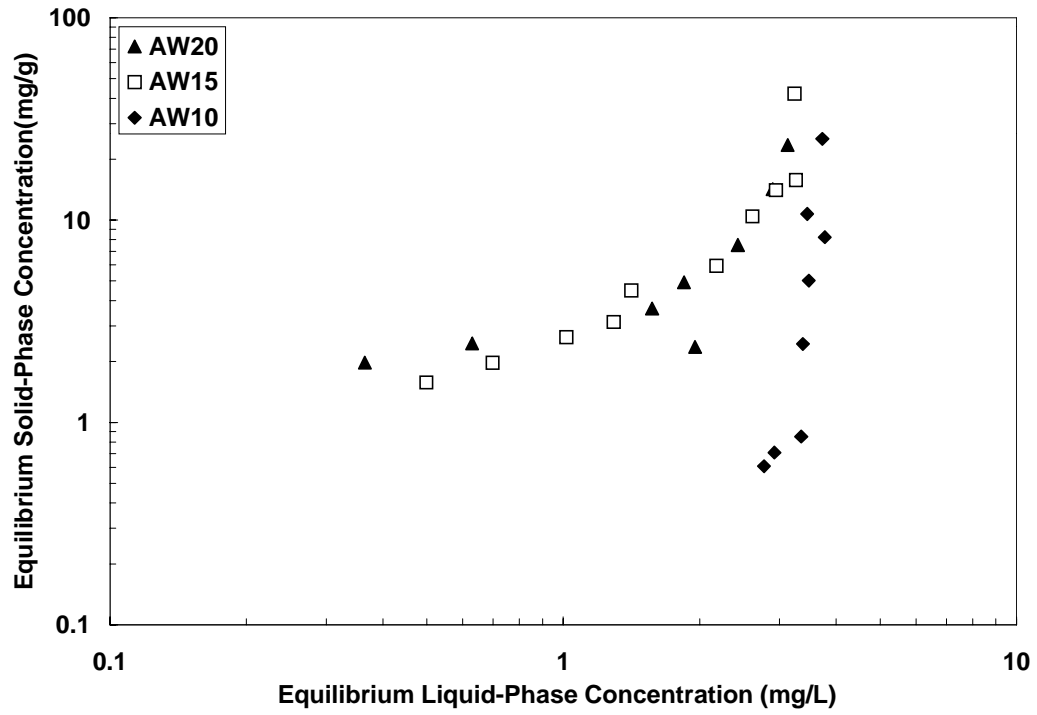
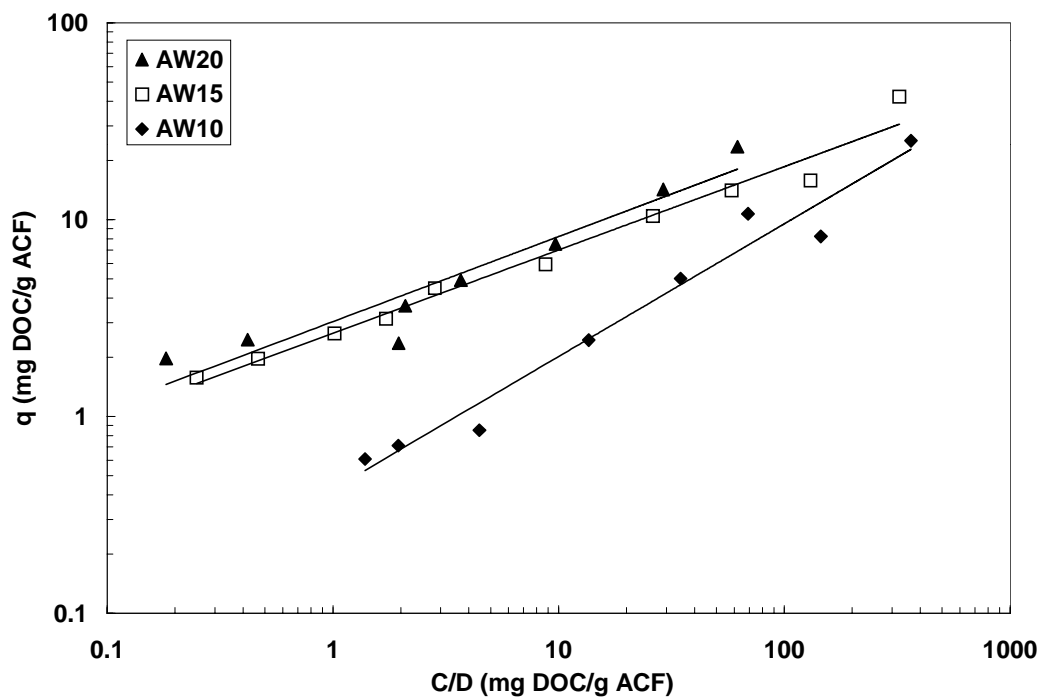


Figure 2.1 DOC isotherms on acid-washed ACF samples.



**Figure 2.2 Dose-normalized DOC isotherms on acid-washed ACF samples.**

Comparing Freundlich K-values between AW10, AW15, and AW20, Table 2.1 shows that the DOC adsorption capacity of AW15 was approximately 6 times larger than that of AW10, depending on the type of treatment the ACFs received. Furthermore, the DOC adsorption capacity of AW20 was approximately 7 times larger than that of AW10.

**Table 2.1 Pore structure effects on Freundlich parameters for dose-normalized DOC isotherms on acid-washed ACFs.**

Carbon	K in (mg/g) <sup>1-1/n</sup> Average (Lower; Upper)	1/n Average (Lower; Upper)
AW10	0.427 (0.278; 0.656)	0.674 (0.553; 0.796)
AW15	2.65 (2.27; 3.09)	0.423 (0.372; 0.474)
AW20	3.03 (2.23; 4.12)	0.432 (0.295; 0.569)

Correlations between Freundlich K-values and ACF pore volumes in a given size range showed that DOC adsorption occurred primarily in pores with pore widths in the 11 to 500 Å range (Figure 2.3). The observation that DOC adsorption occurs in large micropores and mesopores is consistent with the results of prior studies that investigated the adsorption of aquatic NOM (e.g. Ebie et al. 1995, Newcombe et al. 1997).

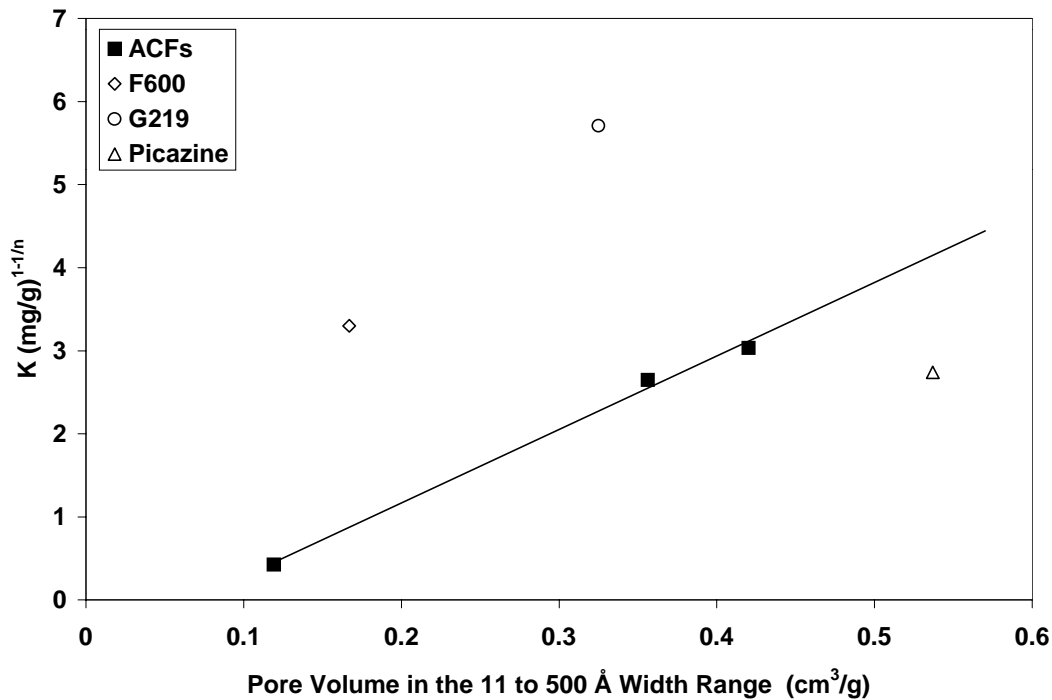


**Figure 2.3. Correlation between DOC adsorption capacity and pore volume in the 11-500 Å width range**

Figure 2.4 depicts the dose-normalized DOC isotherms for the three commercially available GACs. Furthermore, Table 2.2 shows the Freundlich K and 1/n values that resulted from the regression analyses along with their 95% confidence intervals. The results in Figure 2.4 and the Freundlich parameters in Table 2.2 indicate that NOM adsorption was similar on the three GACs despite their differences in pore structure and surface charge. To separate pore structure and surface chemistry effects, Freundlich K-values were plotted as a function of pore volume in the 11 to 500 Å pore width range; i.e. the pore volume in the pore size range in which NOM adsorption dominated on the ACFs (Figure 2.3). As illustrated in Figure 2.3, F600 and G219 GACs exhibited DOC adsorption capacities exceeding those of the ACFs at a given pore volume. Given that

both F600 and G219 are basic adsorbents ( $\text{pH}_{\text{pzc}} = 8.3$  and  $9.7$ , respectively), their positive surface charge may explain enhanced adsorption of negatively charged NOM as a result of attractive electrostatic forces. In contrast, NOM adsorption on Picazine GAC was lower than on the ACFs at a given pore volume. Given the acidic nature of Picazine GAC ( $\text{pH}_{\text{pzc}} = 2.1$ ), Picazine was negatively charged at  $\text{pH } 7.9$ , and electrostatic repulsion between NOM and the activated carbon surface can explain the decrease in NOM adsorption. Furthermore, enhanced water adsorption on this polar GAC may have reduced the pore volume available to NOM as a result of pore blockage or pore constriction.

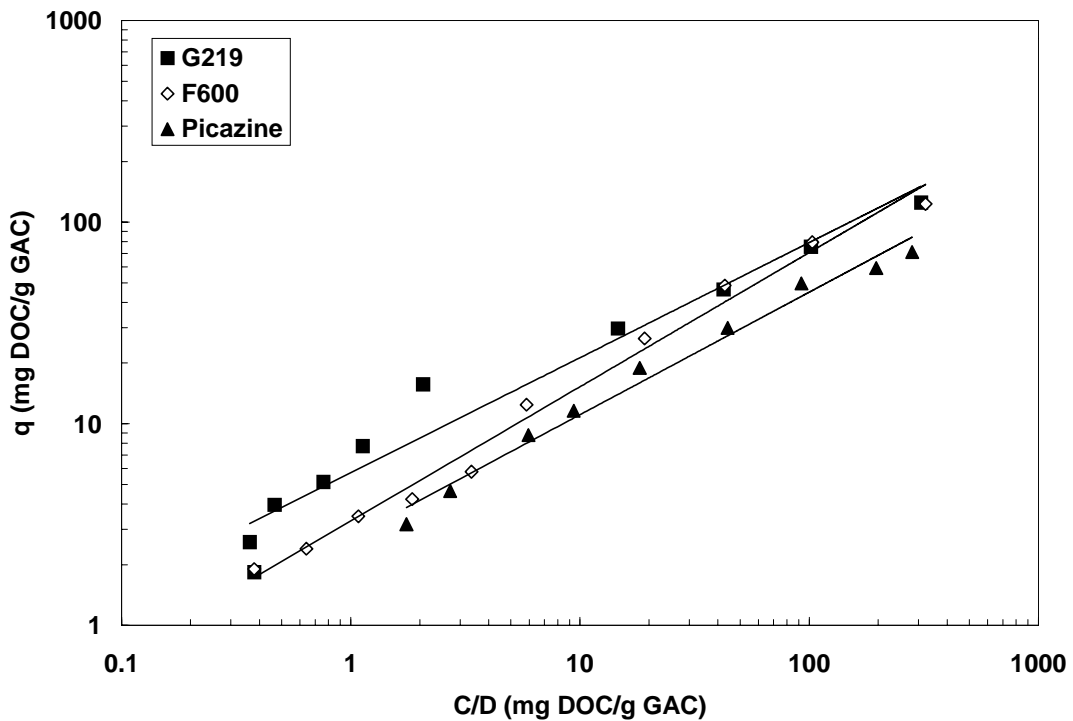


Figure 2.4. Dose-normalized DOC isotherms on GACs.

**Table 2.2 Freundlich parameters for dose-normalized DOC isotherms on GACs.**

Carbon	K in (mg/g) <sup>1-1/n</sup> Average (Lower; Upper)	1/n Average (Lower; Upper)
F600	3.30 (2.79; 3.89)	0.666 (0.608; 0.723)
G219	5.71 (4.32; 7.55)	0.571 (0.472; 0.671)
Picazine	2.74 (2.14; 3.50)	0.608 (0.539; 0.677)

#### 2.4.2 Micropollutant adsorption in the presence of NOM

To evaluate the effects of competition on micropollutant adsorption capacities, MTBE and TCE isotherm experiments were performed in SJDW. Figure 2.5 compares the single-solute TCE isotherm for AW20 to the TCE isotherm in SJDW. Figure 2.5 shows that competition between NOM and TCE lowered the TCE adsorption capacity of AW20 in SJDW. At an equilibrium liquid-phase concentration of 10 µg/L, the equilibrium solid-phase concentration of TCE decreased from 6.1 mg/g in ultrapure water to 2.6 mg/g in the presence of NOM. Thus, the presence of NOM decreased the TCE adsorption capacity of AW20 by about 58%. In the presence of NOM, TCE and MTBE adsorption capacities of all tested adsorbents decreased with capacity reductions ranging from 15-70%.

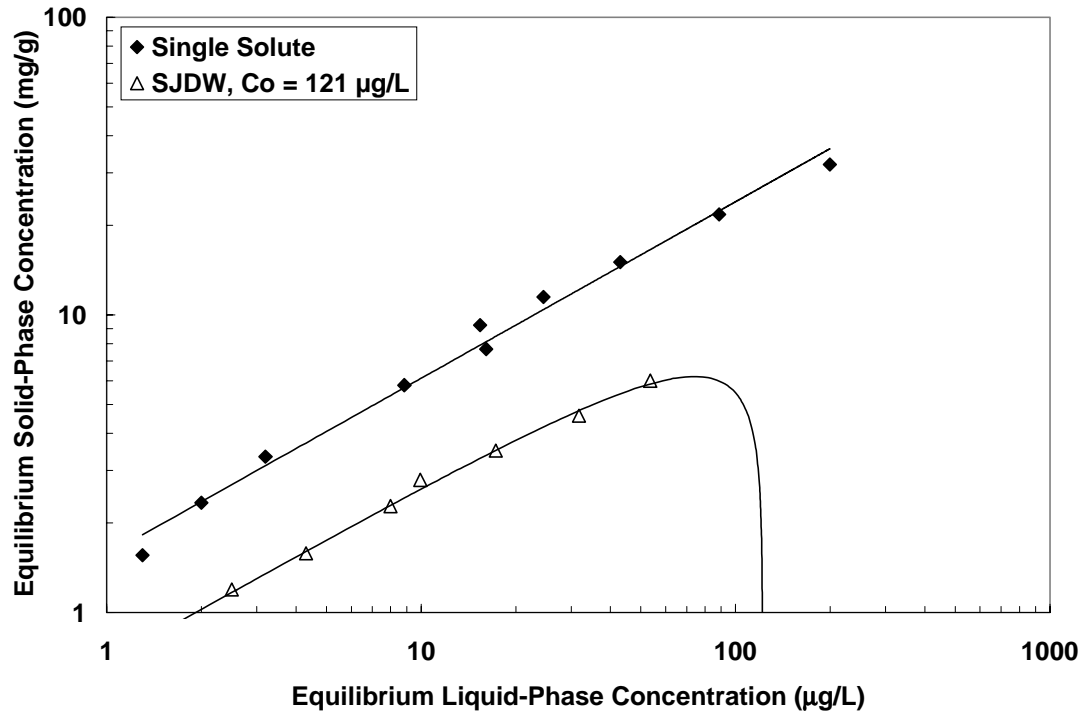


**Figure 2.5. Effect of NOM on TCE adsorption by AW20.**

To assess the effects of adsorbent pore structure on TCE adsorption from SJDW, Figure 2.6 compares TCE isotherms for the three acid-washed carbons in an alternative format, where the percentage of TCE remaining in solution at equilibrium is plotted as a function of the applied ACF dosage. The points on the graph are the experimental data, and the lines through each data set represent the best fits of the IAST model. According to Figure 2.6, AW10 performed the best while AW20 performed the worst at removing TCE from SJDW. Because AW10 had the lowest BET surface area, this result shows that BET surface area is a poor indicator of the ability of a carbon to remove organic micropollutants from natural water. For all four surface chemistry modifications, ACF10 performed significantly better than ACF15 and ACF20 for the removal of TCE from

natural water, a result that concurred with the trends described in Chapter 1 for ultrapure water.

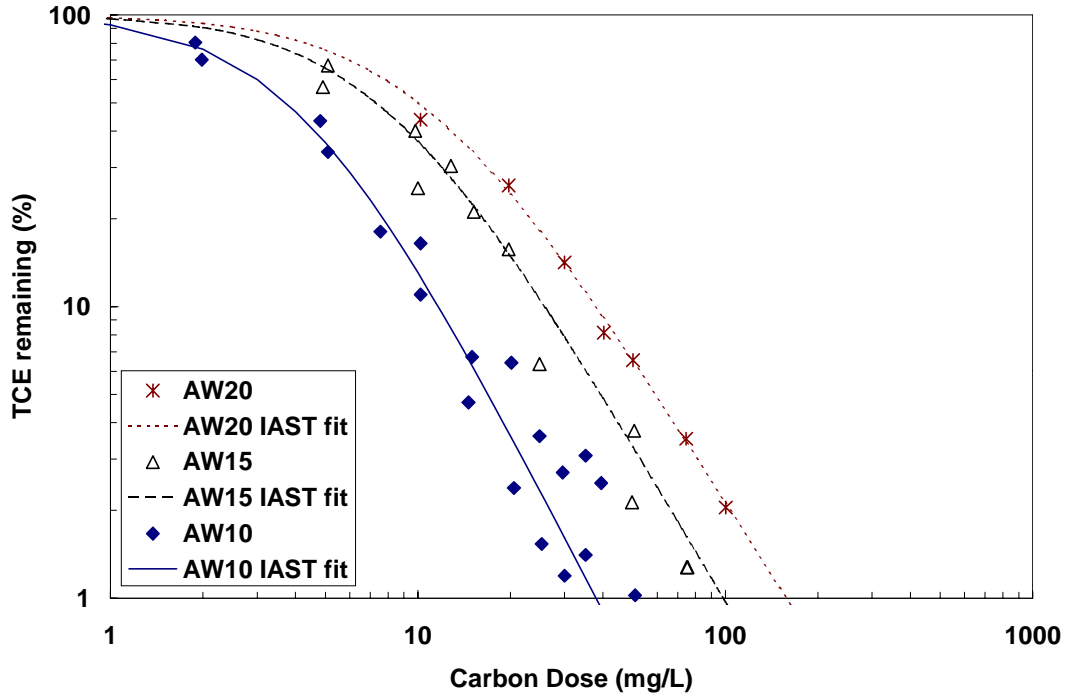


**Figure 2.6. Effect of ACF pore structure on TCE adsorption from SJDW (acid-washed ACFs).**

Figure 2.7 shows the effect of ACF pore structure on the removal of MTBE from SJDW for the acid-washed ACFs. For MTBE, AW10 performed significantly worse than AW15 and AW20. Furthermore, the IAST model could not describe the adsorption behavior of AW10 especially at intermediate adsorbent doses. Because the IAST model is only capable of modeling direct site competition, it is likely that NOM adsorption on AW10 caused pore blockage and/or pore constriction that prevented MTBE from accessing a portion of the pore structure over the tested 4-week equilibration time. One possible explanation is that NOM adsorbed at the openings of the pores thus narrowing the pore

entrances. Because MTBE approximates the shape of a tetrahedron, it would be more difficult for an MTBE molecule to enter this constricted pore entrance than for a flat TCE molecule. The ability of the IAST to describe the MTBE adsorption data on AW10 at the largest carbon doses suggests that the competition mechanism shifted from pore constriction/blockage at high NOM loadings to direct site competition at lower NOM loadings. Figure 2.8 shows MTBE isotherms collected in SJDW for HAW10 and OAW10. As was observed for AW10, the IAST model was also incapable of predicting the adsorption behavior of HAW10 and AAW10 (the latter data set is not shown for clarity). However, the model accurately predicted the behavior of OAW10. The most likely explanation for these results is that the acidic OAW10 carried a negative surface charge and that repulsive electrostatic forces decreased NOM adsorption at the pore entrances. The other surface chemistry modifications resulted in less negative or positive surface charges according to  $\text{pH}_{\text{pzc}}$  data presented in Table 1.3. Another possible explanation is that NOM condenses into a coiled form when the pH is low. Therefore, it is possible that the acidic nature of OAW10 caused the water near the carbon surface to be acidic and therefore, the smaller NOM molecules diffused deeper into the adsorbent pores and competed directly for adsorption sites. Even though pore constriction/blockage was not observed for OAW10, the oxidized carbon was not as effective for MTBE adsorption from SJDW, a result that illustrates that water adsorption in addition to NOM adsorption determines the effectiveness of an adsorbent for the removal of micropollutants from natural water.

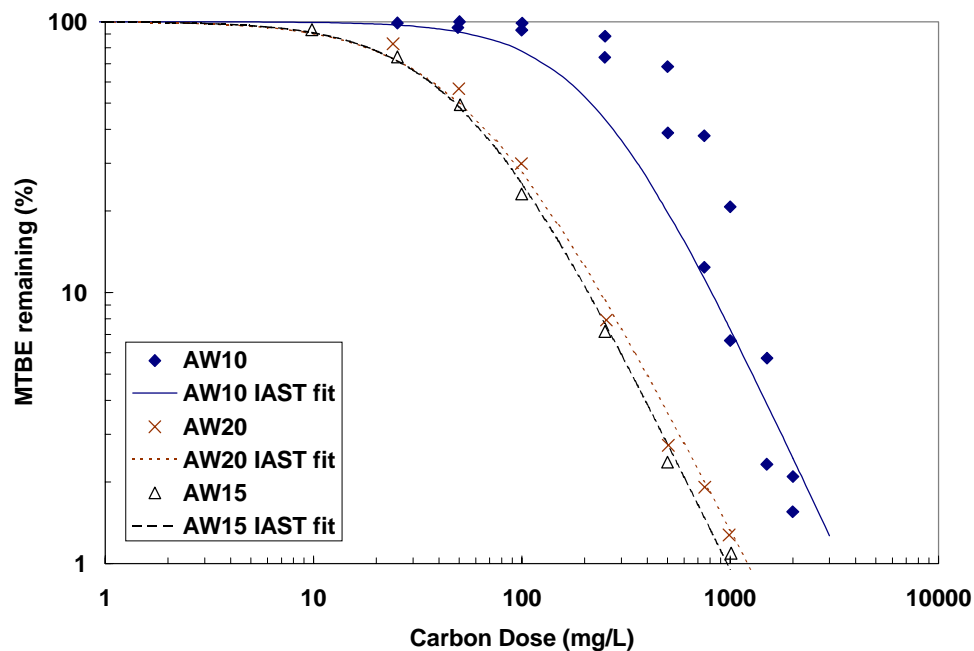


Figure 2.7. Effect of ACF pore structure on MTBE adsorption from SJDW (acid-washed ACFs).

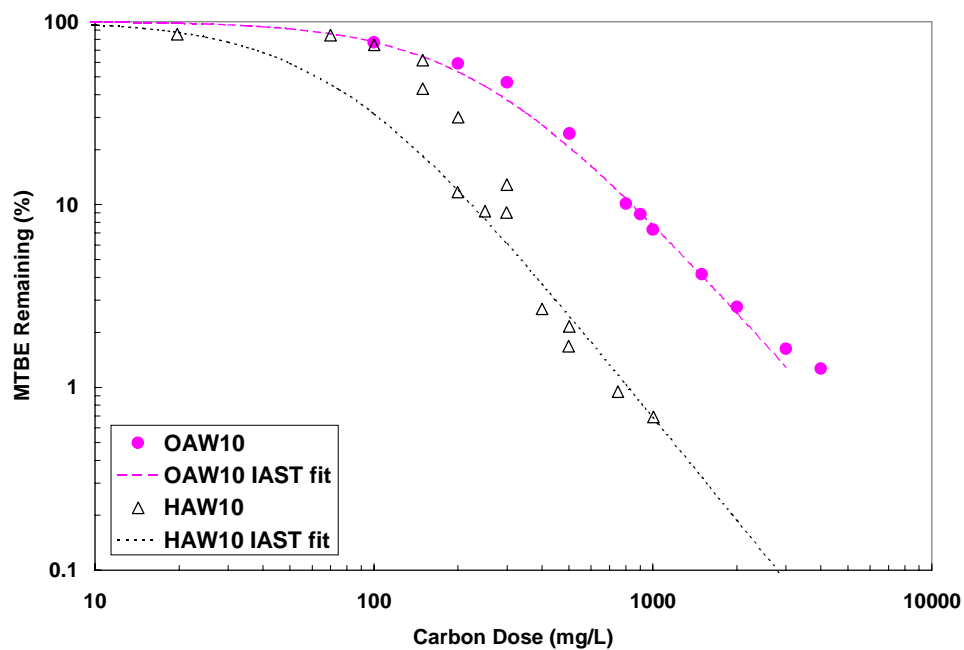
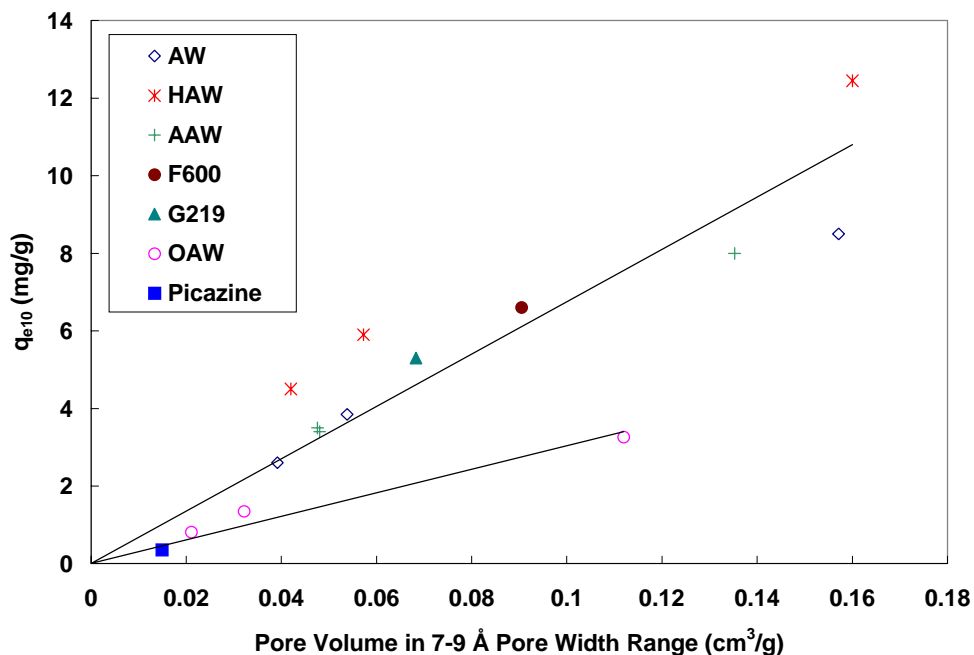


Figure 2.8. Effect of ACF surface chemistry modification on MTBE adsorption from SJDW (ACF10).

To assess in which pore sizes TCE and MTBE adsorb preferentially in the presence of NOM, adsorption capacities at an equilibrium liquid-phase concentration of 10  $\mu\text{g/L}$  ( $q_{e10}$ ) were correlated with ACF pore volumes in a given size range for each surface chemistry modification. Following a trial-and-error approach similar to that described by Ebie et al. (1995) and used for single-solute isotherms in Chapter 1, the results showed that TCE adsorption was controlled by pores in the 7-9  $\text{\AA}$  pore width range while MTBE adsorption was controlled by pores in the 8-11  $\text{\AA}$  pore width range. For TCE, Figure 2.9 illustrates that the available pore volume in the 7-9  $\text{\AA}$  pore width range primarily controlled TCE adsorption on the more hydrophobic ACFs (AW, HAW, AAW) although TCE adsorption capacities of hydrogen-treated ACFs were consistently larger than those of acid-washed and ammonia-treated ACFs. In Chapter 1 it was observed that single-solute TCE adsorption capacities correlated best with the volume of pores in the 7-10  $\text{\AA}$  pore width range. The most likely explanation for this change is that NOM out-competed TCE in pores with pore widths in the 9-10  $\text{\AA}$  range. Figure 2.9 also shows that the correlation established by the more hydrophobic ACFs predicted the adsorption capacity of the relatively hydrophobic F600 and G219 GACs reasonably well. For the oxidized ACFs, a separate correlation indicated that surface chemistry effects in addition to the availability of a suitable pore volume controlled TCE adsorption for ACFs with larger oxygen contents ( $\sim 10\%$ ). The correlation established by the oxidized ACFs appropriately predicted the adsorption capacity of Picazine GAC with an oxygen content of about 16%.



**Figure 2.9. Correlation between adsorption capacity and pore volume in the appropriate size range—TCE.**

As shown in Figure 2.10, a plot of MTBE adsorption capacity versus micropore volume in the 8-11 Å pore width range showed a trend similar to that for TCE, i.e. one correlation described MTBE adsorption on the more hydrophobic adsorbents while a separate correlation described MTBE adsorption on oxidized ACFs. Two hydrophobic adsorbents that deviated from the trend established by the hydrophobic ACFs were AW10 and AAW10, a result that was likely attributable to pore blockage effects. Given that MTBE adsorption occurred primarily in pores with pore widths in the 8-11 Å range and given that the dominant pore sizes of ACF10 were in the 7-11 Å width range, it appears reasonable that even a small quantity of adsorbed NOM caused pore blockage or constrictions in pore size that precluded MTBE access to adsorption sites. MTBE isotherms in SJDW were also poorly described by the IAST, a result that further suggests

that irreversible NOM adsorption led to pore blockage or constrictions that could not be described by the IAST. As a result of pore blockage, MTBE adsorption capacities ( $q_{e10}$ ) of AW10 and AAW10 in SJDW were 69 and 64% smaller, respectively, than in the absence of NOM. These capacity reductions were the most severe among the studied adsorbents and suggest that pore blockage is especially detrimental to the adsorption of micropollutants from natural water, a result that concurs with the findings of Pelekani and Snoeyink (1999). Although the results in Figure 2.8 suggest that NOM adsorption also caused some pore blockage on HAW10, reductions in MTBE adsorption capacity were not as severe as those observed for AW10 and AAW10. Possibly, the lower polarity of HAW10 reduced the severity of pore blockage by lowering the quantity of adsorbed NOM at pore entrances or by reducing the combined effects of water and NOM adsorption on pore blockage. Electrostatic effects most likely did not play a role in reducing pore blockage effects on HAW10 given that its surface charge should be intermediate to those of AW10 and AAW10 based on  $pH_{pzc}$  data (Table 1.3). Pore blockage/constriction effects were not observed for ACF15 and ACF20, adsorbents whose dominant pore sizes were in the 9 to 13 Å width range. Therefore, these results suggest that the adverse effects of pore blockage can be avoided if the micropore size distribution extends to pore widths that are approximately twice the kinetic diameter of the adsorbate molecule.

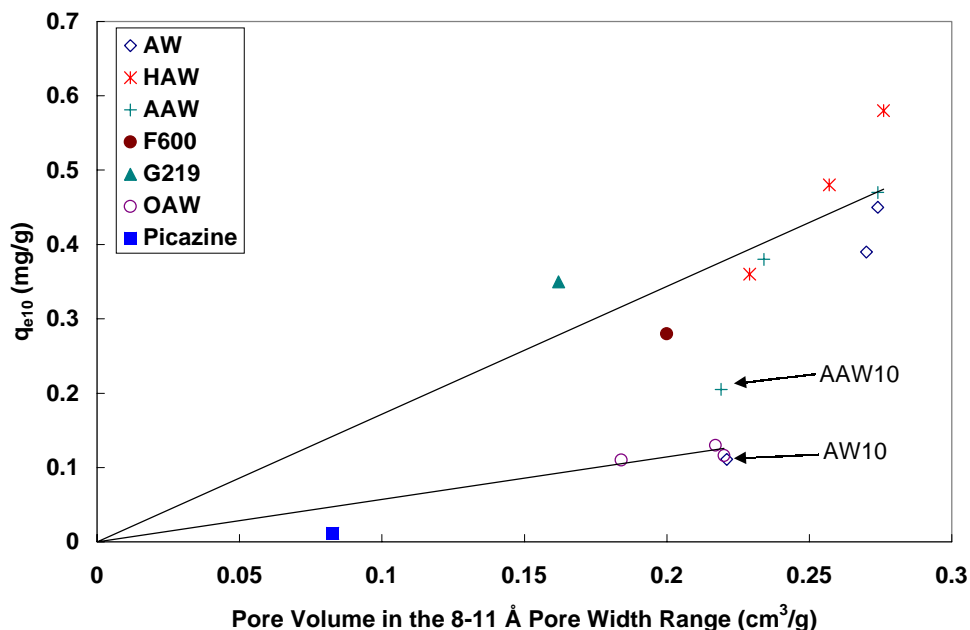


**Figure 2.10. Correlation between adsorption capacity and pore volume in the appropriate size range—MTBE.**

Apart from AW10 and AAW10, differences among the more hydrophobic ACFs at a given activation level were small compared to the decrease in MTBE adsorption capacity that was observed upon oxidation. As indicated before, the detrimental effects of water adsorption explained the poorer performance of the oxidized ACFs. Figure 2.10 further illustrates that the accessible size range for MTBE in natural water did not change from the size range determined in Chapter 1 for the single-solute isotherms. This result suggests that MTBE had to compete with NOM over the entire pore size range that is responsible for MTBE adsorption.

Figure 2.11 illustrates the effect of surface chemistry on TCE adsorption for ACF20. TCE adsorption capacities increased with increasing adsorbent hydrophobicity, and

similar results were observed for ACFs 10 and 15. These results confirm the trends described for single-solute systems in Chapter 1 and illustrate that hydrophobic adsorbents retain their advantage over more polar adsorbents in the presence of NOM.

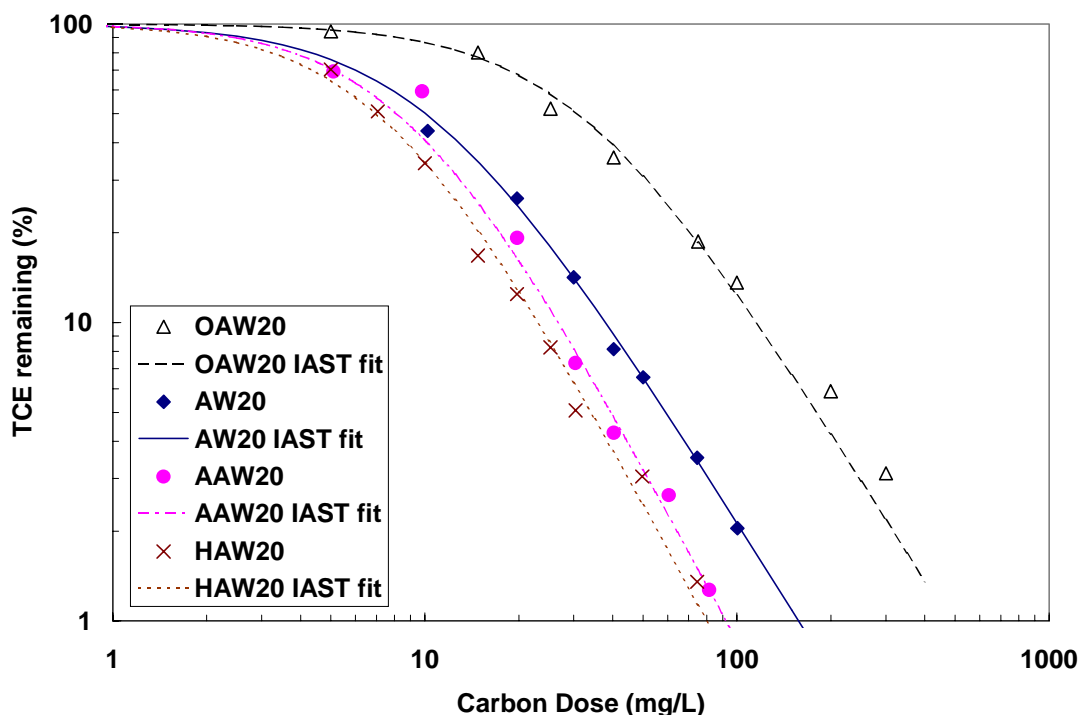


**Figure 2.11. Effect of ACF surface chemistry modifications on TCE adsorption from SJDW (ACF20).**

The effects of surface chemistry on the adsorption of MTBE by ACF20 are shown in Figure 2.12. As was observed for TCE, the more hydrophobic carbons (AW20, HAW20, and AAW20) adsorbed MTBE more effectively than the more hydrophilic carbon (OAW20). Again, these results are similar to those obtained in the absence of NOM and confirm that enhanced water adsorption on polar adsorbents interferes with the adsorption of both nonpolar and polar adsorbates from aqueous solution. Enhanced water adsorption

on polar surface sites therefore negated the potential benefit of providing specific adsorption sites (i.e. oxygen containing functional groups such as carboxylic acid or phenolic groups) capable of forming hydrogen-bonds with MTBE.

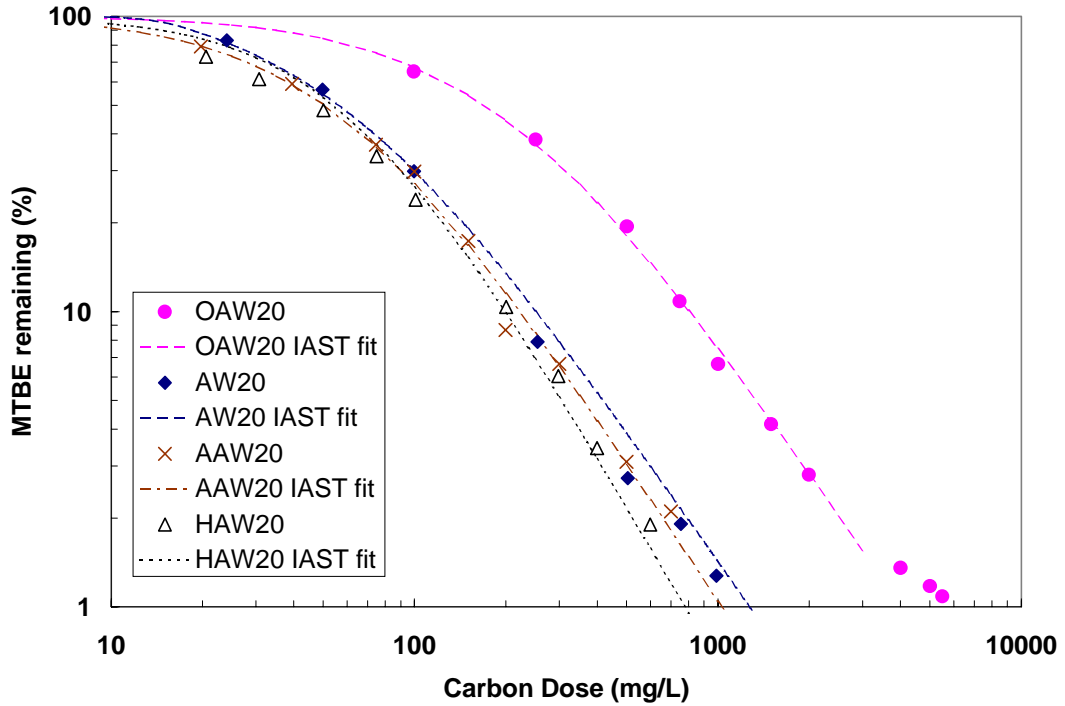


**Figure 2.12. Effect of ACF surface chemistry modifications on MTBE adsorption from SJDW (ACF20).**

Surface chemistry modifications of ACF15 yielded trends similar to those observed for ACF20 in Figure 2.12. However, Figure 2.13 illustrates that OAW10 performed similarly or better than AW10. As explained earlier, a likely explanation for this result is that pore blockage/restriction occurred on AW10 but not on OAW10 as a result of repulsive electrostatic forces between the negatively charged surface of OAW10 and negatively charged NOM.

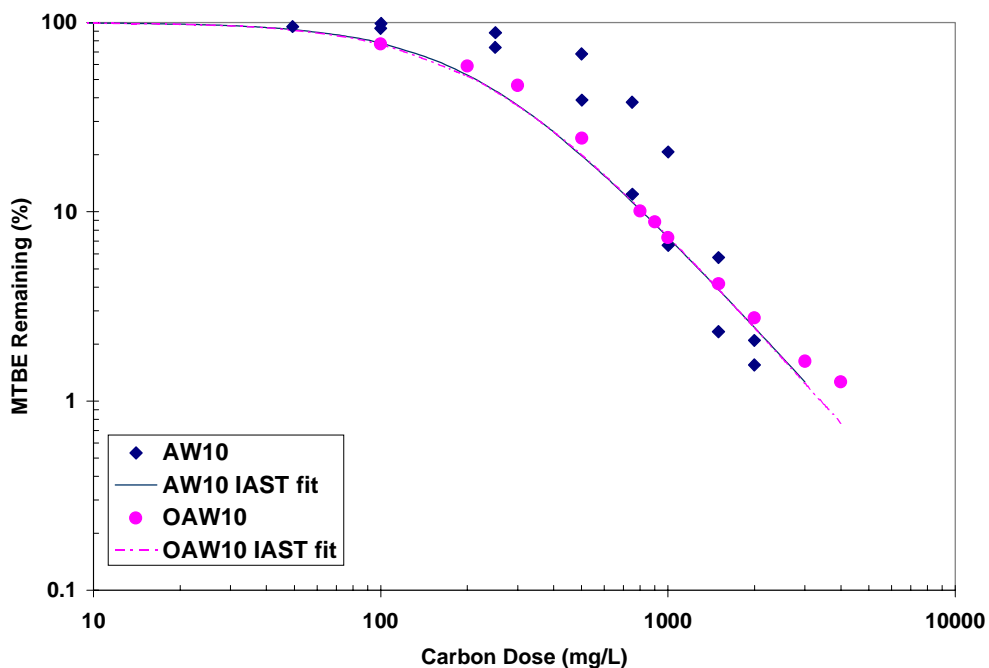


**Figure 2.13. Effect of ACF surface chemistry modifications on MTBE adsorption from SJDW (AW10 vs. OAW10).**

To determine the effects of adsorbent surface chemistry on micropollutant adsorption from SJDW, TCE and MTBE adsorption capacities were plotted as a function of the adsorbent polarity. The polarity of each adsorbent was represented by the sum of its oxygen and nitrogen contents (mmol/g). To eliminate pore structure effects, TCE and MTBE adsorption capacities ( $q_{e10}$ ) were normalized by the pore volume in the appropriate range of pore widths (i.e. 7-9 Å for TCE, 8-11 Å for MTBE). Consequently, normalized TCE and MTBE adsorption capacities ( $q'_{e10}$ ) were expressed in units of mg micropollutant/cm<sup>3</sup> pore volume. Figure 2.14 shows that the normalized TCE adsorption capacity decreased with increasing adsorbent polarity, and a similar trend was observed for MTBE in Figure 2.15.

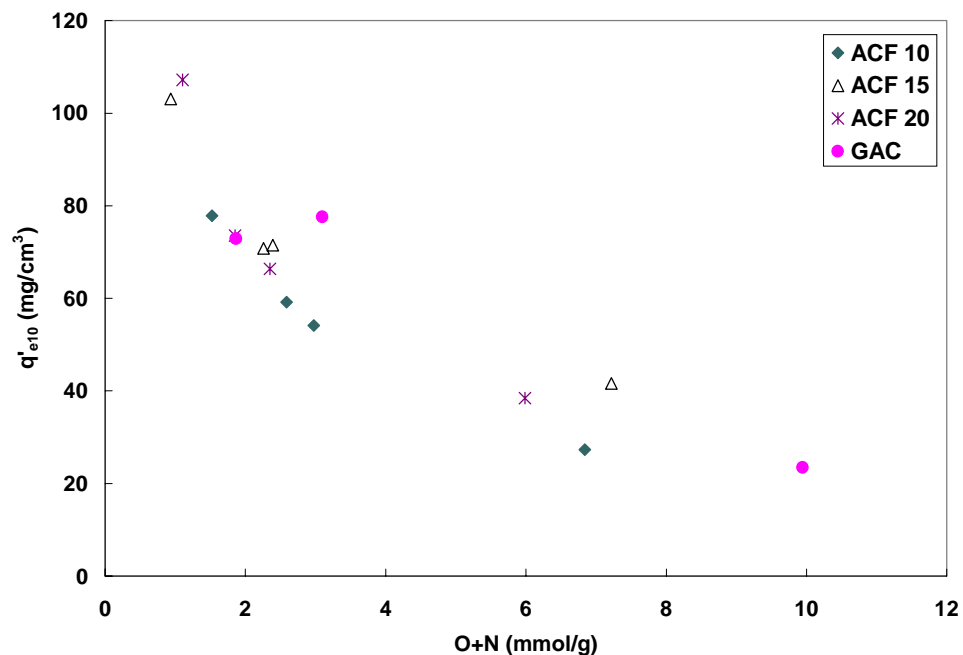


Figure 2.14. Effect of adsorbent hydrophobicity on TCE adsorption capacity in the presence of NOM ( $C_{0, TCE} = 100 \mu\text{g/L}$ ).

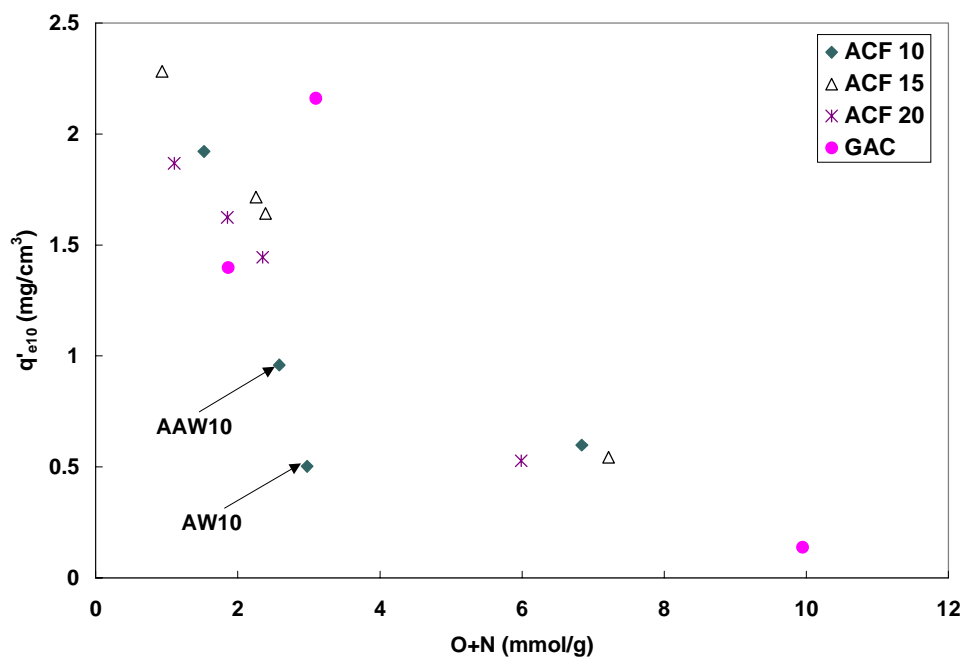


Figure 2.15. Effect of adsorbent hydrophobicity on MTBE adsorption capacity in the presence of NOM ( $C_{0, MTBE} = 100 \mu\text{g/L}$ ).

These results illustrate that hydrophobic adsorbents, i.e. adsorbents with a low heteroatom content, are more effective for the removal of both relatively hydrophobic and relatively hydrophilic pollutants from natural water. Furthermore, Figure 2.14 and 2.15 illustrate that the trends established by the ACF matrix appropriately described the performance of the commercially available GACs. Overall, the results in Figures 2.14 and 2.15 suggest that micropollutant adsorption is most effective on adsorbents that are hydrophobic [ $(O+N) < 2$  to 3 mmol/g] and exhibit a large volume of pores with a diameter that corresponds to approximately 1.5 times the kinetic diameter of the adsorbate. Furthermore, MTBE adsorption data from SJDW suggests that the detrimental effects of pore blockage as a result of NOM adsorption can be avoided if the micropore size distribution extends to pore widths that correspond to approximately twice the kinetic diameter of the adsorbate (i.e. for ACFs 15 and 20).

To illustrate the importance of adsorbent selection, Table 2.3 ranks the studied adsorbents in terms of the carbon dosage required to remove 90% of either TCE or MTBE from SJDW in the order from best to worst. The dosages are based on IAST model results and are in close agreement with the experimental data in the carbon dosage range necessary to remove 90% of TCE or MTBE. In addition, Table 2.3 summarizes the percentage reduction in adsorption capacity ( $q_{e10}$ ) that resulted from the presence of NOM when the initial micropollutant concentration was 100  $\mu\text{g/L}$ .

**Table 2.3 Adsorbent performance rankings in the presence of NOM.**

TCE			MTBE		
Carbon	Reduction in $q_{e10}$ (%)	Carbon Dose for 90% removal	Carbon	Reduction in $q_{e10}$ (%)	Carbon Dose for 90% removal
HAW10	30.9%	8.3	HAW15	22.6%	156
AW10	47.0%	11.6	HAW20	40.4%	199
AAW10	43.3%	12.6	AAW15	32.3%	200
F600	43.8%	15.1	AW15	25.9%	207
HAW15	31.7%	17.5	HAW10	32.2%	222
G219	33.9%	22.0	AAW20	22.8%	222
HAW20	45.1%	23.0	AW20	19.5%	240
AW15	48.9%	26.0	G219	20.4%	255
AAW20	47.5%	26.8	F600	39.2%	315
AAW15	53.4%	27.2	AAW10	64.0%	460
OX10	31.7%	30.1	OX15	26.3%	790
AW20	57.5%	38.0	OX20	16.3%	800
OX15	45.3%	71.0	AW10	68.7%	809
OX20	69.6%	115.0	OX10	37.1%	825
Picazine	14.4%	283.0	Picazine	14.7%	7900

To achieve 90% TCE removal from SJDW, adsorbent doses of about 8 to 300 mg/L were required, and the rankings were affected both by adsorbent pore structure and surface chemistry. The most suitable adsorbents for TCE were hydrophobic adsorbents that exhibited a large pore volume in the 7 to 9 Å range width range, i.e. HAW10, AW10, and AAW10. Among the commercially available GACs, F600 most closely met the requirements for a suitable adsorbent for TCE removal from natural water, and this adsorbent was nearly 20 times as effective as the polar wood-based Picazine. Percentage reductions in TCE adsorption capacities were generally in the range of 30 to 50% and showed little dependence on pore structure or surface chemistry given that none of the studied adsorbents exhibited pore size distributions that caused pore blockage/

constriction effects that affected TCE access to adsorption sites in suitable micropores. Table 2.4 ranks the studied adsorbents in terms of TCE and MTBE adsorption capacities based on the single-solute isotherm data in the order from best to worst. Because the effects of pore structure and surface chemistry had little effect on the competitive effect of NOM, the adsorbent rankings for TCE removal from single-solute systems were similar to those for TCE removal from SJDW.

**Table 2.4 Adsorbent performance rankings in ultrapure water.**

TCE		MTBE	
Carbon	Single-solute $q_{e10}$ (mg/g)	Carbon	Single-solute $q_{e10}$ (mg/g)
HAW10	18.0	HAW15	0.814
AW10	16.0	HAW20	0.805
AAW10	14.1	AAW15	0.694
F600	11.7	HAW10	0.648
HAW15	8.64	AW15	0.607
HAW20	8.20	AAW10	0.597
G219	8.02	AAW20	0.492
AW15	7.53	AW20	0.484
AAW15	7.29	F600	0.460
AAW20	6.66	G219	0.439
AW20	6.12	AW10	0.355
OX10	4.77	OX10	0.175
OX20	2.67	OX15	0.160
OX15	2.45	OX20	0.139
Picazine	0.409	Picazine	0.0134

To achieve 90% MTBE removal from SJDW, adsorbent doses of about 160 to 8000 mg/L were required. MTBE adsorption was most effective with hydrophobic adsorbents that exhibited a large pore volume in the 8 to 11 Å width range and whose micropore widths extended to about 13 Å to prevent pore blockage. Thus, the most effective adsorbents for

MTBE were hydrophobic ACFs 15 and 20 (i.e. hydrogen-treated, acid-washed, and ammonia-treated) whose pores were concentrated in the 9-13 Å width range. Among the commercially available GACs, coconut-shell-based G219 was most effective for MTBE removal from natural water (dominant pore widths: 7-13 Å), while the polar Picazine GAC was again the least effective. In terms of capacity reduction percentage, NOM adsorption had the most detrimental effects on the MTBE adsorption capacities of AAW10 and AW10, a result that was primarily attributable to pore blockage or pore constriction as described above. While capacity reduction percentages were lowest for polar adsorbents with larger micropores (i.e. OAW15, OAW20, or Picazine), a result consistent with the electrostatic repulsion between negatively charged adsorbent surfaces and negatively charged NOM, polar adsorbents still performed poorly in natural water because of the detrimental effects of enhanced water adsorption. Rankings of the adsorbents in terms of MTBE removal effectiveness from SJDW (Table 2.3) were generally similar to those observed in ultrapure water (Table 2.4) with two notable exceptions; the effectiveness of both AAW10 and AW10 decreased greatly because of the detrimental effects of pore blockage or restriction on the MTBE adsorption capacity.

## 2.5 CONCLUSIONS

To evaluate pore structure and surface chemistry effects on the adsorption of TCE and MTBE from natural water, a matrix of activated carbon fibers (ACFs) with three activation levels and four surface chemistry levels was studied along with three commercially available GACs. From the relationships observed between the adsorbent characteristics and the micropollutant adsorption isotherm data in the presence of NOM, the following conclusions were drawn:

- Regardless of the pore structure or surface chemistry, the carbons always had a higher adsorptive capacity for TCE than for MTBE, a result that is consistent with the greater hydrophobicity of TCE.
- For carbons with similar surface chemistry, the pore volume of micropores with widths corresponding to about 1.5 times the kinetic diameter of the target pollutant controlled the adsorption capacity. However, if the dominant pore size range and the range of pore sizes in which the micropollutant adsorbs have similar upper bounds, pore blockage or restriction can occur as a result of NOM adsorption. Consequently, adsorption capacities decreased greatly as was observed for MTBE adsorption from SJDW on AW10 and AAW10. To prevent pore blockage, the dominant micropore range should be extended to pore widths that are approximately twice the kinetic diameter of the target adsorbate.
- Adsorbent polarity, as expressed by the sum of the oxygen and nitrogen contents (mmol/g), can serve as a useful activated carbon selection criterion. As the polarity of a carbon increases, or the molar concentration of O+N increases, the adsorption

capacity decreases. This result can be explained by increased water adsorption on more polar carbons, which in turn lowers the adsorption capacity of the carbon for both hydrophobic and hydrophilic adsorbates. Based on the results of this study, effective adsorbents should have an O+N content of less than 2 to 3 mmol/g.

- Attempts to minimize the adverse effects of NOM adsorption by selecting carbons with a negative surface charge (i.e. oxidized ACFs) were unsuccessful because the carbons contained a larger concentration of polar functional groups. The detrimental effects of enhanced water adsorption on these carbons outweighed any benefits that were derived from minimizing NOM adsorption through repulsive electrostatic forces.

Overall, the results of this study showed that the selection of an effective adsorbent for the removal of micropollutants from natural water requires

- [1] a large pore volume in micropores with widths that are about 1.5 times larger than the kinetic diameter of the target adsorbate,
- [2] a micropore size distribution that extends to widths that are approximately twice the kinetic diameter of the target adsorbate to prevent pore blockage, and
- [3] hydrophobic pore surface chemistry which, when expressed as the sum of the oxygen and nitrogen contents, should not exceed 2 to 3 mmol/g.

## LIST OF REFERENCES

- Adams JQ and Clark RM. Cost estimates for GAC treatment systems. *Journal of the American Water Works Association* 1989; 81(1): 35-42
- Bansal RC, Donnet JB, Stoeckli F. *Active carbon*. New York: Marcel Dekker, Inc. 1988.
- Barton SS, Evans MJB, Holland J, Koresh JE. Water and cyclohexane vapour adsorption on oxidized porous carbon. *Carbon* 1984; 22(3):265-272.
- Barton SS, Evans MJB, Halliop E, MacDonald JAF. Acidic and basic sites on the surface of porous carbon. *Carbon* 1997; 35(9):1361-1366.
- Belfort G. Selective adsorption of organic homologues onto activated carbon from dilute aqueous solutions. Solvophobic interaction approach and correlations of molar adsorptivity with physicochemical parameters. *Environ. Sci. Technol.* 1979; 13(8):939-946.
- Bernazeau F, Mandra V, Charles P, Anselme C, Bersillon J. Pesticides removal of activated carbon: competitive adsorption with natural organic matter. *Water Supply* 1996; 14(2):43-48.
- Biniak S, Szymanski G, Siedlewski J, Swiatkowski A. The characterization of activated carbons with oxygen and nitrogen surface groups. *Carbon* 1997; 35(12):1799-1810.
- Bjelopavic M, Newcombe G, Hayes R. Adsorption of NOM on activated carbon: Effect of surface charge, ionic strength, and pore volume distribution. *Journal of Colloid and Interface Science* 1999; 210:271-280.
- Boehm HP, Diehl E, Heck W, Sappok R. Surface oxides of carbon. *Angew. Chem. Internat. Edit.* 1964; 3:669-677.
- Boehm HP, Voll M. Basische Oberflächenoxide auf Kohlenstoff – I. Adsorption von Säuren. *Carbon* 1970; 8:227-240.
- Bolto B, Abbt-Braun G, Dixon D, Eldridge R, Frimmel F, Hesse S, et al. Experimental evaluation of cationic polyelectrolytes for removing natural organic matter from water. *Water Science and Technology* 1999; 40(9):71-79.
- Cambridge Structural Database. CSD Version 5.20. Cambridge UK: Cambridge Crystallographic Data Centre.
- Carter MC, Kilduff JE, Weber WJ Jr. Site energy distribution analysis of preloaded adsorbents. *Environ. Sci. Technol.* 1995; 29(7):1773-1780.
- Chen G, Dussert W, Suffet H. Evaluation of granular activated carbons for removal of methylisoborneol to below odor threshold concentration in drinking water. *Water Research* 1997; 31(5):1155-1163.

- Chin, YP, Aiken G., O'Loughlin E. Molecular weight, polydispersity, and spectroscopic properties of aquatic humic substances. *Environmental Science and Technology* 1994; 28(11):1853-1858.
- Chintawar PS, Greene HL. Adsorption and catalytic destruction of trichloroethylene in hydrophobic zeolites. *Applied Catalysis B: Environmental* 1997; 14:37-47.
- Considine R, Denoyel R, Pendleton P, Schumann R, Wong SH. The influence of surface chemistry on activated carbon adsorption of 2-methylisoborneol from aqueous solution. *Colloid and Surfaces A: Physicochemical and Engineering Aspects* 2001; 179:271-280.
- Coughlin RW, Ezra FS. Role of surface acidity in the adsorption of organic pollutants on the surface of carbon. *Environ. Sci. Technol.* 1968; 2(4):291-297.
- Coulson CA. The electronic structure of the boundary atoms of a graphite layer. *Proc. of the fourth conf. on carbon*, Oxford: Pergamon Press, 1960: 215-219.
- Crittenden JC, Sanonraj S, Bulloch JL, Hand DW, Rogers TN, Speth, TF, Ulmer M. Correlation of aqueous-phase adsorption isotherms. *Environ. Sci. Technol.* 1999; 33(17):2926-2933.
- Daley MA, Tandon D, Economy J, Hippo EJ. Elucidating the porous structure of activated carbon fibers using direct and indirect methods. *Carbon* 1996; 34(10):1191-1200.
- Davis SW, Powers SE. Alternative sorbents for removing MTBE from gasoline-contaminated ground water. *J. Environ. Engrg.* 2000; 126(4):354-360.
- Derbyshire F, Jagtoyen M, Andrews R, Rao A, Martin-Gullon I, Grulke EA. Carbon materials in environmental applications. In Radovic LR, editor. *Chemistry and Physics of Carbon*, Vol. 27, New York: Marcel Dekker, 2001: 1-66.
- Derylo-Marczewska A, Jaroniec M, Gelbin D, Seidel A. Heterogeneity effects in single-solute adsorption from dilute solutions on solids. *Chemica Scripta* 1984; 24:239-246.
- Dimotakis ED, Cal MP, Economy J, Rood MJ, Larson SM. Chemically treated activated carbon cloths for removal of volatile organic carbons from gas streams: evidence for enhanced physical adsorption. *Environ. Sci. Tech.* 1995; 29(7):1876-1880.
- Dubinlin MM, Zaverina ED, Serpinsky VV. The sorption of water vapor by active carbon. *J. Am. Chem. Soc.* 1955; 77:1760-1766.
- Ebie K, Li F, Hagishita, T. Effect of pore size distribution of activated carbon on the adsorption of humic substances and trace organic compounds. *Water Supply* 1995; 13(3/4):65-70.
- Ebie K, Li F, Azuma Y, Yuasa A, Hagishita T. Pore distribution effect of activated carbon in adsorbing organic micropollutants from natural water. *Water Research* 2001; 35(1):167-179.

- Franz M, Arafat HA, Pinto NG. Effect of chemical surface heterogeneity on the adsorption mechanism of dissolved aromatics on activated carbon. *Carbon* 2000; 38(13):1807-1819.
- Garten, VA, Weiss DE. A new interpretation of the acidic and basic structures in carbons. II. The chromene-carbonium couple in carbon. *Austr. J. Chem.* 1957; 10:309-328.
- Gillogy TET, Snoeyink VL, Elarde JR, Wilson CM, Royal EP. <sup>14</sup>C-MIB adsorption on PAC in natural water. *Journal of the American Water Works Association* 1998; 90(1):98-108.
- Graham MR, Summers RS, Simpson MR, Macleod BW. Modeling equilibrium adsorption of 2-methylisoborneol and geosmin in natural waters. *Water Research* 2000; 34(8):2291-2300.
- Greene BC, Snoeyink VL, Pogue FW. Adsorption of Pesticides by powdered activated carbon. *American Water Works Association: Denver, CO.* 1994.
- Hopman R, Siegers WG, and Kruithof JC. Organic micropollutant removal by activated carbon fiber filtration. *Water Supply* 1995; 13 (3/4):257-261.
- Janssen RJJ, van Bekkum H. Amination and ammoxidation of activated carbons. *Carbon* 1994; 32(8):1507-1516.
- Janssen RJJ, van Bekkum H. XPS of nitrogen-containing functional groups on activated carbon. *Carbon* 1995; 33(8):1021-1027.
- Kaneko Y, Abe M, Ogino K. Adsorption characteristics of organic compounds dissolved in water on surface-improved activated carbon fibers. *Colloids and Surfaces* 1989; 37:211-222.
- Karanfil T, Kitis M, Kilduff JE, Wigton A. Role of granular activated carbon surface chemistry on the adsorption of organic compounds. 2. Natural Organic Matter. *Environmental Science and Technology.* 1999; 33(18):3225-3233.
- Karanfil T, Kilduff JE. Role of granular activated carbon surface chemistry on the adsorption of organic compounds. 1. Priority pollutants. *Environ. Sci. Technol.* 1999; 33(18): 3217-3224.
- Kasaoka S, Sakata Y, Tanaka E, Naitoh R. Preparation of activated fibrous carbon from phenolic fabric and its molecular-sieve properties. *International Chemical Engineering* 1989a; 29(1):101-114.
- Kasaoka S, Sakata Y, Tanaka E, Naitoh R. Design of molecular-sieve carbon. Studies on the adsorption of various dyes in the liquid phase. *International Chemical Engineering* 1989b; 29(4):734-742.
- Kilduff JE. Polyelectrolyte adsorption by activated carbon and the effects of preloading on trichloroethylene adsorption. Ph.D. Dissertation. The University of Michigan: Ann Arbor, MI. 1995.

- Kilduff JE, Karanfil T, Chin Y, Weber WJ. Adsorption of natural organic polyelectrolytes by activated carbon: A size exclusion chromatography study. *Environmental Science and Technology* 1996; 30: 1336-1343.
- Kilduff JE, Karanfil T, Weber WJ Jr. TCE adsorption by GAC preloaded with humic substances. *J. AWWA* 1998; 90(5):76-89.
- Kilduff JE and Wigton A. Sorption of TCE by humic-preloaded activated carbon: Incorporating size-exclusion and pore blockage phenomena in a competitive adsorption model. *Environmental Science and Technology* 1999; 33(2):250-256.
- Knappe D, Matsui Y, Snoeyink VL. Predicting the Capacity of Powdered Activated Carbon for Trace Organic Compounds in Natural Waters. *Environmental Science and Technology* 1998; 32(11):1694-1698.
- Lee MC, Snoeyink VL, Crittenden JC. Activated Carbon Adsorption of humic substances. *Journal of the American Water Works Association* 1981; 73(8):440-446.
- Leon y Leon CA, Solar JM, Calemma V, Radovic LR. Evidence for the protonation of basal plane sites on carbon. *Carbon* 1992; 30(5): 797-811.
- Lundelius EF. Adsorption und Löslichkeit. *Koll. Zeitschr.* 1920; 26(4):145-151.
- Mahajan OP, Moreno-Castilla C, Walker PL Jr. Surface-treated activated carbon for removal of phenol from water. *Sep. Sci. and Technol.* 1980; 15(10):1733-1752.
- Mamchenko AV, Yakimova TI, Koganovskii AM. The mechanism of the filling of the micropores in activated charcoals during the adsorption of organic substances dissolved in water. *Russian Journal of Physical Chemistry* 1982; 56(5): 1221-1224.
- Mangun CL, Benak KR, Daley MA, Economy J. Oxidation of activated carbon fibers: effect on pore size, surface chemistry, and adsorption properties. *Chem. Mater.* 1999; 11:3476-3483.
- Matsumoto A, Zhao JX, Tsutsumi K. Adsorption behavior of hydrocarbons on slit-shaped micropores. *Langmuir* 1997; 13:496-501.
- Mattson JS and Mark HB Jr. *Activated carbon - surface chemistry and adsorption from solution.* New York: Marcel Dekker. 1971.
- McCallum CL, Bandosz TJ, McGrother SC, Müller EA, Gubbins KE. A molecular model for adsorption of water on activated carbon: comparison of simulation and experiment. *Langmuir* 1999; 15:533-544.
- McGuire MJ, Suffet IH, Radziul JV. Assessment of unit processes for the removal of trace organic compounds from drinking water. *J. AWWA* 1978; 70(10):565-572.
- Menendez JA, Phillips J, Xia B, Radovic LR. On the modification and characterization of chemical surface properties of activated carbon: in the search of carbons with stable basic properties. *Langmuir* 1996a; 12(18):4404-4410.

- Menendez JA, Radovic LR, Xia B, Phillips J. Low-temperature generation of basic carbon surfaces by hydrogen spillover." J. Phys. Chem. 1996b; 100(43):17243-17248.
- Morris G and Newcombe G. Granular activated carbon: The variation of surface properties with the adsorption of humic substances. Journal of Colloid and Interface Science 1993; 159:413-420.
- Müller EA, Rull LF, Vega LF, Gubbins KE. Adsorption of water on activated carbons: a molecular simulation study. J. Phys. Chem. 1996; 100:1189-1196.
- Müller EA, Gubbins KE. Molecular simulation study of hydrophilic and hydrophobic behavior of activated carbon surfaces. Carbon 1998; 36(10):1433-1438.
- Müller EA, Hung, FR, Gubbins KE. Adsorption of water vapor-methane mixtures on activated carbons. Langmuir 2000, 16:5418-5424.
- Muller G, Radke CJ, Prausnitz JM. Adsorption of weak organic electrolytes from dilute aqueous solution into activated carbon. 1. Single-solute systems. Journal of Colloid and Interface Science 1985; 103(2):466-483.
- Müller U, Hess F, Worch E. Impact of organic matter adsorbability on micropollutant removal by activated carbon. Journal of Water Supply Research and Technology-Aqua 1996; 45(6):273-280.
- Najm, IN, Snoeyink VL, Richard Y. Effect of initial concentration of a SOC in natural water on its adsorption by activated carbon. Journal of the American Water Works Association 1991a; 83(8):57-63.
- Najm IN, Snoeyink VL, Lykins BW, Adams JQ. Using powdered activated carbon: A critical review. Journal of the American Water Works Association 1991b; 83(1): 65-76.
- Narbaitz RM and Benedek A. Adsorption of 1,1,2-trichloroethane from river water. Journal of Environmental Engineering 1994; 120(6):1400-1415.
- Newcombe G, Hayes R, and Drikas M. Granular activated carbon: importance of surface properties in the adsorption of naturally occurring organics. Colloids and Surfaces: Physicochemical and Engineering Aspects 1993; 78:65-71.
- Newcombe G and Drikas M. Adsorption of NOM onto activated carbon: Electrostatic and non-electrostatic effects. Carbon 1997; 35(9):1239-1250.
- Newcombe G, Drikas M, Hayes R. Influence of characterised natural organic matter on activated carbon adsorption: II. Effect on pore volume distribution and adsorption of 2-methylisoborneol. Water Research 1997; 31(5):1065-1073.
- Newcombe G. Charge vs. porosity – Some influences on the adsorption of natural organic matter (NOM) by activated carbon. Water Science and Technology 1999; 40(9):191-198.

- Newcombe G. Removal of natural microcontaminants from drinking water. *Encyclopedia of Colloid and Interface Science* 2001; in press.
- Nichols EM, Einarson MD, Beadle SC. Strategies for characterizing subsurface releases of gasoline containing MTBE, Publication No. 4699. Washington DC: American Petroleum Institute. 2000.
- Noh JS, Schwarz JA. Estimation of the point of zero charge of simple oxides by mass titration. *J. Coll. Interf. Sci.* 1989; 130(1):157-164.
- Okouchi S, Saegusa H, Nojima O. Prediction of environmental parameters by adsorbability index: water solubilities of hydrophobic organic pollutants. *Environment International* 1992; 18: 249-261.
- Pan D, Jaroniec M. Adsorption and thermogravimetric studies of unmodified and oxidized active carbons. *Langmuir* 1996; 12:3657-3665.
- Pauling L. The nature of the chemical bond, and the structure of molecules and crystals: an introduction to modern structural chemistry; 3<sup>rd</sup> edition. Ithaca NY: Cornell University Press. 1960.
- Pelekani C, Snoeyink VL. Competitive adsorption in natural water: role of activated carbon pore size. *Water Research* 1999; 33(5):1209-1219.
- Pelekani C, Newcombe G, Snoeyink VL, Hepplewhite C, Assemi S, Beckett R. Characterization of natural organic matter using high performance size exclusion chromatography. *Environmental Science & Technology* 1999; 33(16):2807-2813.
- Pelekani C, Snoeyink VL. Competitive adsorption between atrazine and methylene blue on activated carbon: the importance of pore size distribution. *Carbon* 2000; 38:1423-1436.
- Pelekani C, Snoeyink VL. A kinetic and equilibrium study of competitive adsorption between atrazine and Congo red dye on activated carbon: the importance of pore size distribution. *Carbon* 2001; 39:25-37.
- Pendleton P, Wong SH, Schumann R, Levay G, Denoyel R, Rouquerol J. Properties of activated carbon controlling 2-methylisoborneol adsorption. *Carbon* 1997; 35(8):1141-1149.
- Perdue EM, Reuter, JH, Ghosal M. The operational nature of acidic functional group analyses and its impact on mathematical descriptions of acid-base equilibria in humic substances. *Geochimica et Cosmochimica Acta* 1980; 44(11):1841-1851.
- Perdue EM and Lytle CR. Distribution model for binding of protons and metal ions by humic substances. *Environmental Science & Technology* 1983; 17(11):654-660.
- Perdue EM, Reuter JH, Parrish RS. A statistical model of proton binding by humus. *Geochimica et Cosmochimica Acta* 1984; 48(6):1257-1263.
- Polovina M, Babic B, Kaluderovic B, Dekanski A. Surface characterization of oxidized activated carbon cloth. *Carbon* 1997; 35(8):1047-1052.

- Puri, BR and Bansal, RC. Studies in surface chemistry of carbon blacks part I. High temperature evacuation. *Carbon* 1964; 1: 451-455.
- Puri BR. Chemisorbed oxygen evolved as carbon dioxide and its influence on surface reactivity of carbons. *Carbon* 1966; 4:391-400.
- Puri BR. Surface complexes on carbons. In Walker PL Jr., editor. *Chemistry and Physics of Carbon*, Vol. 6, New York: Marcel Dekker, 1970: 191-282.
- Puri BR. Physicochemical aspects of carbon affecting adsorption from the aqueous phase. In McGuire MJ and Suffet IH, editors. *Advances in Chemistry Series*, Vol. 202, Washington DC: American Chemical Society, 1983: 77-93.
- Qi S, Adham SS, Snoeyink VL, Lykins BW. Prediction and verification of atrazine adsorption by PAC. *Journal of Environmental Engineering* 1994; 120(1):202-218.
- Sano T, Hasegawa M, Kawakami K, Yanagishita H. Separation of methanol/methyl tert-butyl ether mixture by pervaporation using silicalite membrane. *J. Membrane Science* 1995; 107: 193-196.
- Schlautman MA and Morgan JJ. Adsorption of aquatic humic substances on colloidal-size aluminum oxide particles: Influence of solution chemistry. *Geochimica et Cosmochimica Acta* 1994; 58(20):4293-4303.
- Schwarzenbach RP, Gschwend PM, Imboden DM. *Environmental Organic Chemistry*. New York: John Wiley and Sons, Inc. 1993.
- Sing KSW, Everett DH, Haul RAW, Moscou L, Pierotti RA, Rouquerol J, Siemieniewska T. *Pure and Applied Chemistry* 1985; 57:603-619.
- Smisek M, Cerny S. *Active carbon. Manufacture, properties and applications*. New York: Elsevier Publishing Company, 1970.
- Snoeyink VL, Weber WJ Jr. Surface functional groups on carbon and silica. *Progress in Surface and Membrane Science*, Vol. 5, New York: Academic Press, 1972: 63-119.
- Sontheimer H, Crittenden JC, Summers RS. *Activated carbon for water treatment*. DVGW-Forschungsstelle, Engler-Bunte-Institute, University of Karlsruhe: FRG. 1988.
- Summers RS and Roberts PV. Activated carbon adsorption of humic substances II. Size exclusion and electrostatic interactions. *Journal of Colloid and Interface Science* 1988; 122(2):382-397.
- Weber WJ Jr. *Physicochemical processes for water quality control*. New York: John Wiley and Sons, 1972, pp 199-259.

## **APPENDICES**

## Appendix A. Raw Data

**Table A.1 DOC isotherms for AW10**

**Carbon Type: AW10**  
**Solvent: SJDW**  
**Initial DOC Concentration (mg/L): 3.988 mg/L**

Weight of Carbon (mg)	Solvent Volume (mL)	Carbon Conc. (mg/L)	Equilibrium DOC Conc. (mg/L)	Qe (mg/g)
4.1	400	10.3	3.730	25.220
5.2	200	26.0	3.774	8.231
10.0	200	50.0	3.452	10.720
20.1	200	100.5	3.483	5.0249
49.8	200	249.0	3.380	2.4418
75.1	100	751.0	3.349	0.8515
149.9	100	1499.0	2.924	0.7101
200.0	100	2000.0	2.773	0.6078

**Table A.2 DOC isotherms for AW15**

**Carbon Type: AW15**

**Solvent: SJDW**

**Initial DOC Concentration (mg/L): 3.657 mg/L**

Weight of Carbon (mg)	Solvent Volume (mL)	Carbon Conc. (mg/L)	Equilibrium DOC Conc. (mg/L)	Qe (mg/g)
4.0	400	10.0	3.235	42.250
5.0	200	25.0	3.262	15.820
10.1	200	50.5	2.9455	14.089
20.0	200	100.0	2.613	10.440
49.8	200	249.0	2.176	5.948
50.0	100	500.0	1.4115	4.491
75.2	100	752.0	1.292	3.145
100.0	100	1000.0	1.0160	2.641
150.0	100	1500.0	0.698	1.973
200.1	100	2001.0	0.4985	1.578

**Table A.3 DOC isotherms for AW20**

**Carbon Type: AW20**

**Solvent: SJDW**

**Initial DOC Concentration (mg/L): 4.316 mg/L**

Weight of Carbon (mg)	Solvent Volume (mL)	Carbon Conc. (mg/L)	Equilibrium DOC Conc. (mg/L)	Qe (mg/g)
10.1	200	50.5	3.128	23.520
19.9	200	99.5	2.898	14.249
50.1	200	250.5	2.428	7.536
50.1	100	501.0	1.847	4.928
75.1	100	751.0	1.5705	3.655
100.0	100	1000.0	1.954	2.362
150.0	100	1500.0	0.6295	2.458
199.9	100	1999.0	0.3650	1.976

**Table A.4 DOC isotherms for F600**

**Carbon Type: F600**

**Solvent: SJDW**

**Initial DOC Concentration (mg/L): 4.564 mg/L**

Weight of Carbon (mg)	Solvent Volume (mL)	Carbon Conc. (mg/L)	Equilibrium DOC Conc. (mg/L)	Qe (mg/g)
4.1	400	10.3	3.3025	123.11
5.0	200	25.0	2.5765	79.51
10.0	200	50.0	2.1415	48.46
20.0	200	100.0	1.9140	26.50
49.9	200	249.5	1.4585	12.45
49.9	100	499.0	1.6790	5.78
75.0	100	750.0	1.3905	4.23
100.1	100	1001.0	1.0815	3.48
150.1	100	1501.0	0.9620	2.40
200.0	100	2000.0	0.7585	1.90

**Table A.5 DOC isotherms for G219**

**Carbon Type: G219**  
**Solvent: SJDW**  
**Initial DOC Concentration (mg/L): 4.435 mg/L**

Weight of Carbon (mg)	Solvent Volume (mL)	Carbon Conc. (mg/L)	Equilibrium DOC Conc. (mg/L)	Qe (mg/g)
4.1	400	10.3	3.1505	125.28
5.0	200	25.0	2.5450	75.59
10.0	200	50.0	2.1140	46.41
20.0	200	100.0	1.4625	29.72
49.9	200	249.5	0.5155	15.71
49.9	100	499.0	0.5625	7.76
75.0	100	750.0	0.5700	5.15
100.1	100	1001.0	0.4665	3.96
150.1	100	1501.0	0.5440	2.59
200.0	100	2000.0	0.7590	1.84

**Table A.6 DOC isotherms for Picazine**

**Carbon Type: Picazine**  
**Solvent: SJDW**  
**Initial DOC Concentration (mg/L): 3.698 mg/L**

Weight of Carbon (mg)	Solvent Volume (mL)	Carbon Conc. (mg/L)	Equilibrium DOC Conc. (mg/L)	Qe (mg/g)
4.2	400	10.5	2.9505	71.14
2.9	200	14.5	2.8385	59.24
5.2	200	26.0	2.4045	49.73
10.0	200	50.0	2.2025	29.90
19.9	200	99.5	1.8120	18.95
35.2	200	176.0	1.6540	11.61
50.2	200	251.0	1.4950	8.77
50.2	100	502.0	1.3650	4.65
75.1	100	751.0	1.3140	3.17

**Table A.7 Single-solute TCE isotherm data for AW10**

**Carbon Type: AW10**  
**Solvent: ultrapure water**  
**Micropollutant: TCE**

Weight of Carbon (mg)	Solvent Volume (mL)	Carbon Conc. (mg/L)	Initial TCE Conc (µg/L)	Equilibrium TCE Conc. (µg/L)	Qe (mg/g)
5.0	253.4	19.7	1170.5	118.6	53.31
6.2	253.4	24.5	1170.5	78.3	44.64
7.7	253.4	30.4	1170.5	46.3	36.99
8.8	253.4	34.7	1170.5	37.0	32.64
10.0	253.4	39.5	1170.5	54.3	28.28
12.7	253.4	50.1	1170.5	19.1	22.97
19.1	253.4	75.4	1170.5	7.4	15.43
25.4	253.4	100.2	1170.5	4.4	11.63
41.9	253.4	165.4	1170.5	2.6	7.06

**Table A.8 Single-solute TCE isotherm data for AW15**

**Carbon Type: AW15**  
**Solvent: ultrapure water**  
**Micropollutant: TCE**

Weight of Carbon (mg)	Solvent Volume (mL)	Carbon Conc. (mg/L)	Initial TCE Conc (µg/L)	Equilibrium TCE Conc. (µg/L)	Qe (mg/g)
5.0	253.4	19.7	1170.5	295.2	44.36
7.6	253.4	30.0	1170.5	141.7	34.30
12.7	253.4	50.1	1170.5	69.1	21.97
19.0	253.4	75.0	1170.5	31.6	15.19
25.4	253.4	100.2	1170.5	17.4	11.50
31.6	253.4	124.7	1170.5	16.3	9.26
37.9	253.4	149.6	1170.5	11.5	7.75
50.7	253.4	200.1	1170.5	5.0	5.82
69.7	253.4	275.1	1170.5	3.8	4.24
109.0	253.4	430.1	1170.5	1.9	2.72

**Table A.9 Single-solute TCE isotherm data for AW20**

**Carbon Type: AW20**

**Solvent: ultrapure water**

**Micropollutant: TCE**

Weight of Carbon (mg)	Solvent Volume (mL)	Carbon Conc. (mg/L)	Initial TCE Conc (µg/L)	Equilibrium TCE Conc. (µg/L)	Q <sub>e</sub> (mg/g)
7.7	253.4	30.4	1170.5	199.6	31.95
12.6	253.4	49.7	1170.5	88.8	21.75
19.0	253.4	75.0	1170.5	43.0	15.04
25.3	253.4	99.8	1170.5	24.5	11.48
31.7	253.4	125.1	1170.5	15.4	9.23
38.1	253.4	150.4	1170.5	16.1	7.68
50.7	253.4	200.1	1170.5	8.9	5.81
88.7	253.4	350.0	1170.5	3.2	3.33
126.7	253.4	500.0	1170.5	2.0	2.34
190.1	253.4	750.2	1170.5	1.3	1.56

**Table A.10 Single-solute TCE isotherm data for OAW10 – Run 1**

**Carbon Type: OAW10**  
**Solvent: ultrapure water**  
**Micropollutant: TCE**

Weight of Carbon (mg)	Solvent Volume (mL)	Carbon Conc. (mg/L)	Initial TCE Conc (µg/L)	Equilibrium TCE Conc. (µg/L)	Qe (mg/g)
5.2	253.4	20.5	1279.4	393.6	43.17
7.7	253.4	30.4	1279.4	259.4	33.57
10.0	253.4	39.5	1279.4	215.5	26.96
12.8	253.4	50.5	1279.4	127.1	22.81
19.0	253.4	75.0	1279.4	62.9	16.22
25.3	253.4	99.8	1279.4	47.7	12.34
31.8	253.4	125.5	1279.4	29.8	9.96
38.1	253.4	150.4	1279.4	26.2	8.33
44.2	253.4	174.4	1279.4	20.2	7.22
50.7	253.4	200.1	1279.4	14.4	6.32

**Table A.11 Single-solute TCE isotherm data for OAW10 – Run 2**

**Carbon Type: OAW10**  
**Solvent: ultrapure water**  
**Micropollutant: TCE**

Weight of Carbon (mg)	Solvent Volume (mL)	Carbon Conc. (mg/L)	Initial TCE Conc (µg/L)	Equilibrium TCE Conc. (µg/L)	Qe (mg/g)
5.0	253.4	19.7	112.2	10.8	5.14
7.5	253.4	29.6	112.2	6.0	3.59
12.6	253.4	49.7	112.2	3.5	2.19

**Table A.12 Single-solute TCE isotherm data for OAW15 – Run 1**

**Carbon Type: OAW15**  
**Solvent: ultrapure water**  
**Micropollutant: TCE**

Weight of Carbon (mg)	Solvent Volume (mL)	Carbon Conc. (mg/L)	Initial TCE Conc (µg/L)	Equilibrium TCE Conc. (µg/L)	Qe (mg/g)
5.1	253.4	20.1	1279.4	683.8	29.59
8.8	253.4	34.7	1279.4	458.7	23.63
12.8	253.4	50.5	1279.4	291.9	19.55
19.1	253.4	75.4	1279.4	193.1	14.41
25.4	253.4	100.2	1279.4	125.7	11.51
50.6	253.4	199.7	1279.4	40.9	6.20
76.0	253.4	299.9	1279.4	19.6	4.20
101.4	253.4	400.2	1279.4	34.3	3.11
152.0	253.4	599.8	1279.4	7.8	2.12
202.7	253.4	799.9	1279.4	4.5	1.59

**Table A.13 Single-solute TCE isotherm data for OAW15 – Run 2**

**Carbon Type: OAW15**  
**Solvent: ultrapure water**  
**Micropollutant: TCE**

Weight of Carbon (mg)	Solvent Volume (mL)	Carbon Conc. (mg/L)	Initial TCE Conc (µg/L)	Equilibrium TCE Conc. (µg/L)	Qe (mg/g)
15.2	253.4	60.0	112.2	5.6	1.78
28.0	253.4	110.5	112.2	2.1	1.00

**Table A.14 Single-solute TCE isotherm data for OAW20 – Run 1**

**Carbon Type: OAW20**  
**Solvent: ultrapure water**  
**Micropollutant: TCE**

Weight of Carbon (mg)	Solvent Volume (mL)	Carbon Conc. (mg/L)	Initial TCE Conc (µg/L)	Equilibrium TCE Conc. (µg/L)	Qe (mg/g)
5.0	500.0	10.0	1200.8	816.4	38.44
12.7	253.4	50.1	1355.6	339.4	20.28
25.3	253.4	99.8	1355.6	145.9	12.12
38.0	253.4	150.0	1355.6	72.3	8.56
50.6	253.4	199.7	1355.6	44.3	6.57
88.8	253.4	350.4	1355.6	15.0	3.83

**Table A.15 Single-solute TCE isotherm data for OAW20 – Run 2**

**Carbon Type: OAW20**  
**Solvent: ultrapure water**  
**Micropollutant: TCE**

Weight of Carbon (mg)	Solvent Volume (mL)	Carbon Conc. (mg/L)	Initial TCE Conc (µg/L)	Equilibrium TCE Conc. (µg/L)	Qe (mg/g)
12.6	253.4	49.7	129.4	7.8	2.45
25.4	253.4	100.2	129.4	2.5	1.27
50.6	253.4	199.7	129.4	1.2	0.64

**Table A.16 Single-solute TCE isotherm data for HAW10**

**Carbon Type: HAW10**  
**Solvent: ultrapure water**  
**Micropollutant: TCE**

Weight of Carbon (mg)	Solvent Volume (mL)	Carbon Conc. (mg/L)	Initial TCE Conc (µg/L)	Equilibrium TCE Conc. (µg/L)	Qe (mg/g)
5.0	253.4	19.7	1130.3	110.1	51.70
6.4	253.4	25.3	1130.3	81.1	41.54
7.6	253.4	30.0	1130.3	50.2	36.01
9.0	253.4	35.5	1130.3	35.0	30.84
10.1	253.4	39.9	1130.3	37.6	27.41
11.4	253.4	45.0	1130.3	16.5	24.76
12.7	253.4	50.1	1130.3	12.9	22.29
19.0	253.4	75.0	1130.3	6.0	14.99
41.7	253.4	164.6	1130.3	1.3	6.86

**Table A.17 Single-solute TCE isotherm data for HAW15**

**Carbon Type: HAW15**  
**Solvent: ultrapure water**  
**Micropollutant: TCE**

Weight of Carbon (mg)	Solvent Volume (mL)	Carbon Conc. (mg/L)	Initial TCE Conc (µg/L)	Equilibrium TCE Conc. (µg/L)	Qe (mg/g)
5.0	253.4	19.7	1130.3	258.8	44.17
7.5	253.4	29.6	1130.3	127.2	33.89
12.7	253.4	50.1	1130.3	102.2	20.51
19.1	253.4	75.4	1130.3	22.7	14.69
25.2	253.4	99.4	1130.3	15.1	11.21
31.8	253.4	125.5	1130.3	8.6	8.94
38.0	253.4	150.0	1130.3	9.8	7.47
50.7	253.4	200.1	1130.3	6.6	5.62
69.6	253.4	274.7	1130.3	1.7	4.11

**Table A.18 Single-solute TCE isotherm data for HAW20**

**Carbon Type: HAW20**  
**Solvent: ultrapure water**  
**Micropollutant: TCE**

Weight of Carbon (mg)	Solvent Volume (mL)	Carbon Conc. (mg/L)	Initial TCE Conc (µg/L)	Equilibrium TCE Conc. (µg/L)	Qe (mg/g)
7.7	253.4	30.4	1130.3	132.6	32.83
12.7	253.4	50.1	1130.3	62.9	21.30
25.3	253.4	99.8	1130.3	22.2	11.10
31.8	253.4	125.5	1130.3	12.1	8.91
38.0	253.4	150.0	1130.3	9.1	7.48
50.7	253.4	200.1	1130.3	4.0	5.63

**Table A.19 Single-solute TCE isotherm data for AAW10**

**Carbon Type: AAW10**  
**Solvent: ultrapure water**  
**Micropollutant: TCE**

Weight of Carbon (mg)	Solvent Volume (mL)	Carbon Conc. (mg/L)	Initial TCE Conc (µg/L)	Equilibrium TCE Conc. (µg/L)	Qe (mg/g)
5.1	253.4	20.1	1075.1	111.8	47.86
6.2	253.4	24.5	1075.1	84.1	40.50
7.6	253.4	30.0	1075.1	53.2	34.07
8.8	253.4	34.7	1075.1	49.2	29.54
10.0	253.4	39.5	1075.1	37.4	26.30
11.4	253.4	45.0	1075.1	26.7	23.30
12.8	253.4	50.5	1075.1	24.7	20.79
19.1	253.4	75.4	1075.1	15.0	14.06
25.2	253.4	99.4	1075.1	4.2	10.77
41.8	253.4	165.0	1075.1	2.1	6.50

**Table A.20 Single-solute TCE isotherm data for AAW15**

**Carbon Type: AAW15**  
**Solvent: ultrapure water**  
**Micropollutant: TCE**

Weight of Carbon (mg)	Solvent Volume (mL)	Carbon Conc. (mg/L)	Initial TCE Conc (µg/L)	Equilibrium TCE Conc. (µg/L)	Qe (mg/g)
5.0	253.4	19.7	1075.1	246.3	42.00
12.8	253.4	50.5	1075.1	72.5	19.85
19.0	253.4	75.0	1075.1	22.6	14.04
25.4	253.4	100.2	1075.1	17.2	10.55
31.6	253.4	124.7	1075.1	12.6	8.52
37.9	253.4	149.6	1075.1	9.1	7.13
50.7	253.4	200.1	1075.1	4.8	5.35
69.8	253.4	275.5	1075.1	3.0	3.89
109.0	253.4	430.1	1075.1	2.5	2.49

**Table A.21 Single-solute TCE isotherm data for AAW20**

**Carbon Type: AAW20**  
**Solvent: ultrapure water**  
**Micropollutant: TCE**

Weight of Carbon (mg)	Solvent Volume (mL)	Carbon Conc. (mg/L)	Initial TCE Conc (µg/L)	Equilibrium TCE Conc. (µg/L)	Qe (mg/g)
7.6	253.4	30.0	1075.1	187.1	29.61
12.7	253.4	50.1	1075.1	81.3	19.83
19.0	253.4	75.0	1075.1	38.3	13.83
25.3	253.4	99.8	1075.1	25.8	10.51
31.6	253.4	124.7	1075.1	14.1	8.51
38.1	253.4	150.4	1075.1	14.6	7.05
50.6	253.4	199.7	1075.1	6.0	5.35
88.7	253.4	350.0	1075.1	2.2	3.07

**Table A.22 Single-solute TCE isotherm data for F600**

**Carbon Type: F600**  
**Solvent: ultrapure water**  
**Micropollutant: TCE**

Weight of Carbon (mg)	Solvent Volume (mL)	Carbon Conc. (mg/L)	Initial TCE Conc (µg/L)	Equilibrium TCE Conc. (µg/L)	Qe (mg/g)
5.1	253.4	20.1	1020.6	168.9	42.32
6.3	253.4	24.9	1020.6	129.6	35.84
7.6	253.4	30.0	1020.6	65.0	31.86
9.0	253.4	35.5	1020.6	69.9	26.77
10.2	253.4	40.3	1020.6	44.7	24.24
11.4	253.4	45.0	1020.6	40.4	21.79
12.8	253.4	50.5	1020.6	28.7	19.64
19.0	253.4	75.0	1020.6	12.3	13.45
25.2	253.4	99.4	1020.6	7.3	10.19
41.9	253.4	165.4	1020.6	2.8	6.16

**Table A.23 Single-solute TCE isotherm data for G219 – Run 1**

**Carbon Type: G219**  
**Solvent: ultrapure water**  
**Micropollutant: TCE**

Weight of Carbon (mg)	Solvent Volume (mL)	Carbon Conc. (mg/L)	Initial TCE Conc (µg/L)	Equilibrium TCE Conc. (µg/L)	Qe (mg/g)
5.1	253.4	20.1	1049.5	292.8	37.60
6.3	253.4	24.9	1049.5	198.8	34.22
7.6	253.4	30.0	1049.5	148.2	30.05
8.9	253.4	35.1	1049.5	106.1	26.86
10.1	253.4	39.9	1049.5	79.0	24.35
11.3	253.4	44.6	1049.5	64.0	22.10
12.6	253.4	49.7	1049.5	53.8	20.02
19.0	253.4	75.0	1049.5	31.2	13.58
25.3	253.4	99.8	1049.5	30.3	10.21
37.3	253.4	147.2	1049.5	10.5	7.06

**Table A.24 Single-solute TCE isotherm data for G219 – Run 2**

**Carbon Type: G219**  
**Solvent: ultrapure water**  
**Micropollutant: TCE**

Weight of Carbon (mg)	Solvent Volume (mL)	Carbon Conc. (mg/L)	Initial TCE Conc (µg/L)	Equilibrium TCE Conc. (µg/L)	Qe (mg/g)
50.9	253.4	200.9	1192.3	4.2	5.91
44.5	126.8	350.9	1423.3	2.3	4.05

**Table A.25 Single-solute TCE isotherm data for Picazine – Run 1**

**Carbon Type: Picazine**  
**Solvent: ultrapure water**  
**Micropollutant: TCE**

Weight of Carbon (mg)	Solvent Volume (mL)	Carbon Conc. (mg/L)	Initial TCE Conc (µg/L)	Equilibrium TCE Conc. (µg/L)	Qe (mg/g)
76.0	253.4	299.9	1192.3	263.0	3.10
76.1	126.8	600.2	1423.3	151.6	2.12

**Table A.26 Single-solute TCE isotherm data for Picazine – Run 2**

**Carbon Picazine**  
**Type:**  
**Solvent: ultrapure water**  
**Micropollutant: TCE**

Weight of Carbon (mg)	Solvent Volume (mL)	Carbon Conc. (mg/L)	Initial TCE Conc (µg/L)	Equilibrium TCE Conc. (µg/L)	Qe (mg/g)
5.1	253.4	20.1	124.5	88.1	1.81
10.1	253.4	39.9	124.5	76.3	1.21
25.2	253.4	99.4	124.5	34.7	0.90
38.1	253.4	150.4	124.5	22.7	0.68
50.8	253.4	200.5	124.5	15.2	0.55
38.1	126.8	300.5	148.4	12.1	0.45
50.9	126.8	401.4	148.4	7.0	0.35
63.4	126.8	500.0	148.4	6.3	0.28

**Table A.27 Single-solute MTBE isotherm data for AW10 – Run 1**

**Carbon Type: AW10**  
**Solvent: ultrapure water**  
**Micropollutant: MTBE**

Weight of Carbon (mg)	Solvent Volume (mL)	Carbon Conc. (mg/L)	Initial TCE Conc (µg/L)	Equilibrium TCE Conc. (µg/L)	Qe (mg/g)
25.3	253.4	99.8	864.8	486.7	3.787
63.4	253.4	250.2	864.8	276.9	2.350
126.7	253.4	500.0	864.8	92.7	1.544
190.2	253.4	750.6	864.8	55.6	1.078
253.5	253.4	1000.4	864.8	37.7	0.827
380.1	253.4	1500.0	864.8	19.9	0.563
506.9	253.4	2000.4	864.8	13.9	0.425
887.1	253.4	3500.8	864.8	7.3	0.245

**Table A.28 Single-solute MTBE isotherm data for AW10 – Run 2**

**Carbon Type: AW10**  
**Solvent: ultrapure water**  
**Micropollutant: MTBE**

Weight of Carbon (mg)	Solvent Volume (mL)	Carbon Conc. (mg/L)	Initial TCE Conc (µg/L)	Equilibrium TCE Conc. (µg/L)	Qe (mg/g)
63.5	253.4	250.6	1108.9	379.5	2.911
126.8	253.4	500.4	1108.9	157.5	1.901
190.2	253.4	750.6	1108.9	93.1	1.353
253.5	253.4	1000.4	1108.9	56.2	1.052
380.2	253.4	1500.4	1108.9	32.1	0.718
506.9	253.4	2000.4	1108.9	20.0	0.544
886.9	253.4	3500.0	1108.9	10.2	0.314

**Table A.29 Single-solute MTBE isotherm data for AW10 – Run 3**

**Carbon Type: AW10**  
**Solvent: ultrapure water**  
**Micropollutant: MTBE**

Weight of Carbon (mg)	Solvent Volume (mL)	Carbon Conc. (mg/L)	Initial TCE Conc (µg/L)	Equilibrium TCE Conc. (µg/L)	Qe (mg/g)
50.7	126.8	399.8	119.7	6.0	0.284
85.7	126.8	675.9	119.7	2.8	0.173

**Table A.30 Single-solute MTBE isotherm data for AW15**

**Carbon Type: AW15**  
**Solvent: ultrapure water**  
**Micropollutant: MTBE**

Weight of Carbon (mg)	Solvent Volume (mL)	Carbon Conc. (mg/L)	Initial TCE Conc (µg/L)	Equilibrium TCE Conc. (µg/L)	Qe (mg/g)
12.6	253.4	49.7	864.8	498.1	7.375
25.4	253.4	100.2	864.8	329.2	5.344
63.4	253.4	250.2	864.8	130.9	2.933
126.7	253.4	500.0	864.8	48.0	1.634
190.2	253.4	750.6	864.8	25.1	1.119
253.5	253.4	1000.4	864.8	15.3	0.849
380.1	253.4	1500.0	864.8	8.2	0.571
506.7	253.4	1999.6	864.8	5.5	0.430
760.0	253.4	2999.2	864.8	3.0	0.287
1140.6	253.4	4501.2	864.8	2.0	0.192

**Table A.31 Single-solute MTBE isotherm data for AW20**

**Carbon Type: AW20**  
**Solvent: ultrapure water**  
**Micropollutant: MTBE**

Weight of Carbon (mg)	Solvent Volume (mL)	Carbon Conc. (mg/L)	Initial TCE Conc (µg/L)	Equilibrium TCE Conc. (µg/L)	Qe (mg/g)
25.3	253.4	99.8	864.8	359.1	5.065
63.3	253.4	249.8	864.8	151.2	2.857
126.7	253.4	500.0	864.8	57.9	1.614
190.0	253.4	749.8	864.8	32.0	1.111
253.5	253.4	1000.4	864.8	21.2	0.843
380.1	253.4	1500.0	864.8	11.9	0.569
506.9	253.4	2000.4	864.8	7.8	0.428
761.0	253.4	3003.2	864.8	4.6	0.286
1267.3	253.4	5001.2	864.8	2.1	0.173
1900.2	253.4	7498.8	864.8	1.4	0.115

**Table A.32 Single-solute MTBE isotherm data for OAW10 – Run 1**

**Carbon Type: OAW10**  
**Solvent: ultrapure water**  
**Micropollutant: MTBE**

Weight of Carbon (mg)	Solvent Volume (mL)	Carbon Conc. (mg/L)	Initial TCE Conc (µg/L)	Equilibrium TCE Conc. (µg/L)	Qe (mg/g)
12.7	253.4	50.1	1575.8	1401.5	3.477
25.2	253.4	99.4	1575.8	1264.3	3.132
63.5	253.4	250.6	1575.8	950.4	2.496
126.6	253.4	499.6	1575.8	606.5	1.940
190.0	253.4	749.8	1575.8	392.7	1.578
253.3	253.4	999.6	1575.8	297.0	1.279
380.2	253.4	1500.4	1575.8	174.1	0.934
506.9	253.4	2000.4	1575.8	120.4	0.728
886.9	253.4	3500.0	1575.8	53.6	0.435
1394.3	253.4	5502.4	1575.8	27.1	0.281

**Table A.33 Single-solute MTBE isotherm data for OAW10 – Run 2**

**Carbon Type: OAW10**  
**Solvent: ultrapure water**  
**Micropollutant: MTBE**

Weight of Carbon (mg)	Solvent Volume (mL)	Carbon Conc. (mg/L)	Initial TCE Conc (µg/L)	Equilibrium TCE Conc. (µg/L)	Qe (mg/g)
76.1	126.8	76.2	119.7	600.9	10.550
126.8	126.8	126.9	119.7	1000.8	4.700
221.9	126.8	221.1	119.7	1743.7	1.700

**Table A.34 Single-solute MTBE isotherm data for OAW15 – Run 1**

**Carbon Type: OAW15**  
**Solvent: ultrapure water**  
**Micropollutant: MTBE**

Weight of Carbon (mg)	Solvent Volume (mL)	Carbon Conc. (mg/L)	Initial TCE Conc (µg/L)	Equilibrium TCE Conc. (µg/L)	Qe (mg/g)
25.4	253.4	100.2	1575.8	1219.6	3.554
63.4	253.4	250.2	1575.8	888.7	2.746
126.8	253.4	500.4	1575.8	550.7	2.049
190.0	253.4	749.8	1575.8	395.1	1.575
253.4	253.4	1000.0	1575.8	278.4	1.297
380.0	253.4	1499.6	1575.8	171.9	0.936
506.7	253.4	1999.6	1575.8	118.6	0.729
760.2	253.4	3000.0	1575.8	66.7	0.503
1013.4	253.4	3999.2	1575.8	43.3	0.383
1647.1	253.4	6500.0	1575.8	19.9	0.239

**Table A.35 Single-solute MTBE isotherm data for OAW15 – Run 2**

**Carbon Type: OAW15**  
**Solvent: ultrapure water**  
**Micropollutant: MTBE**

Weight of Carbon (mg)	Solvent Volume (mL)	Carbon Conc. (mg/L)	Initial TCE Conc (µg/L)	Equilibrium TCE Conc. (µg/L)	Qe (mg/g)
76.0	126.8	599.4	119.7	10.3	0.182
253.3	126.8	1997.6	119.7	2.0	0.059

**Table A.36 Single-solute MTBE isotherm data for OAW20 – Run 1**

**Carbon Type: OAW20**  
**Solvent: ultrapure water**  
**Micropollutant: MTBE**

Weight of Carbon (mg)	Solvent Volume (mL)	Carbon Conc. (mg/L)	Initial TCE Conc (µg/L)	Equilibrium TCE Conc. (µg/L)	Q <sub>e</sub> (mg/g)
25.3	253.4	100.0	949.0	711.8	2.373
44.4	126.8	350.2	981.0	446.1	1.528
126.8	126.8	1000.0	981.0	160.4	0.821

**Table A.37 Single-solute MTBE isotherm data for OAW20 – Run 2**

**Carbon Type: OAW20**  
**Solvent: ultrapure water**  
**Micropollutant: MTBE**

Weight of Carbon (mg)	Solvent Volume (mL)	Carbon Conc. (mg/L)	Initial TCE Conc (µg/L)	Equilibrium TCE Conc. (µg/L)	Q <sub>e</sub> (mg/g)
12.7	253.4	50.1	106.4	77.6	0.575
25.3	253.4	99.8	106.4	62.5	0.440
31.7	126.8	250.0	116.4	31.1	0.341
63.4	126.8	500.0	116.4	13.5	0.206
126.8	126.8	1000.0	116.4	6.0	0.110
253.6	126.8	2000.0	116.4	2.7	0.057
380.4	126.8	3000.0	116.4	2.1	0.038

**Table A.38 Single-solute MTBE isotherm data for HAW10**

**Carbon Type: HAW10**  
**Solvent: ultrapure water**  
**Micropollutant: MTBE**

Weight of Carbon (mg)	Solvent Volume (mL)	Carbon Conc. (mg/L)	Initial TCE Conc ( $\mu\text{g/L}$ )	Equilibrium TCE Conc. ( $\mu\text{g/L}$ )	Qe (mg/g)
63.4	253.4	250.2	1213.3	256.2	3.826
126.6	253.4	499.6	1213.3	87.1	2.254
190.2	253.4	750.6	1213.3	65.0	1.530
253.3	253.4	999.6	1213.3	31.7	1.182
380.1	253.4	1500.0	1213.3	14.6	0.799
506.8	253.4	2000.0	1213.3	9.9	0.602
886.8	253.4	3499.6	1213.3	2.7	0.346

**Table A.39 Single-solute MTBE isotherm data for HAW15**

**Carbon Type: HAW15**  
**Solvent: ultrapure water**  
**Micropollutant: MTBE**

Weight of Carbon (mg)	Solvent Volume (mL)	Carbon Conc. (mg/L)	Initial TCE Conc ( $\mu\text{g/L}$ )	Equilibrium TCE Conc. ( $\mu\text{g/L}$ )	Qe (mg/g)
12.7	253.4	50.1	1213.3	719.9	9.845
25.2	253.4	99.4	1213.3	455.0	7.625
63.3	253.4	249.8	1213.3	157.4	4.227
126.8	253.4	500.4	1213.3	53.5	2.318
190.0	253.4	749.8	1213.3	28.3	1.580
253.4	253.4	1000.0	1213.3	15.9	1.197
380.2	253.4	1500.4	1213.3	9.5	0.802
506.8	253.4	2000.0	1213.3	5.4	0.604
760.2	253.4	3000.0	1213.3	3.2	0.403
1140.3	253.4	4500.0	1213.3	2.1	0.269

**Table A.40 Single-solute MTBE isotherm data for HAW20**

**Carbon Type: HAW20**  
**Solvent: ultrapure water**  
**Micropollutant: MTBE**

Weight of Carbon (mg)	Solvent Volume (mL)	Carbon Conc. (mg/L)	Initial TCE Conc (µg/L)	Equilibrium TCE Conc. (µg/L)	Qe (mg/g)
25.4	253.4	100.2	1213.3	470.3	7.413
63.4	253.4	250.2	1213.3	188.0	4.098
126.7	253.4	500.0	1213.3	64.9	2.297
190.0	253.4	749.8	1213.3	33.8	1.573
253.3	253.4	999.6	1213.3	21.6	1.192
380.0	253.4	1499.6	1213.3	9.8	0.803
506.9	253.4	2000.4	1213.3	5.9	0.604
760.2	253.4	3000.0	1213.3	2.8	0.404

**Table A.41 Single-solute MTBE isotherm data for AAW10 – Run 1**

**Carbon Type: AAW10**  
**Solvent: ultrapure water**  
**Micropollutant: MTBE**

Weight of Carbon (mg)	Solvent Volume (mL)	Carbon Conc. (mg/L)	Initial TCE Conc (µg/L)	Equilibrium TCE Conc. (µg/L)	Qe (mg/g)
25.3	253.4	99.8	1031.1	507.0	5.249
63.5	253.4	250.6	1031.1	196.2	3.332
126.6	253.4	499.6	1031.1	73.1	1.917
506.8	253.4	2000.0	1031.1	8.3	0.516

**Table A.42 Single-solute MTBE isotherm data for AAW10 – Run 2**

**Carbon Type: AAW10**  
**Solvent: ultrapure water**  
**Micropollutant: MTBE**

Weight of Carbon (mg)	Solvent Volume (mL)	Carbon Conc. (mg/L)	Initial TCE Conc (µg/L)	Equilibrium TCE Conc. (µg/L)	Qe (mg/g)
8.9	253.4	35.1	385.8	369.6	0.462
190.2	253.4	750.6	385.8	36.0	0.466
886.9	253.4	3500.0	385.8	1.9	0.110

**Table A.43 Single-solute MTBE isotherm data for AAW15 – Run 1**

**Carbon Type: AAW15**  
**Solvent: ultrapure water**  
**Micropollutant: MTBE**

Weight of Carbon (mg)	Solvent Volume (mL)	Carbon Conc. (mg/L)	Initial TCE Conc (µg/L)	Equilibrium TCE Conc. (µg/L)	Qe (mg/g)
12.7	253.4	50.1	1031.1	652.9	7.545
25.4	253.4	100.2	1031.1	487.8	5.420
126.6	253.4	499.6	1031.1	72.3	1.919
190.1	253.4	750.2	1031.1	39.4	1.322
1140.5	253.4	4500.8	1031.1	1.4	0.229

**Table A.44 Single-solute MTBE isotherm data for AAW15 – Run 2**

**Carbon Type: AAW15**  
**Solvent: ultrapure water**  
**Micropollutant: MTBE**

Weight of Carbon (mg)	Solvent Volume (mL)	Carbon Conc. (mg/L)	Initial TCE Conc (µg/L)	Equilibrium TCE Conc. (µg/L)	Qe (mg/g)
63.3	253.4	249.8	385.8	112.5	1.094
253.4	253.4	1000.0	385.8	13.3	0.373
506.9	253.4	2000.4	385.8	3.7	0.191
760.1	253.4	2999.6	385.8	2.2	0.128

**Table A.45 Single-solute MTBE isotherm data for AAW20 – Run 1**

**Carbon Type: AAW20**  
**Solvent: ultrapure water**  
**Micropollutant: MTBE**

Weight of Carbon (mg)	Solvent Volume (mL)	Carbon Conc. (mg/L)	Initial TCE Conc (µg/L)	Equilibrium TCE Conc. (µg/L)	Qe (mg/g)
63.3	253.4	249.8	1031.1	207.8	3.296
253.4	253.4	1000.0	1031.1	27.8	1.003
380.1	253.4	1500.0	1031.1	14.1	0.678
506.7	253.4	1999.6	1031.1	9.1	0.511
760.1	253.4	2999.6	1031.1	6.6	0.342
1267.1	253.4	5000.4	1031.1	2.4	0.206
1900.6	253.4	7500.4	1031.1	1.7	0.137

**Table A.46 Single-solute MTBE isotherm data for AAW20 – Run 2**

**Carbon Type: AAW20**  
**Solvent: ultrapure water**  
**Micropollutant: MTBE**

Weight of Carbon (mg)	Solvent Volume (mL)	Carbon Conc. (mg/L)	Initial TCE Conc (µg/L)	Equilibrium TCE Conc. (µg/L)	Qe (mg/g)
25.3	253.4	99.8	385.8	236.2	1.499
126.8	253.4	500.4	385.8	59.2	0.653
190.1	253.4	750.2	385.8	31.8	0.472

**Table A.47 Single-solute MTBE isotherm data for F600**

**Carbon Type: F600**  
**Solvent: ultrapure water**  
**Micropollutant: MTBE**

Weight of Carbon (mg)	Solvent Volume (mL)	Carbon Conc. (mg/L)	Initial TCE Conc (µg/L)	Equilibrium TCE Conc. (µg/L)	Qe (mg/g)
6.2	253.4	24.5	1057.7	954.3	4.227
12.7	253.4	50.1	1057.7	866.5	3.815
25.4	253.4	100.2	1057.7	695.0	3.619
63.4	253.4	250.2	1057.7	372.2	2.740
126.8	253.4	500.4	1057.7	158.6	1.797
190.2	253.4	750.6	1057.7	82.7	1.299
253.4	253.4	1000.0	1057.7	46.9	1.011
380.1	253.4	1500.0	1057.7	22.6	0.690
506.7	253.4	1999.6	1057.7	13.1	0.522
887.0	253.4	3500.4	1057.7	4.5	0.301

**Table A.48 Single-solute MTBE isotherm data for G219**

**Carbon Type: G219**  
**Solvent: ultrapure water**  
**Micropollutant: MTBE**

Weight of Carbon (mg)	Solvent Volume (mL)	Carbon Conc. (mg/L)	Initial TCE Conc (µg/L)	Equilibrium TCE Conc. (µg/L)	Q <sub>e</sub> (mg/g)
6.4	253.4	25.3	1057.7	929.9	5.061
12.8	253.4	50.5	1057.7	817.5	4.756
25.3	253.4	99.8	1057.7	650.4	4.080
63.4	253.4	250.2	1057.7	341.3	2.863
126.7	253.4	500.0	1057.7	142.7	1.830
190.0	253.4	749.8	1057.7	73.1	1.313
253.3	253.4	999.6	1057.7	43.8	1.014
380.1	253.4	1500.0	1057.7	20.0	0.692
506.9	253.4	2000.4	1057.7	12.7	0.522
886.9	253.4	3500.0	1057.7	6.2	0.300

**Table A.49 Single-solute MTBE isotherm data for Picazine – Run 1**

**Carbon Type: Picazine**  
**Solvent: ultrapure water**  
**Micropollutant: MTBE**

Weight of Carbon (mg)	Solvent Volume (mL)	Carbon Conc. (mg/L)	Initial TCE Conc (µg/L)	Equilibrium TCE Conc. (µg/L)	Q <sub>e</sub> (mg/g)
25.3	253.4	99.8	1063.1	995.6	0.676
63.4	253.4	250.2	1063.1	902.7	0.641
126.8	253.4	500.4	1063.1	816.4	0.493
253.5	253.4	1000.4	1063.1	661.1	0.402
380.2	253.4	1500.4	1063.1	528.7	0.356
506.8	253.4	2000.0	1063.1	426.3	0.318
887.0	253.4	3500.4	1063.1	256.8	0.230

**Table A.50 Single-solute MTBE isotherm data for Picazine – Run 2**

**Carbon Type: Picazine**  
**Solvent: ultrapure water**  
**Micropollutant: MTBE**

Weight of Carbon (mg)	Solvent Volume (mL)	Carbon Conc. (mg/L)	Initial TCE Conc (µg/L)	Equilibrium TCE Conc. (µg/L)	Qe (mg/g)
126.7	126.8	999.2	105.4	50.7	0.0548
253.8	126.8	2001.6	105.4	32.3	0.0365
507.5	126.8	4002.4	105.4	19.2	0.0215

**Table A.51 Data from TCE isotherms in the presence of NOM for AW10 – Run 1**

**Carbon Type: AW10**  
**Solvent: SJDW**  
**Micropollutant: TCE**

Weight of Carbon (mg)	Solvent Volume (mL)	Carbon Conc. (mg/L)	Initial TCE Conc (µg/L)	Equilibrium TCE Conc. (µg/L)	Qe (mg/g)
2.0	1060.0	1.9	117.4	94.4	12.172
5.1	1060.0	4.8	117.4	50.8	13.835
5.1	500.0	10.2	117.4	12.9	10.242
7.3	500.0	14.6	117.4	5.5	7.662
5.2	253.4	20.5	117.4	2.8	5.583
6.4	253.4	25.3	117.4	1.8	4.576
7.6	253.4	30.0	117.4	1.4	3.867
8.9	253.4	35.1	117.4	1.7	3.295
10.0	253.4	39.5	117.4	1.1	2.946
12.9	253.4	50.9	117.4	1.2	2.282

**Table A.52 Data from TCE isotherms in the presence of NOM for AW10 – Run 2**

**Carbon Type: AW10  
Solvent: SJDW  
Micropollutant: TCE**

Weight of Carbon (mg)	Solvent Volume (mL)	Carbon Conc. (mg/L)	Initial TCE Conc (µg/L)	Equilibrium TCE Conc. (µg/L)	Qe (mg/g)
2.1	1060.0	2.0	123.0	86.4	18.449
5.4	1060.0	5.1	123.0	41.7	15.949
8.0	1060.0	7.5	123.0	22.2	13.349
5.1	500.0	10.2	108.7	17.9	8.902
7.5	500.0	15.0	108.7	7.3	6.760
5.1	253.4	20.1	116.8	7.5	5.431
6.3	253.4	24.9	116.8	4.2	4.529
7.5	253.4	29.6	116.8	3.2	3.840
8.9	253.4	35.1	116.8	3.6	3.223
10.0	253.4	39.5	116.8	2.9	2.886

**Table A.53 Data from TCE isotherms in the presence of NOM for AW15 – Run 1**

**Carbon Type: AW15  
Solvent: SJDW  
Micropollutant: TCE**

Weight of Carbon (mg)	Solvent Volume (mL)	Carbon Conc. (mg/L)	Initial TCE Conc (µg/L)	Equilibrium TCE Conc. (µg/L)	Qe (mg/g)
5.2	1060.0	4.9	117.4	66.4	10.39
5.0	500.0	10.0	117.4	29.9	8.75
6.3	253.4	24.9	117.4	7.5	4.42
12.6	253.4	49.7	117.4	2.5	2.31
19.0	253.4	75.0	117.4	1.5	1.55
25.5	253.4	100.6	117.4	1.1	1.16

**Table A.54 Data from TCE isotherms in the presence of NOM for AW15 – Run 2**

**Carbon Type: AW15  
Solvent: SJDW  
Micropollutant: TCE**

Weight of Carbon (mg)	Solvent Volume (mL)	Carbon Conc. (mg/L)	Initial TCE Conc (µg/L)	Equilibrium TCE Conc. (µg/L)	Qe (mg/g)
5.4	1060.0	5.1	125.3	84.1	8.09
4.9	500.0	9.8	125.3	50.2	7.66
6.4	500.0	12.8	125.3	38.1	6.82
7.6	500.0	15.2	125.3	26.5	6.50
5.0	253.4	19.7	125.3	19.7	5.35
12.8	253.4	50.5	125.3	4.7	2.39
19.1	253.4	75.4	125.3	1.6	1.64
25.3	253.4	99.8	125.3	1.2	1.24

**Table A.55 Data from TCE isotherms in the presence of NOM for AW20**

**Carbon Type: AW20  
Solvent: SJDW  
Micropollutant: TCE**

Weight of Carbon (mg)	Solvent Volume (mL)	Carbon Conc. (mg/L)	Initial TCE Conc (µg/L)	Equilibrium TCE Conc. (µg/L)	Qe (mg/g)
5.1	500.0	10.2	114.8	53.5	6.01
5.0	253.4	19.7	122.2	31.8	4.58
7.6	253.4	30.0	122.2	17.3	3.50
10.2	253.4	40.3	122.2	10.0	2.79
12.7	253.4	50.1	122.2	8.0	2.28
18.9	253.4	74.6	122.2	4.3	1.58
25.4	253.4	100.2	122.2	2.5	1.19

**Table A.56 Data from TCE isotherms in the presence of NOM for OAW10**

**Carbon Type: OAW10  
Solvent: SJDW  
Micropollutant: TCE**

Weight of Carbon (mg)	Solvent Volume (mL)	Carbon Conc. (mg/L)	Initial TCE Conc (µg/L)	Equilibrium TCE Conc. (µg/L)	Qe (mg/g)
5.2	1060.0	4.9	119.2	62.4	11.59
5.0	500.0	10.0	117.2	39.6	7.76
7.5	500.0	15.0	117.2	29.3	5.86
5.1	253.4	20.1	118.2	20.8	4.84
7.1	235.4	30.2	118.2	13.4	3.47
9.5	235.4	40.4	118.2	9.0	2.71
11.8	235.4	50.1	118.2	6.2	2.23
14.1	235.4	59.9	118.2	4.6	1.90

**Table A.57 Data from TCE isotherms in the presence of NOM for OAW15 – Run 1**

**Carbon Type: OAW15  
Solvent: SJDW  
Micropollutant: TCE**

Weight of Carbon (mg)	Solvent Volume (mL)	Carbon Conc. (mg/L)	Initial TCE Conc (µg/L)	Equilibrium TCE Conc. (µg/L)	Qe (mg/g)
5.0	500.0	10.0	117.2	77.9	3.93
5.1	253.4	20.1	118.2	46.3	3.57
10.2	253.4	40.3	118.2	29.6	2.20
15.3	253.4	60.4	118.2	14.3	1.72
20.3	253.4	80.1	118.2	9.7	1.35
25.3	253.4	99.8	118.2	7.3	1.11
38.0	253.4	150.0	118.2	4.8	0.76
50.9	253.4	200.9	118.2	3.6	0.57

**Table A.58 Data from TCE isotherms in the presence of NOM for OAW15 – Run 2**

**Carbon Type: OAW15  
Solvent: SJDW  
Micropollutant: TCE**

Weight of Carbon (mg)	Solvent Volume (mL)	Carbon Conc. (mg/L)	Initial TCE Conc (µg/L)	Equilibrium TCE Conc. (µg/L)	Qe (mg/g)
5.1	500.0	10.2	107.9	88.5	1.90
5.1	253.4	20.1	108.8	42.9	3.27
10.0	253.4	39.5	108.8	21.9	2.20
15.3	253.4	60.4	108.8	11.0	1.62
25.4	253.4	100.2	108.8	8.6	1.00
38.1	253.4	150.4	108.8	5.4	0.69
50.7	253.4	200.1	108.8	4.3	0.52

**Table A.59 Data from TCE isotherms in the presence of NOM for OAW20**

**Carbon Type: OAW20  
Solvent: SJDW  
Micropollutant: TCE**

Weight of Carbon (mg)	Solvent Volume (mL)	Carbon Conc. (mg/L)	Initial TCE Conc (µg/L)	Equilibrium TCE Conc. (µg/L)	Qe (mg/g)
5.3	1060.0	5.0	110.2	104.1	1.22
7.4	500.0	14.8	107.9	86.5	1.45
6.4	253.4	25.3	108.8	56.6	2.07
10.2	253.4	40.3	108.8	38.8	1.74
19.0	253.4	75.0	108.8	20.3	1.18
25.3	253.4	99.8	108.8	14.8	0.94
50.6	253.4	199.7	108.8	6.4	0.51
76.0	253.4	299.9	108.8	3.4	0.35

**Table A.60 Data from TCE isotherms in the presence of NOM for HAW10 – Run 1**

**Carbon Type: HAW10  
Solvent: SJDW  
Micropollutant: TCE**

Weight of Carbon (mg)	Solvent Volume (mL)	Carbon Conc. (mg/L)	Initial TCE Conc (µg/L)	Equilibrium TCE Conc. (µg/L)	Qe (mg/g)
2.7	1060.0	2.5	131.2	74.5	22.25
5.4	1060.0	5.1	131.2	30.8	19.70
8.1	1060.0	7.6	131.2	15.8	15.10
5.1	500.0	10.2	131.2	5.3	12.34
6.4	500.0	12.8	131.2	2.9	10.02
7.5	500.0	15.0	131.2	2.3	8.59
8.8	500.0	17.6	131.2	2.9	7.29
5.1	253.4	20.1	131.2	1.9	6.42

**Table A.61 Data from TCE isotherms in the presence of NOM for HAW10 – Run 2**

**Carbon Type: HAW10  
Solvent: SJDW  
Micropollutant: TCE**

Weight of Carbon (mg)	Solvent Volume (mL)	Carbon Conc. (mg/L)	Initial TCE Conc (µg/L)	Equilibrium TCE Conc. (µg/L)	Qe (mg/g)
3.7	1060.0	3.5	118.3	60.3	16.60
8.6	1060.0	8.1	118.3	18.2	12.34

**Table A.62 Data from TCE isotherms in the presence of NOM for HAW10 – Run 3**

**Carbon Type: HAW10  
Solvent: SJDW  
Micropollutant: TCE**

Weight of Carbon (mg)	Solvent Volume (mL)	Carbon Conc. (mg/L)	Initial TCE Conc (µg/L)	Equilibrium TCE Conc. (µg/L)	Qe (mg/g)
5.1	500.0	10.2	114.8	5.2	10.75
5.5	500.0	11.0	114.8	5.3	9.95
6.6	500.0	13.2	114.8	2.3	8.52

**Table A.63 Data from TCE isotherms in the presence of NOM for HAW15 – Run 1**

**Carbon Type: HAW15  
Solvent: SJDW  
Micropollutant: TCE**

Weight of Carbon (mg)	Solvent Volume (mL)	Carbon Conc. (mg/L)	Initial TCE Conc (µg/L)	Equilibrium TCE Conc. (µg/L)	Qe (mg/g)
2.0	1060.0	1.9	131.2	107.6	12.49
5.4	1060.0	5.1	131.2	60.3	13.92
5.1	500.0	10.2	131.2	25.4	10.37
5.1	253.4	20.1	131.2	9.5	6.05
8.8	253.4	34.7	131.2	3.5	3.68
12.6	253.4	49.7	131.2	1.8	2.60

**Table A.64 Data from TCE isotherms in the presence of NOM for HAW15 – Run 2**

**Carbon Type: HAW15  
Solvent: SJDW  
Micropollutant: TCE**

Weight of Carbon (mg)	Solvent Volume (mL)	Carbon Conc. (mg/L)	Initial TCE Conc (µg/L)	Equilibrium TCE Conc. (µg/L)	Qe (mg/g)
7.2	1060.0	6.8	118.3	45.8	10.67
7.7	500.0	15.4	118.3	13.4	6.81

**Table A.65 Data from TCE isotherms in the presence of NOM for HAW20 – Run 1**

**Carbon Type: HAW20  
Solvent: SJDW  
Micropollutant: TCE**

Weight of Carbon (mg)	Solvent Volume (mL)	Carbon Conc. (mg/L)	Initial TCE Conc (µg/L)	Equilibrium TCE Conc. (µg/L)	Qe (mg/g)
5.3	1060.0	5.0	131.2	83.2	9.59
5.0	500.0	10.0	131.2	40.4	9.08
6.4	253.4	25.3	131.2	9.8	4.81
12.6	253.4	49.7	131.2	3.6	2.57
18.9	253.4	74.6	131.2	1.6	1.74

**Table A.66 Data from TCE isotherms in the presence of NOM for HAW20 – Run 2**

**Carbon Type: HAW20  
Solvent: SJDW  
Micropollutant: TCE**

Weight of Carbon (mg)	Solvent Volume (mL)	Carbon Conc. (mg/L)	Initial TCE Conc (µg/L)	Equilibrium TCE Conc. (µg/L)	Qe (mg/g)
7.5	1060	7.07547	118.3	60.2	8.20
7.4	500	14.8	118.3	19.8	6.65
5	253.4	19.7316	118.3	14.7	5.25
7.7	253.4	30.3867	118.3	6	3.69

**Table A.67 Data from TCE isotherms in the presence of NOM for AAW10**

**Carbon Type: AAW10  
Solvent: SJDW  
Micropollutant: TCE**

Weight of Carbon (mg)	Solvent Volume (mL)	Carbon Conc. (mg/L)	Initial TCE Conc (µg/L)	Equilibrium TCE Conc. (µg/L)	Qe (mg/g)
5.2	1060.0	4.9	132.2	49.9	16.77
7.9	1060.0	7.5	132.2	35.7	12.94
5.1	500.0	10.2	114.8	19.4	9.35
7.6	500.0	15.2	114.8	5.2	7.21
5.1	253.4	20.1	122.2	5.4	5.80
7.5	253.4	29.6	122.2	2.4	4.05
10.0	253.4	39.5	122.2	1.3	3.06

**Table A.68 Data from TCE isotherms in the presence of NOM for AAW15**

**Carbon Type: AAW15  
Solvent: SJDW  
Micropollutant: TCE**

Weight of Carbon (mg)	Solvent Volume (mL)	Carbon Conc. (mg/L)	Initial TCE Conc (µg/L)	Equilibrium TCE Conc. (µg/L)	Qe (mg/g)
5.2	1060.0	4.9	110.1	69.1	8.35
5.0	500.0	10.0	110.1	52.1	5.80
6.4	253.4	25.3	110.1	12.3	3.87
12.7	253.4	50.1	110.1	4.1	2.12
19.0	253.4	75.0	110.1	1.6	1.45

**Table A.69 Data from TCE isotherms in the presence of NOM for AAW20**

**Carbon Type: AAW20  
Solvent: SJDW  
Micropollutant: TCE**

Weight of Carbon (mg)	Solvent Volume (mL)	Carbon Conc. (mg/L)	Initial TCE Conc (µg/L)	Equilibrium TCE Conc. (µg/L)	Qe (mg/g)
5.4	1060.0	5.1	110.1	76.3	6.63
4.9	500.0	9.8	110.1	65.4	4.56
5.0	253.4	19.7	110.1	21.1	4.51
7.7	253.4	30.4	110.1	8.1	3.36
10.2	253.4	40.3	110.1	4.7	2.62
15.3	253.4	60.4	110.1	2.9	1.78
20.6	253.4	81.3	110.1	1.4	1.34

**Table A.70 Data from TCE isotherms in the presence of NOM for F600**

**Carbon Type: F600  
Solvent: SJDW  
Micropollutant: TCE**

Weight of Carbon (mg)	Solvent Volume (mL)	Carbon Conc. (mg/L)	Initial TCE Conc (µg/L)	Equilibrium TCE Conc. (µg/L)	Qe (mg/g)
2.3	1060.0	2.2	118.2	69.3	22.54
5.1	500.0	10.2	105.4	17.9	8.58
7.7	500.0	15.4	105.4	8.7	6.28
5.2	253.4	20.5	124.2	6.7	5.73
7.6	253.4	30.0	124.2	3.4	4.03
10.2	253.4	40.3	124.2	2.3	3.03

**Table A.71 Data from TCE isotherms in the presence of NOM for G219**

**Carbon Type: G219  
Solvent: SJDW  
Micropollutant: TCE**

Weight of Carbon (mg)	Solvent Volume (mL)	Carbon Conc. (mg/L)	Initial TCE Conc (µg/L)	Equilibrium TCE Conc. (µg/L)	Qe (mg/g)
5.0	500.0	10.0	165.3	50.4	11.49
7.5	500.0	15.0	165.3	26.6	9.24
5.3	253.4	20.9	165.3	19.5	6.97
6.5	253.4	25.7	165.3	14.3	5.88
7.7	253.4	30.4	165.3	9.2	5.14
8.9	253.4	35.1	165.3	6.5	4.52
10.1	253.4	39.9	165.3	9.2	3.92

**Table A.72 Data from TCE isotherms in the presence of NOM for Picazine**

**Carbon Type: Picazine  
Solvent: SJDW  
Micropollutant: TCE**

Weight of Carbon (mg)	Solvent Volume (mL)	Carbon Conc. (mg/L)	Initial TCE Conc (µg/L)	Equilibrium TCE Conc. (µg/L)	Qe (mg/g)
12.8	253.4	50.5	124.2	75.5	0.964
25.4	253.4	100.2	124.2	44.7	0.793
32.0	126.8	252.4	138.2	17.0	0.480
63.7	126.8	502.4	138.2	6.8	0.262
126.9	126.8	1000.8	138.2	3.0	0.135

**Table A.73 Data from MTBE isotherms in the presence of NOM for AW10 – Run 1**

**Carbon Type: AW10  
Solvent: SJDW  
Micropollutant: MTBE**

Weight of Carbon (mg)	Solvent Volume (mL)	Carbon Conc. (mg/L)	Initial TCE Conc (µg/L)	Equilibrium TCE Conc. (µg/L)	Qe (mg/g)
25.4	253.4	100.2	109.9	108.6	0.013
63.5	253.4	250.6	109.9	97.2	0.051
126.8	253.4	500.4	109.9	75.0	0.070
190.2	253.4	750.6	109.9	41.7	0.091
253.5	253.4	1000.4	109.9	22.8	0.087
380.2	253.4	1500.4	109.9	6.3	0.069
506.7	253.4	1999.6	109.9	2.3	0.054

**Table A.74 Data from MTBE isotherms in the presence of NOM for AW10 – Run 2**

**Carbon Type: AW10  
Solvent: SJDW  
Micropollutant: MTBE**

Weight of Carbon (mg)	Solvent Volume (mL)	Carbon Conc. (mg/L)	Initial TCE Conc (µg/L)	Equilibrium TCE Conc. (µg/L)	Qe (mg/g)
12.5	253.4	49.3	83.8	79.8	0.081
25.3	253.4	99.8	83.8	78.1	0.057
63.4	253.4	250.2	83.8	61.9	0.088
63.6	126.8	501.6	90.3	35.2	0.110
95.3	126.8	751.6	90.3	11.2	0.105
127.0	126.8	1001.6	90.3	6.0	0.084
190.1	126.8	1499.2	90.3	2.1	0.059
253.4	126.8	1998.4	90.3	1.4	0.044

**Table A.75 Data from MTBE isotherms in the presence of NOM for AW15**

**Carbon Type: AW15  
Solvent: SJDW  
Micropollutant: MTBE**

Weight of Carbon (mg)	Solvent Volume (mL)	Carbon Conc. (mg/L)	Initial TCE Conc (µg/L)	Equilibrium TCE Conc. (µg/L)	Qe (mg/g)
4.9	500.0	9.8	109.9	102.7	0.736
6.4	253.4	25.3	109.9	81.5	1.125
12.8	253.4	50.5	109.9	54.3	1.101
25.3	253.4	99.8	109.9	25.4	0.847
63.5	253.4	250.6	109.9	7.9	0.407
126.6	253.4	499.6	109.9	2.6	0.215
255.9	253.4	1009.9	109.9	1.2	0.108

**Table A.76 Data from MTBE isotherms in the presence of NOM for AW20**

**Carbon Type: AW20  
Solvent: SJDW  
Micropollutant: MTBE**

Weight of Carbon (mg)	Solvent Volume (mL)	Carbon Conc. (mg/L)	Initial TCE Conc ( $\mu\text{g/L}$ )	Equilibrium TCE Conc. ( $\mu\text{g/L}$ )	Qe (mg/g)
6.1	253.4	24.1	109.9	91.1	0.782
12.6	253.4	49.7	109.9	62.2	0.960
25.2	253.4	99.4	109.9	32.9	0.774
64.5	253.4	254.5	109.9	8.7	0.398
127.8	253.4	504.3	109.9	3.0	0.212
191.1	253.4	754.1	109.9	2.1	0.143
250.6	253.4	989.0	109.9	1.4	0.110

**Table A.77 Data from MTBE isotherms in the presence of NOM for OAW10 – Run 1**

**Carbon Type: OAW10  
Solvent: SJDW  
Micropollutant: MTBE**

Weight of Carbon (mg)	Solvent Volume (mL)	Carbon Conc. (mg/L)	Initial TCE Conc ( $\mu\text{g/L}$ )	Equilibrium TCE Conc. ( $\mu\text{g/L}$ )	Qe (mg/g)
101.6	126.8	801.3	110.7	11.2	0.124
114.3	126.8	901.4	110.7	9.8	0.112
126.8	126.8	1000.0	110.7	8.1	0.103
190.1	126.8	1499.2	110.7	4.6	0.071
253.9	126.8	2002.4	110.7	3.1	0.054
380.5	126.8	3000.8	110.7	1.8	0.036
507.4	126.8	4001.6	110.7	1.4	0.027

**Table A.78 Data from MTBE isotherms in the presence of NOM for OAW10 – Run  
2**

**Carbon Type: OAW10  
Solvent: SJDW  
Micropollutant: MTBE**

Weight of Carbon (mg)	Solvent Volume (mL)	Carbon Conc. (mg/L)	Initial TCE Conc (µg/L)	Equilibrium TCE Conc. (µg/L)	Qe (mg/g)
25.3	253.4	99.8	84.2	64.9	0.193
50.8	253.4	200.5	84.2	49.7	0.172
76.0	253.4	299.9	84.2	39.2	0.150
63.6	126.8	501.6	90.3	22.1	0.136

**Table A.79 Data from MTBE isotherms in the presence of NOM for OAW15**

**Carbon Type: OAW15  
Solvent: SJDW  
Micropollutant: MTBE**

Weight of Carbon (mg)	Solvent Volume (mL)	Carbon Conc. (mg/L)	Initial TCE Conc (µg/L)	Equilibrium TCE Conc. (µg/L)	Qe (mg/g)
19.0	253.4	75.0	110.7	82.1	0.383
25.3	253.4	99.8	110.7	73.1	0.377
50.7	253.4	200.1	110.7	49.9	0.304
50.7	126.8	399.8	110.7	28.5	0.206
95.2	126.8	750.8	110.7	11.9	0.132
127.0	126.8	1001.6	110.7	8.2	0.102
190.6	126.8	1503.2	110.7	5.0	0.070
253.4	126.8	1998.4	110.7	3.3	0.054
380.4	126.8	3000.0	110.7	2.2	0.036
507.6	126.8	4003.2	110.7	1.7	0.027

**Table A.80 Data from MTBE isotherms in the presence of NOM for OAW20**

**Carbon Type: OAW20  
Solvent: SJDW  
Micropollutant: MTBE**

Weight of Carbon (mg)	Solvent Volume (mL)	Carbon Conc. (mg/L)	Initial TCE Conc (µg/L)	Equilibrium TCE Conc. (µg/L)	Qe (mg/g)
25.2	253.4	99.4	110.7	72.1	0.389
63.6	253.4	251.0	110.7	42.4	0.272
63.5	126.8	500.8	110.7	21.5	0.178
95.0	126.8	749.2	110.7	12.0	0.132
127.0	126.8	1001.6	110.7	7.4	0.103
190.4	126.8	1501.6	110.7	4.6	0.071
253.5	126.8	1999.2	110.7	3.1	0.054
507.3	126.8	4000.8	110.7	1.5	0.027
633.9	126.8	4999.2	110.7	1.3	0.022
697.5	126.8	5500.8	110.7	1.2	0.020

**Table A.81 Data from MTBE isotherms in the presence of NOM for HAW10 – Run 1**

**Carbon Type: HAW10  
Solvent: SJDW  
Micropollutant: MTBE**

Weight of Carbon (mg)	Solvent Volume (mL)	Carbon Conc. (mg/L)	Initial TCE Conc (µg/L)	Equilibrium TCE Conc. (µg/L)	Qe (mg/g)
37.9	253.4	149.6	115.8	71.5	0.296
50.8	253.4	200.5	115.8	34.8	0.404
37.9	126.8	298.9	115.8	10.5	0.352
63.2	126.8	498.4	115.8	2.0	0.228
95.1	126.8	750.0	115.8	1.1	0.153
127.2	126.8	1003.2	115.8	0.8	0.115

**Table A.82 Data from MTBE isotherms in the presence of NOM for HAW10 – Run  
2**

**Carbon Type: HAW10  
Solvent: SJDW  
Micropollutant: MTBE**

Weight of Carbon (mg)	Solvent Volume (mL)	Carbon Conc. (mg/L)	Initial TCE Conc (µg/L)	Equilibrium TCE Conc. (µg/L)	Q <sub>e</sub> (mg/g)
5.0	253.4	19.7	115.9	105.0	0.552
17.7	253.4	69.9	115.9	103.6	0.175
25.4	253.4	100.2	115.9	91.6	0.242
37.9	253.4	149.6	115.9	52.9	0.421
50.6	253.4	199.7	115.9	14.4	0.508
31.7	126.8	250.0	129.6	11.3	0.473
38.0	126.8	299.7	129.6	15.8	0.380
50.7	126.8	399.8	129.6	3.3	0.316
63.5	126.8	500.8	129.6	2.7	0.254

**Table A.83 Data from MTBE isotherms in the presence of NOM for HAW15**

**Carbon Type: HAW15**  
**Solvent: SJDW**  
**Micropollutant: MTBE**

Weight of Carbon (mg)	Solvent Volume (mL)	Carbon Conc. (mg/L)	Initial TCE Conc (µg/L)	Equilibrium TCE Conc. (µg/L)	Qe (mg/g)
5.0	500.0	10.0	115.8	91.2	2.458
5.1	253.4	20.1	115.8	76.4	1.959
7.6	253.4	30.0	115.8	65.2	1.687
12.8	253.4	50.5	115.8	47.3	1.356
19.0	253.4	75.0	115.8	31.9	1.119
25.2	253.4	99.4	115.8	22.7	0.936
50.8	253.4	200.5	115.8	7.8	0.539
37.9	126.8	298.9	115.8	4.4	0.373
50.5	126.8	398.3	115.8	3.1	0.283
76.1	126.8	600.2	115.8	1.6	0.190

**Table A.84 Data from MTBE isotherms in the presence of NOM for HAW20**

**Carbon Type: HAW20**  
**Solvent: SJDW**  
**Micropollutant: MTBE**

Weight of Carbon (mg)	Solvent Volume (mL)	Carbon Conc. (mg/L)	Initial TCE Conc (µg/L)	Equilibrium TCE Conc. (µg/L)	Qe (mg/g)
4.9	500.0	9.8	115.8	97.4	1.876
5.2	253.4	20.5	115.8	84.6	1.520
7.8	253.4	30.8	115.8	71.1	1.452
12.7	253.4	50.1	115.8	55.7	1.199
19.0	253.4	75.0	115.8	38.9	1.025
25.5	253.4	100.6	115.8	27.8	0.875
50.8	253.4	200.5	115.8	12.0	0.518
37.8	126.8	298.1	115.8	7.0	0.365
50.7	126.8	399.8	115.8	4.0	0.280
75.9	126.8	598.6	115.8	2.2	0.190

**Table A.85 Data from MTBE isotherms in the presence of NOM for AAW10 – Run  
1**

**Carbon Type: AAW10  
Solvent: SJDW  
Micropollutant: MTBE**

Weight of Carbon (mg)	Solvent Volume (mL)	Carbon Conc. (mg/L)	Initial TCE Conc (µg/L)	Equilibrium TCE Conc. (µg/L)	Qe (mg/g)
50.6	253.4	199.7	108.0	81.5	0.133
31.7	126.8	250.0	108.0	72.6	0.142
38.3	126.8	302.1	108.0	73.5	0.114
51.1	126.8	403.0	108.0	36.8	0.177
76.1	126.8	600.2	108.0	6.8	0.169
101.7	126.8	802.1	108.0	2.5	0.132
126.8	126.8	1000.0	108.0	1.9	0.106
158.7	126.8	1251.6	108.0	1.0	0.086
190.0	126.8	1498.4	108.0	1.0	0.071
253.7	126.8	2000.8	108.0	0.8	0.054

**Table A.86 Data from MTBE isotherms in the presence of NOM for AAW10 – Run  
2**

**Carbon Type: AAW10  
Solvent: SJDW  
Micropollutant: MTBE**

Weight of Carbon (mg)	Solvent Volume (mL)	Carbon Conc. (mg/L)	Initial TCE Conc (µg/L)	Equilibrium TCE Conc. (µg/L)	Qe (mg/g)
7.6	253.4	30.0	115.9	108.4	0.248
17.7	253.4	69.9	115.9	99.4	0.236
37.9	253.4	149.6	115.9	78.6	0.249
57.0	253.4	224.9	115.9	60.9	0.244
44.3	126.8	349.4	129.6	35.6	0.269
60.1	126.8	474.0	129.6	12.5	0.247
66.5	126.8	524.4	129.6	7.9	0.232
76.0	126.8	599.4	129.6	7.1	0.204
88.8	126.8	700.3	129.6	10.9	0.169
101.2	126.8	798.1	129.6	4.7	0.156

**Table A.87 Data from MTBE isotherms in the presence of NOM for AAW15**

**Carbon Type: AAW15  
Solvent: SJDW  
Micropollutant: MTBE**

Weight of Carbon (mg)	Solvent Volume (mL)	Carbon Conc. (mg/L)	Initial TCE Conc ( $\mu\text{g/L}$ )	Equilibrium TCE Conc. ( $\mu\text{g/L}$ )	Qe (mg/g)
5.0	500.0	10.0	108.0	92.9	1.512
6.2	253.4	24.5	108.0	80.6	1.123
12.7	253.4	50.1	108.0	53.7	1.084
19.0	253.4	75.0	108.0	40.2	0.904
25.3	253.4	99.8	108.0	32.4	0.757
37.9	253.4	149.6	108.0	17.2	0.607
50.8	253.4	200.5	108.0	10.0	0.489
38.0	126.8	299.7	108.0	6.2	0.340
50.7	126.8	399.8	108.0	3.7	0.261
76.0	126.8	599.4	108.0	2.4	0.176

**Table A.88 Data from MTBE isotherms in the presence of NOM for AAW20**

**Carbon Type: AAW20  
Solvent: SJDW  
Micropollutant: MTBE**

Weight of Carbon (mg)	Solvent Volume (mL)	Carbon Conc. (mg/L)	Initial TCE Conc ( $\mu\text{g/L}$ )	Equilibrium TCE Conc. ( $\mu\text{g/L}$ )	Qe (mg/g)
5.0	253.4	19.7	84.2	66.6	0.889
10.0	253.4	39.5	84.2	49.8	0.870
18.9	253.4	74.6	84.2	31.0	0.713
25.3	253.4	99.8	84.2	25.1	0.591
38.1	253.4	150.4	84.2	14.6	0.463
50.6	253.4	199.7	84.2	7.3	0.385
76.0	253.4	299.9	84.2	5.6	0.262
63.4	126.8	500.0	90.3	2.8	0.175
88.9	126.8	701.1	90.3	1.9	0.126

**Table A.89 Data from MTBE isotherms in the presence of NOM for F600 – Run 1**

**Carbon Type: F600  
Solvent: SJDW  
Micropollutant: MTBE**

Weight of Carbon (mg)	Solvent Volume (mL)	Carbon Conc. (mg/L)	Initial TCE Conc (µg/L)	Equilibrium TCE Conc. (µg/L)	Qe (mg/g)
50.8	253.4	200.5	107.6	20.8	0.449
50.8	126.8	400.6	110.8	8.5	0.247
76.2	126.8	600.9	110.8	4.8	0.171
101.5	126.8	800.5	110.8	3.3	0.130
127.0	126.8	1001.6	110.8	2.6	0.105

**Table A.90 Data from MTBE isotherms in the presence of NOM for F600 – Run 2**

**Carbon Type: F600  
Solvent: SJDW  
Micropollutant: MTBE**

Weight of Carbon (mg)	Solvent Volume (mL)	Carbon Conc. (mg/L)	Initial TCE Conc (µg/L)	Equilibrium TCE Conc. (µg/L)	Qe (mg/g)
12.7	253.4	50.1	84.2	55.1	0.581
25.3	253.4	99.8	84.2	36.5	0.477
38.0	253.4	150.0	84.2	24.5	0.398
63.4	253.4	250.2	84.2	12.9	0.285

**Table A.91 Data from MTBE isotherms in the presence of NOM for G219 – Run 1**

**Carbon Type: G219  
Solvent: SJDW  
Micropollutant: MTBE**

Weight of Carbon (mg)	Solvent Volume (mL)	Carbon Conc. (mg/L)	Initial TCE Conc (µg/L)	Equilibrium TCE Conc. (µg/L)	Qe (mg/g)
10.2	253.4	40.3	107.6	69.1	1.035
19.0	253.4	75.0	107.6	48.0	0.837
25.4	253.4	100.2	107.6	38.1	0.725
31.8	126.8	250.8	110.8	11.3	0.384
63.4	126.8	500.0	110.8	3.8	0.208

**Table A.92 Data from MTBE isotherms in the presence of NOM for G219 – Run 2**

**Carbon Type: G219  
Solvent: SJDW  
Micropollutant: MTBE**

Weight of Carbon (mg)	Solvent Volume (mL)	Carbon Conc. (mg/L)	Initial TCE Conc (µg/L)	Equilibrium TCE Conc. (µg/L)	Qe (mg/g)
44.4	253.4	175.2	84.2	16.95	0.384
88.8	253.4	350.4	84.2	6.00	0.223

**Table A.93 Data from MTBE isotherms in the presence of NOM for Picazine**

**Carbon Type: Picazine  
Solvent: SJDW  
Micropollutant: MTBE**

Weight of Carbon (mg)	Solvent Volume (mL)	Carbon Conc. (mg/L)	Initial TCE Conc ( $\mu\text{g/L}$ )	Equilibrium TCE Conc. ( $\mu\text{g/L}$ )	Qe (mg/g)
63.3	126.8	499.2	107.6	77.7	0.060
95.2	126.8	750.8	107.6	70.3	0.050
126.9	126.8	1000.8	107.6	61.9	0.046
190.1	126.8	1499.2	107.6	48.5	0.039
253.8	126.8	2001.6	107.6	38.7	0.034
507.2	126.8	4000.0	107.6	21.9	0.021

## Appendix B. Isotherm Plots

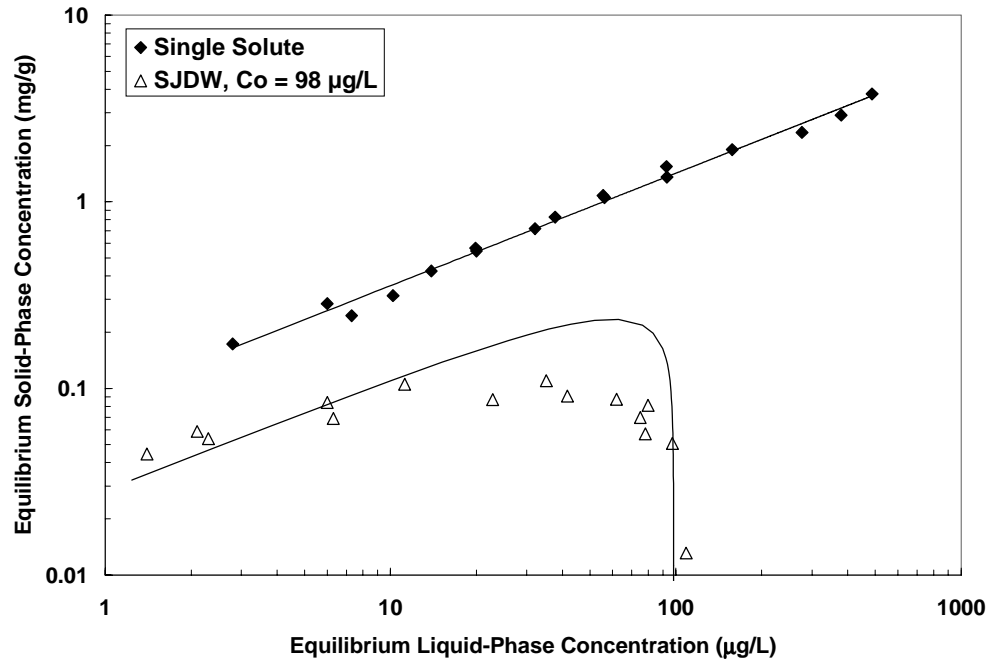


Figure B.1 Effect of NOM on MTBE Adsorption by AW10

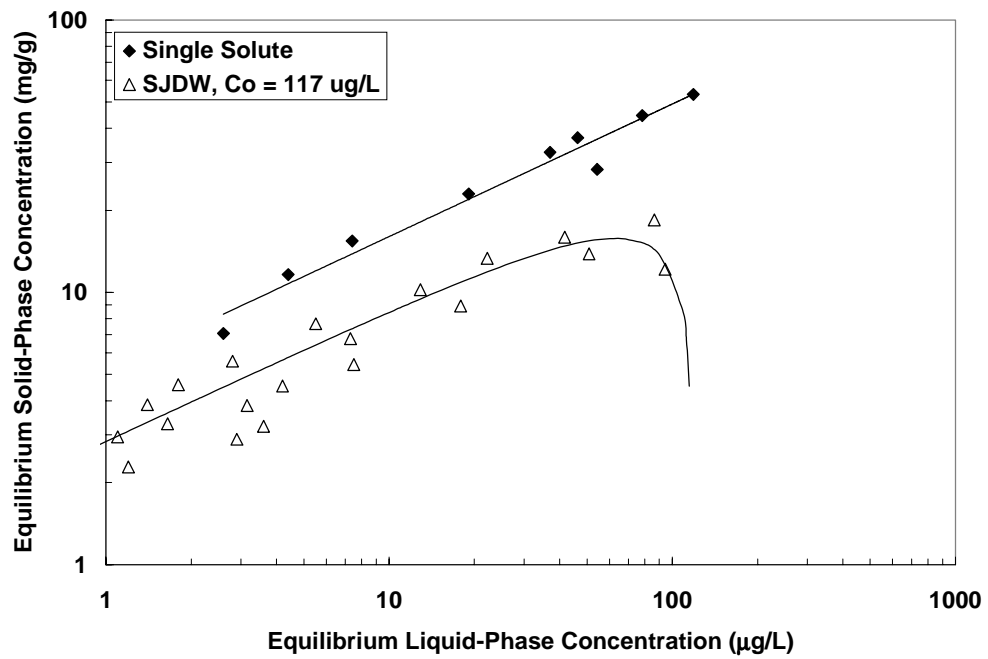


Figure B.2 Effect of NOM on TCE adsorption by AW10

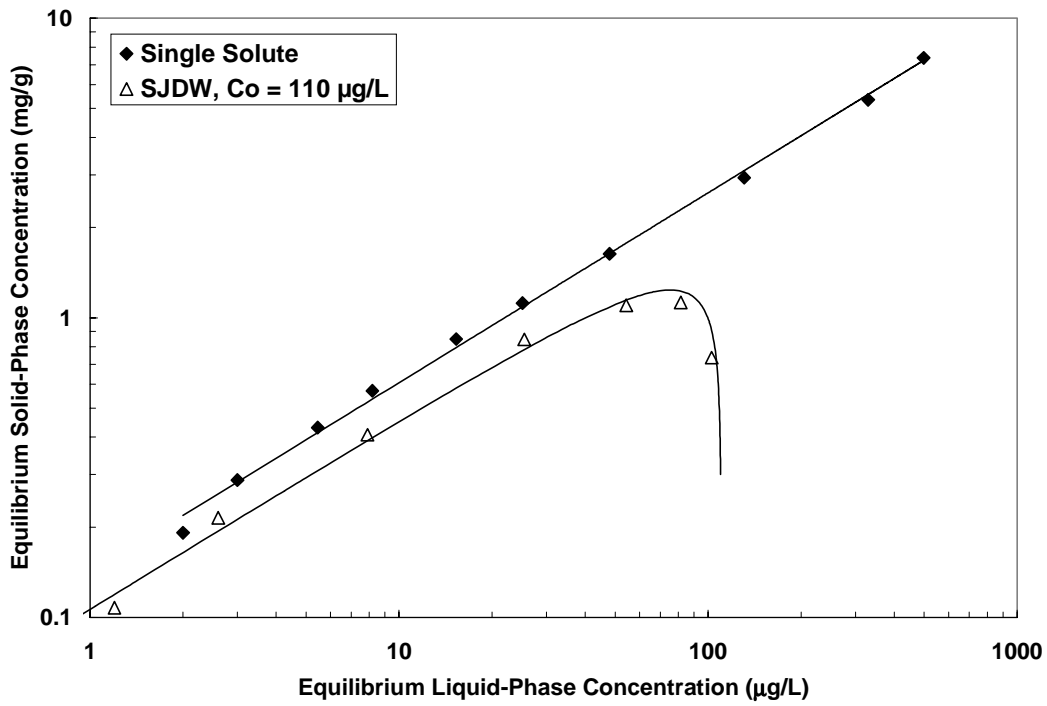


Figure B.3 Effect of NOM on MTBE Adsorption by AW15

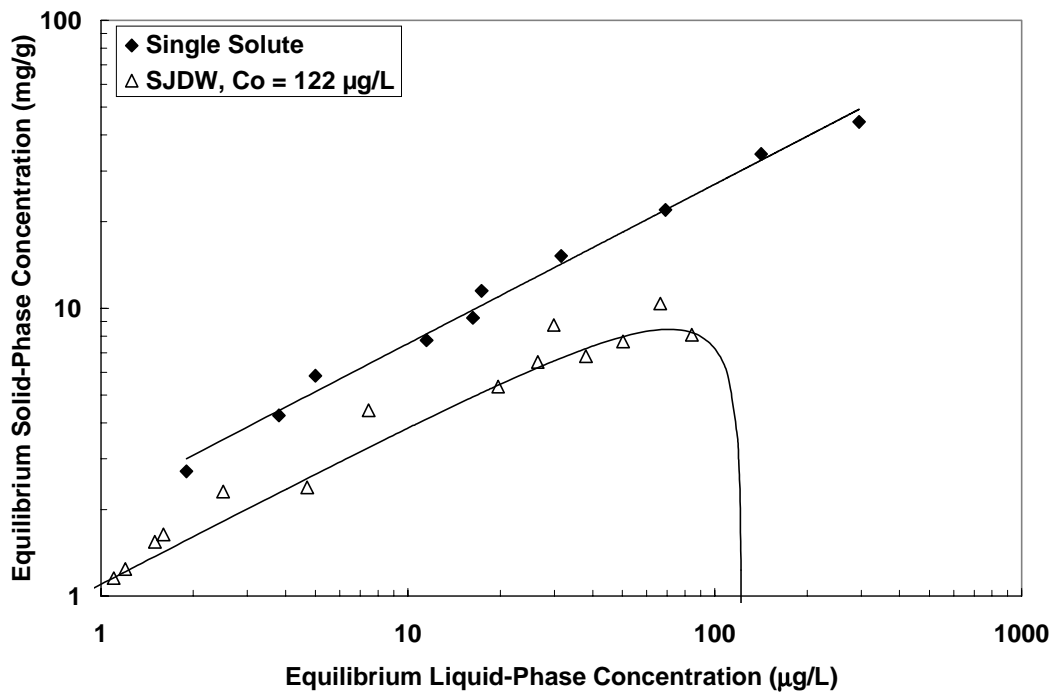


Figure B. 4 Effect of NOM on TCE Adsorption by AW15

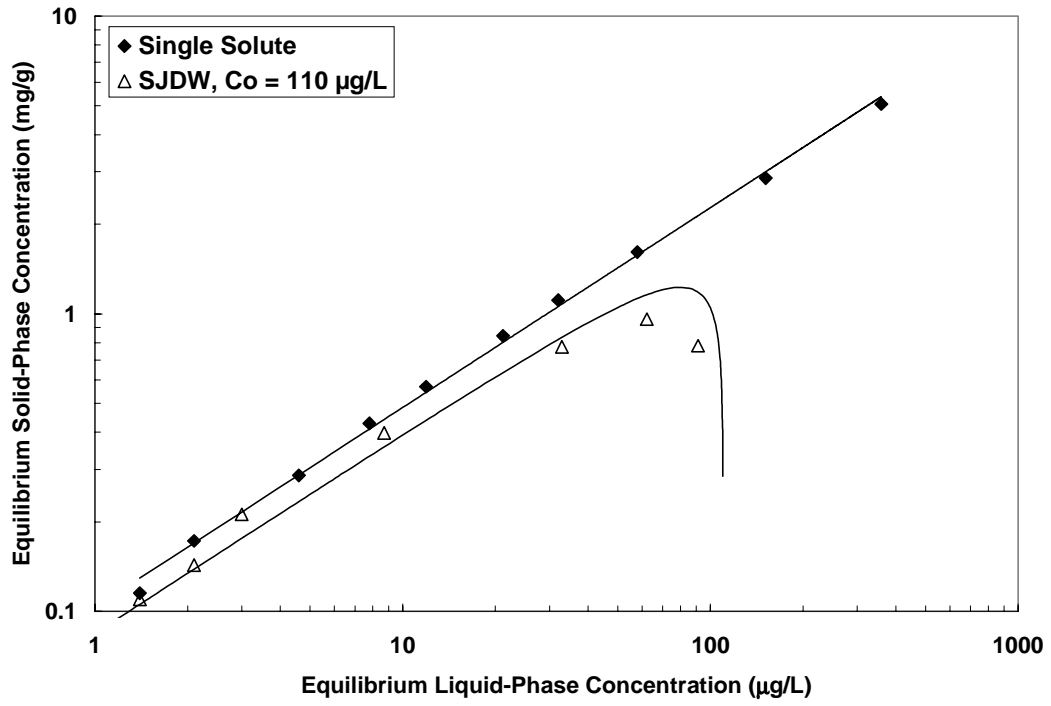


Figure B.5 Effect of NOM on MTBE Adsorption by AW20

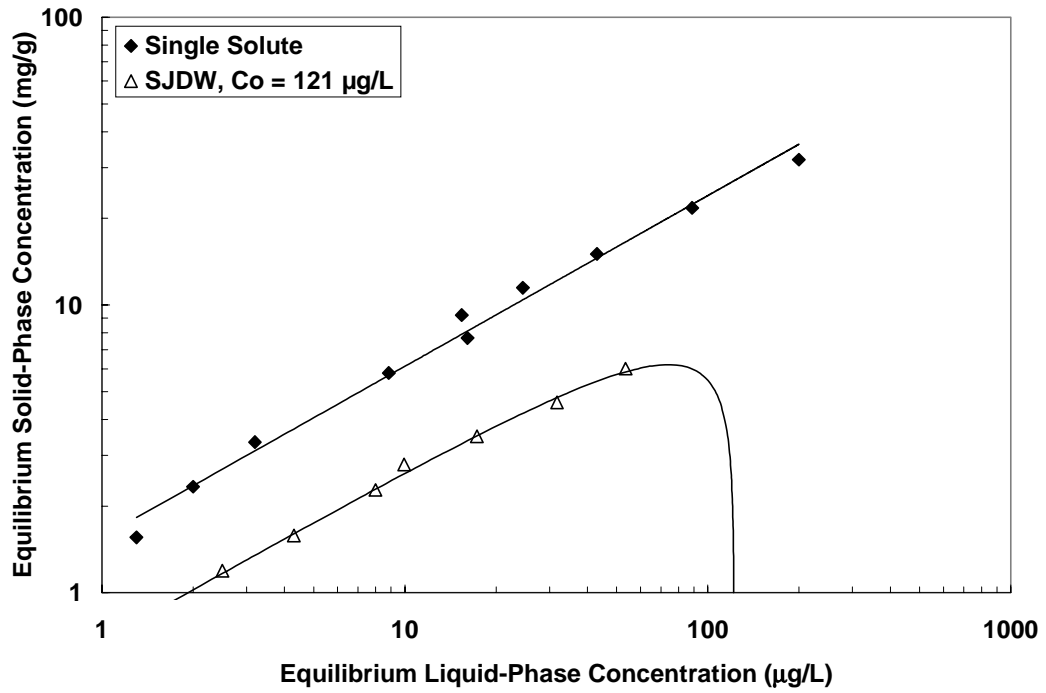


Figure B.6 Effect of NOM on TCE Adsorption by AW20

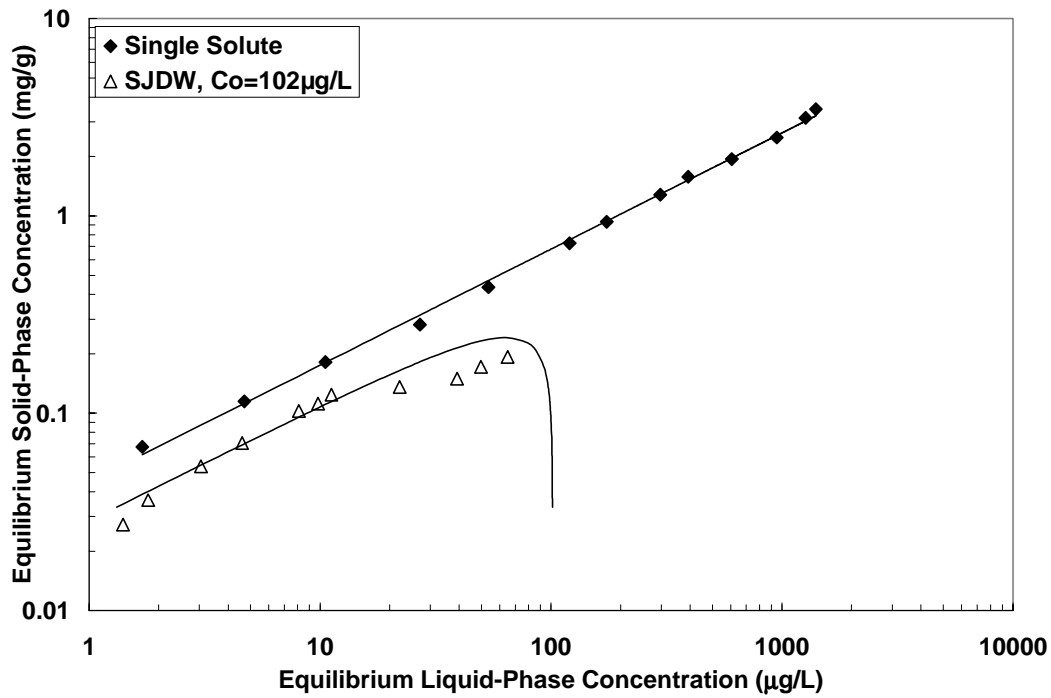


Figure B.7 Effect of NOM on MTBE Adsorption by OAW10

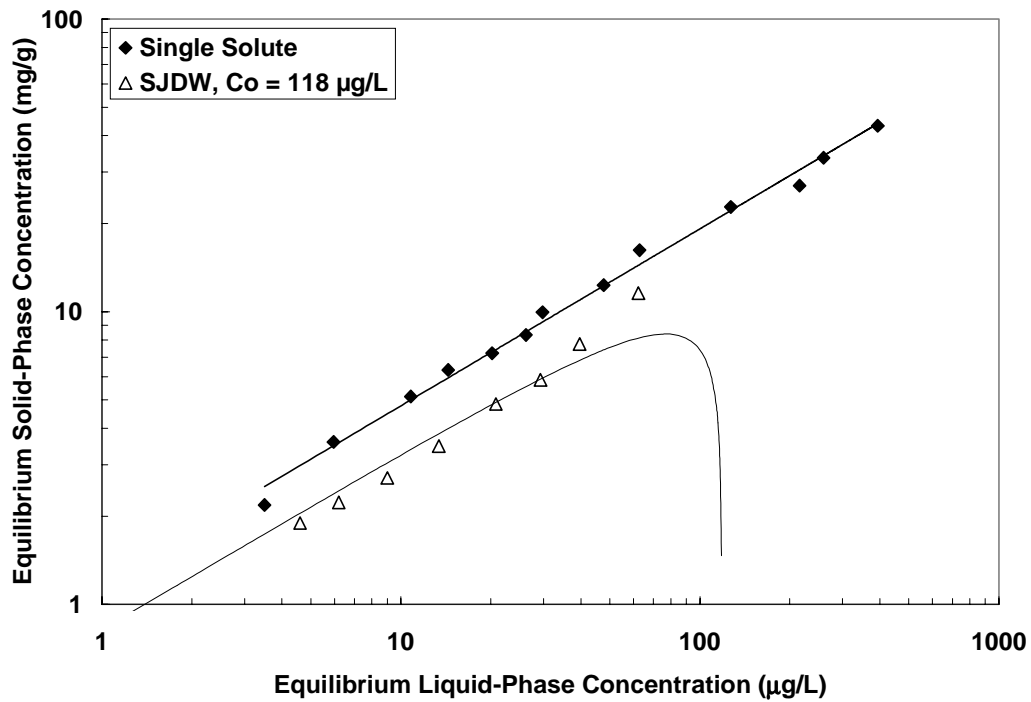


Figure B.8 Effect of NOM on TCE Adsorption by OAW10

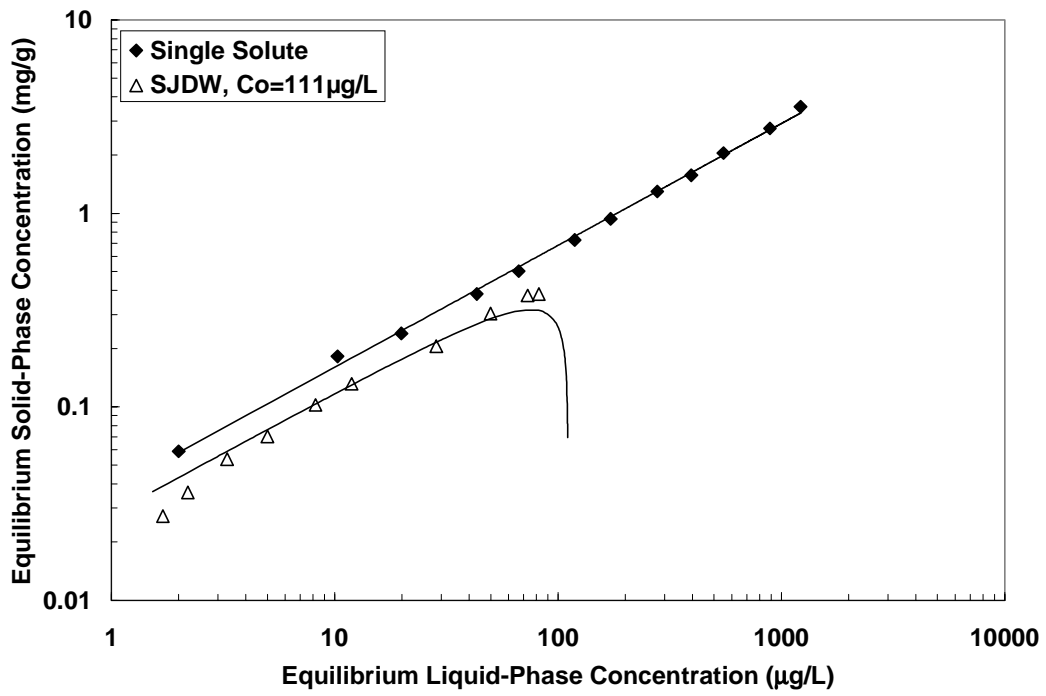


Figure B. 9 Effect of NOM on MTBE Adsorption by OAW15

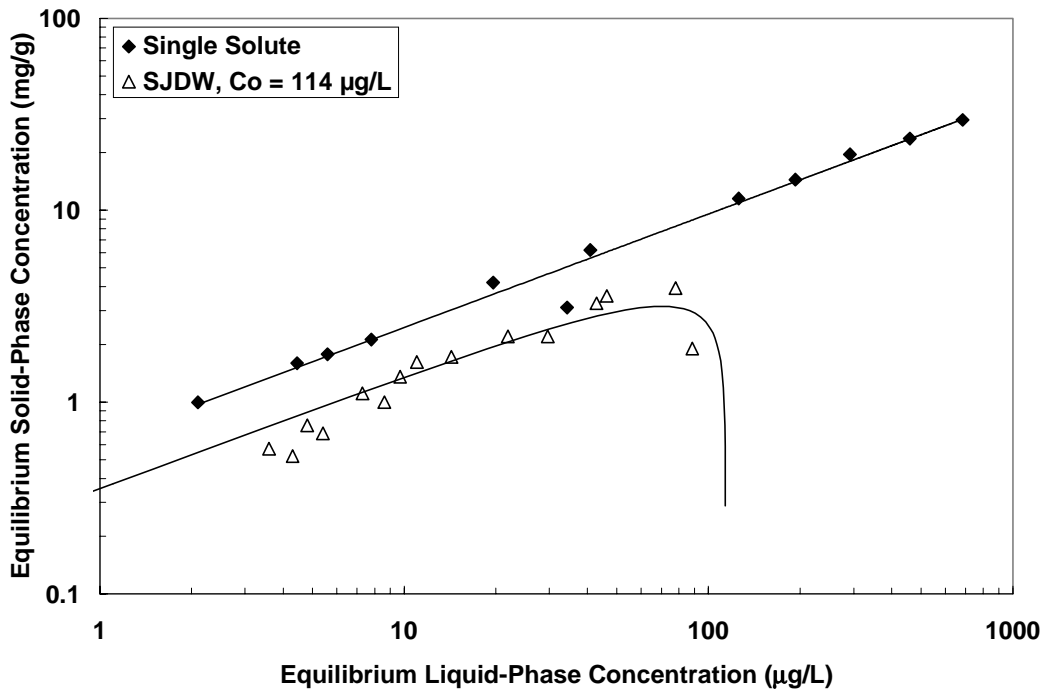


Figure B.10 Effect of NOM on TCE Adsorption by OAW15

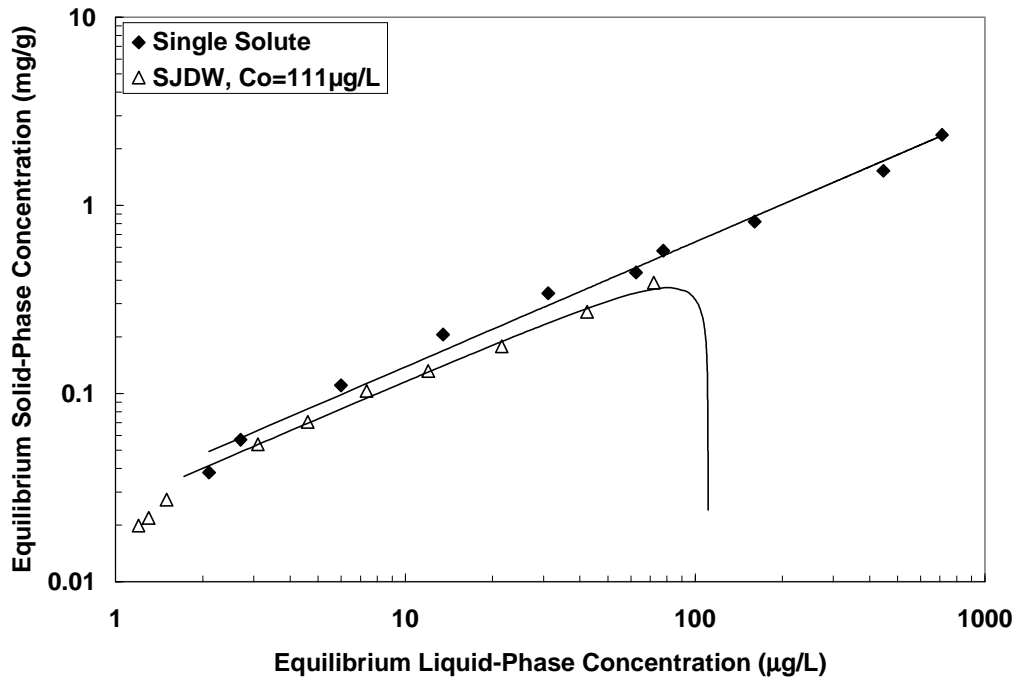


Figure B.11 Effect of NOM on MTBE Adsorption by OAW20

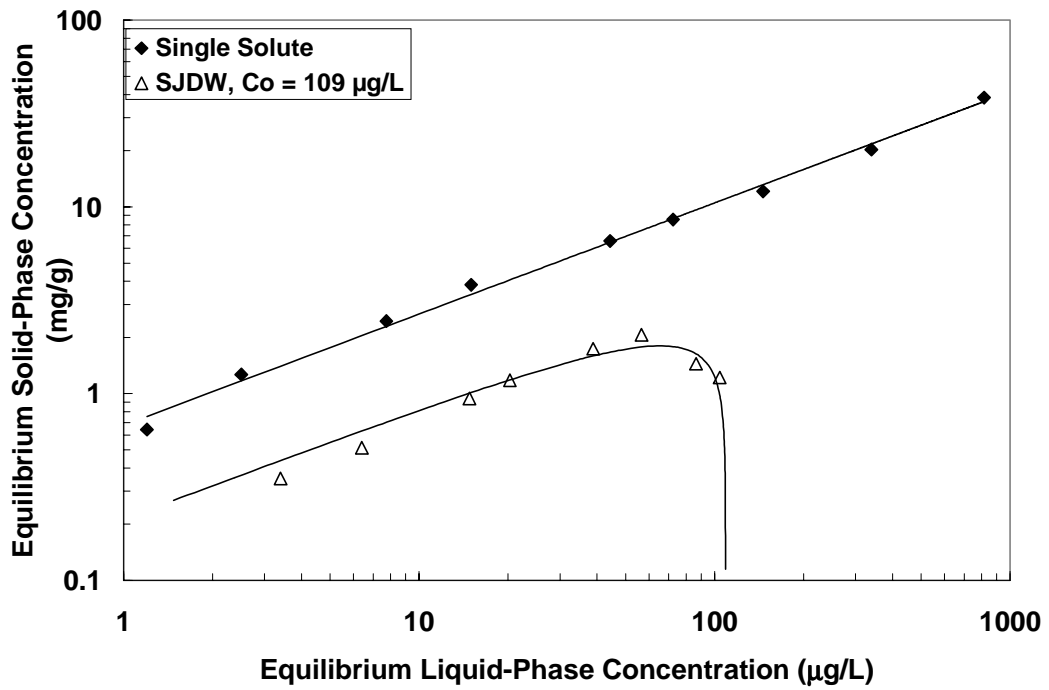


Figure B.12 Effect of NOM on TCE Adsorption by OAW20

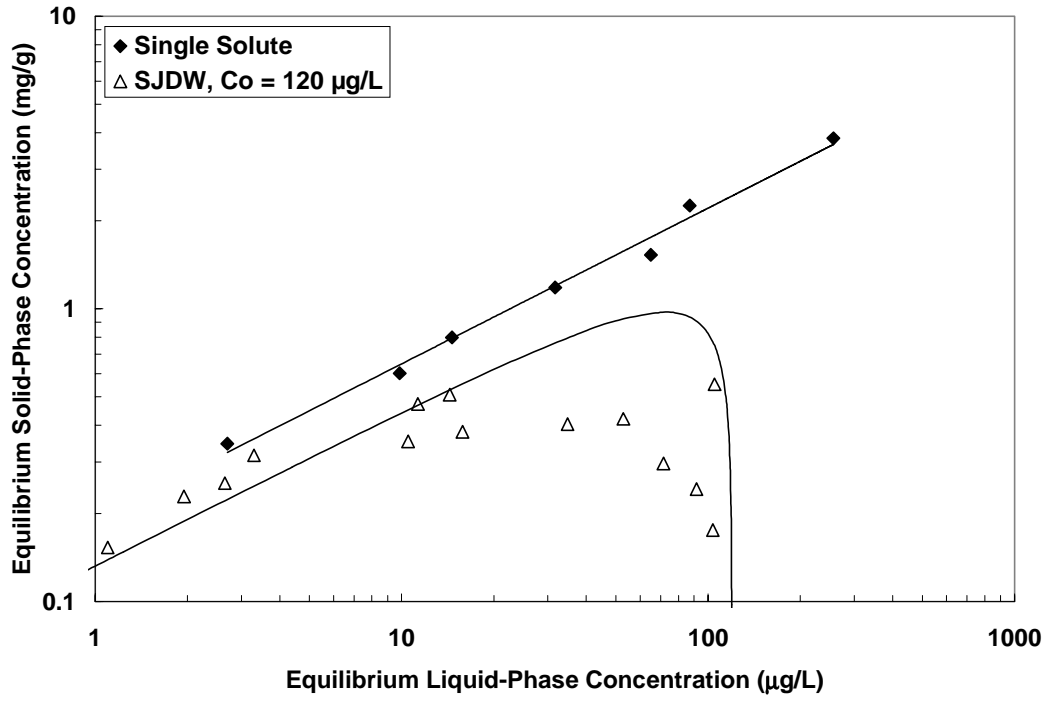


Figure B.13 Effect of NOM on MTBE Adsorption by HAW10

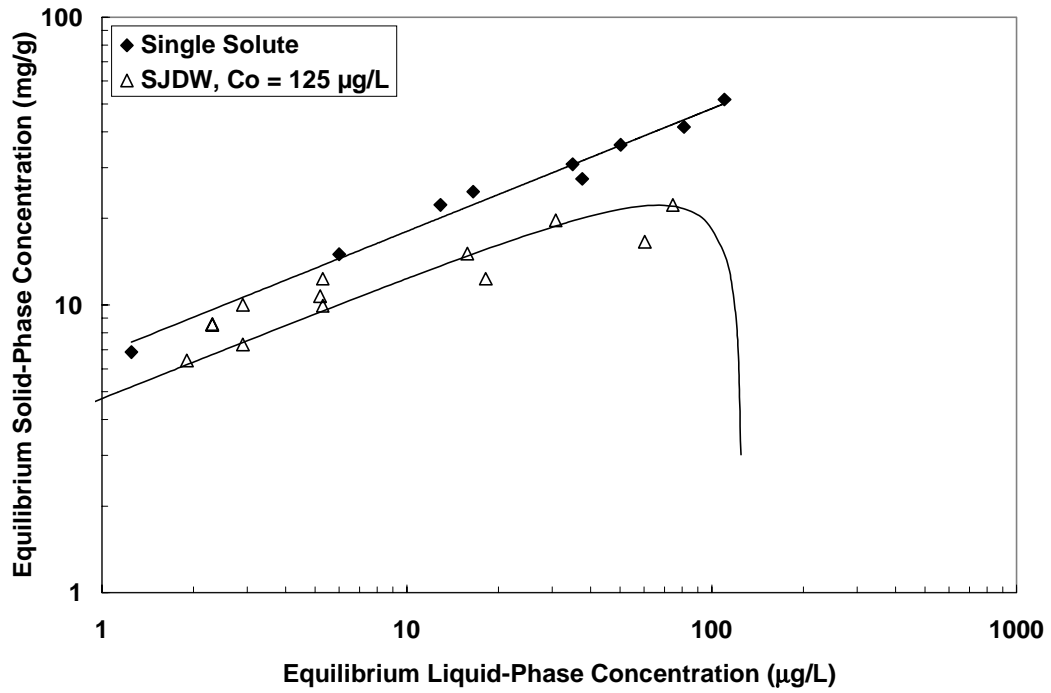


Figure B.14 Effect of NOM on TCE Adsorption by HAW10

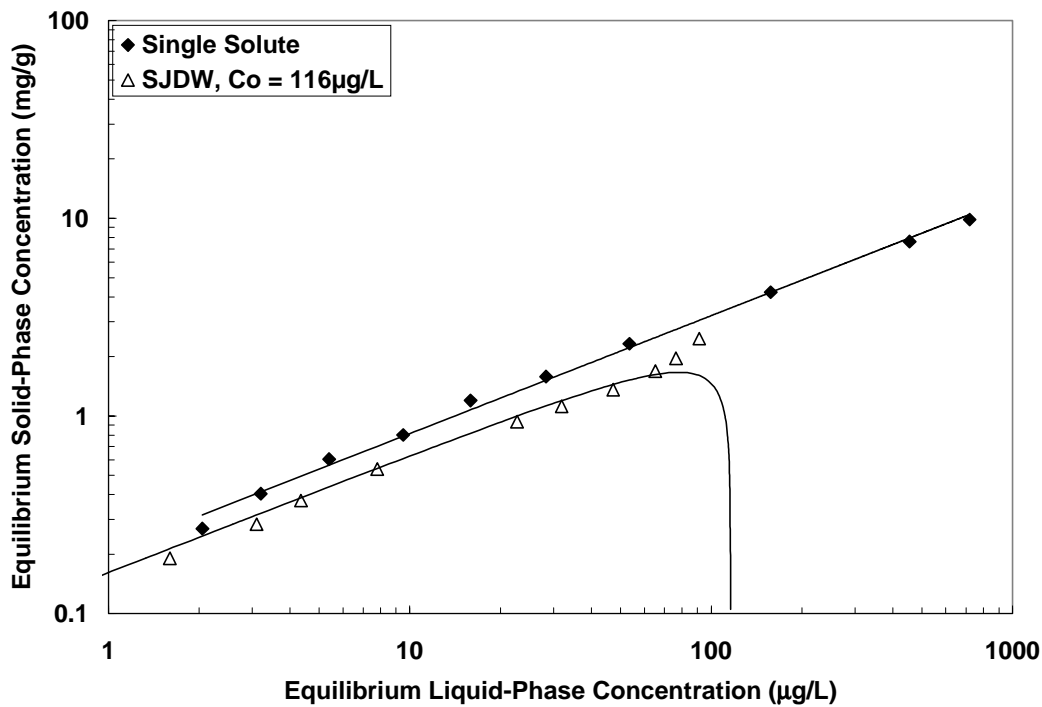


Figure B.15 Effect of NOM on MTBE Adsorption by HAW15

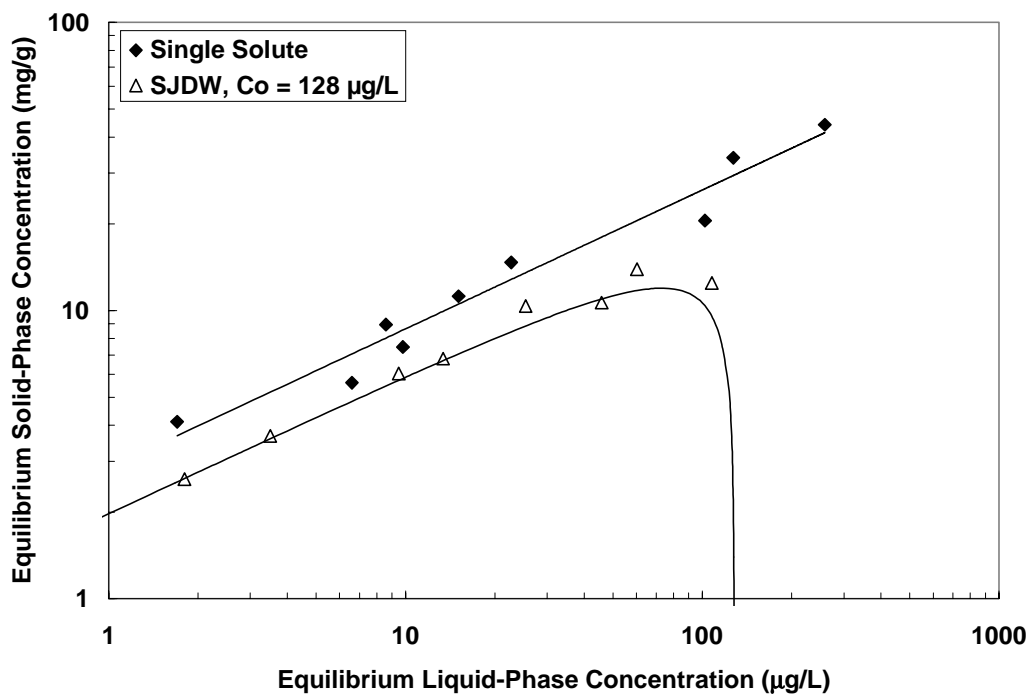


Figure B.16 Effect of NOM on TCE Adsorption by HAW15

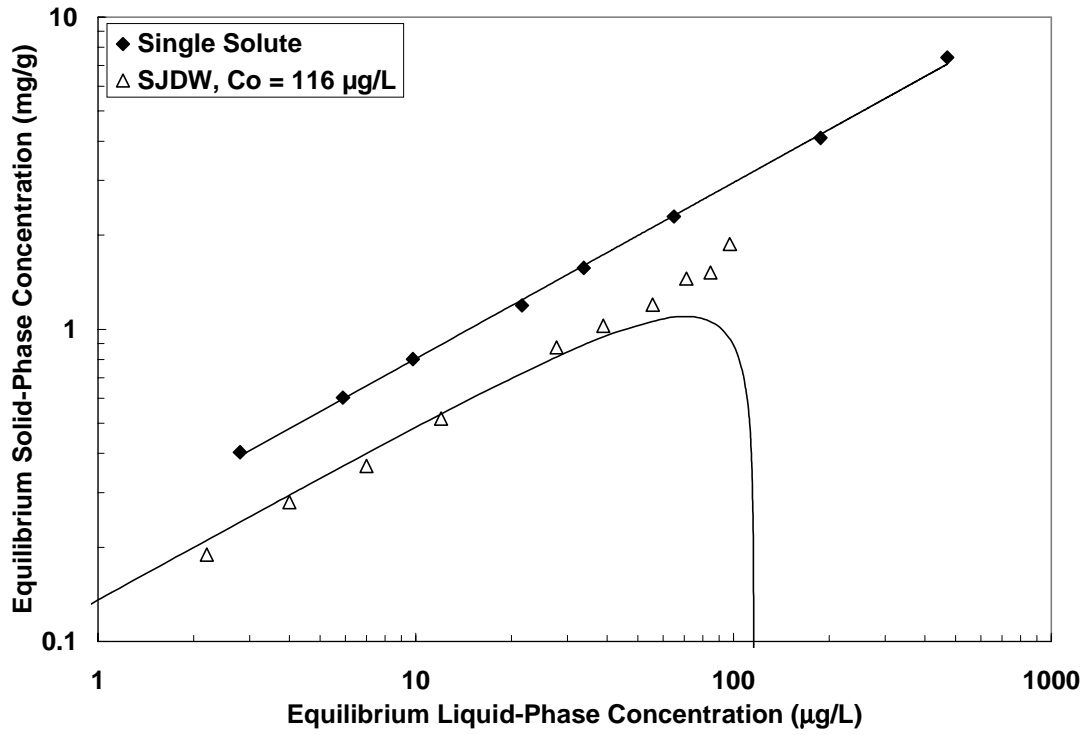


Figure B.17 Effect of NOM on MTBE Adsorption by HAW20

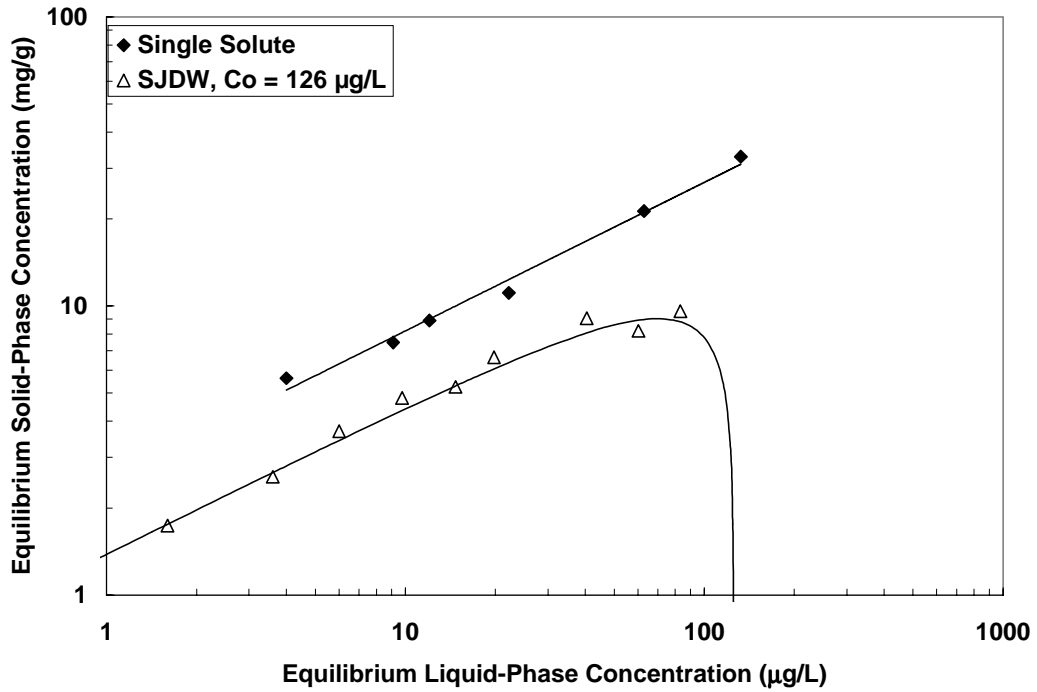


Figure B.18 Effect of NOM on TCE Adsorption by HAW20

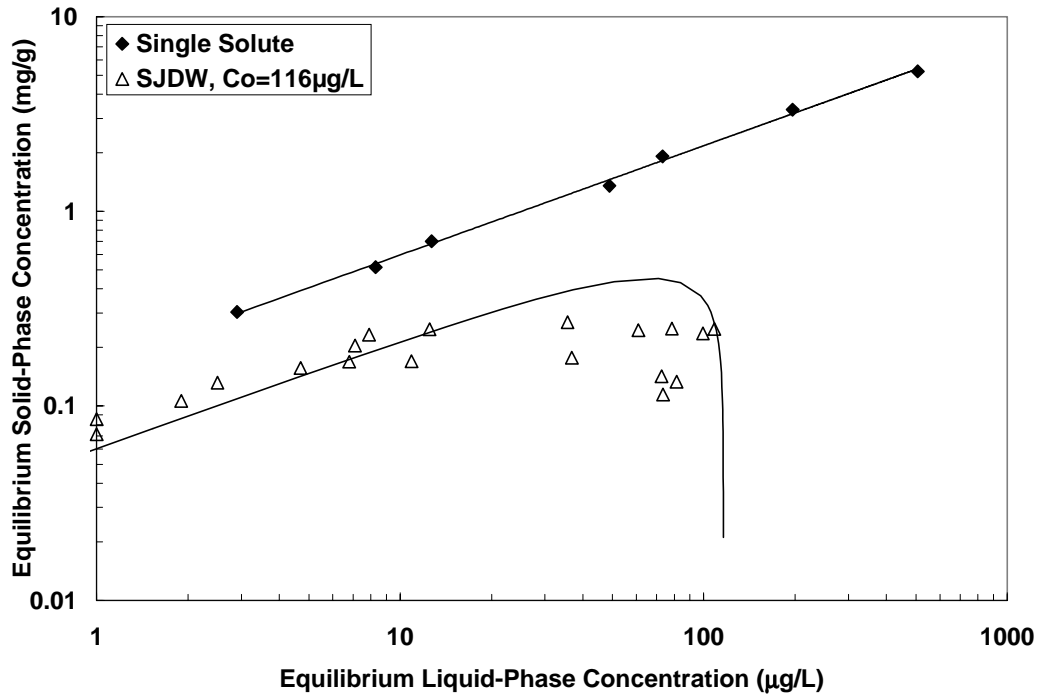


Figure B.19 Effect of NOM on MTBE Adsorption by AAW10

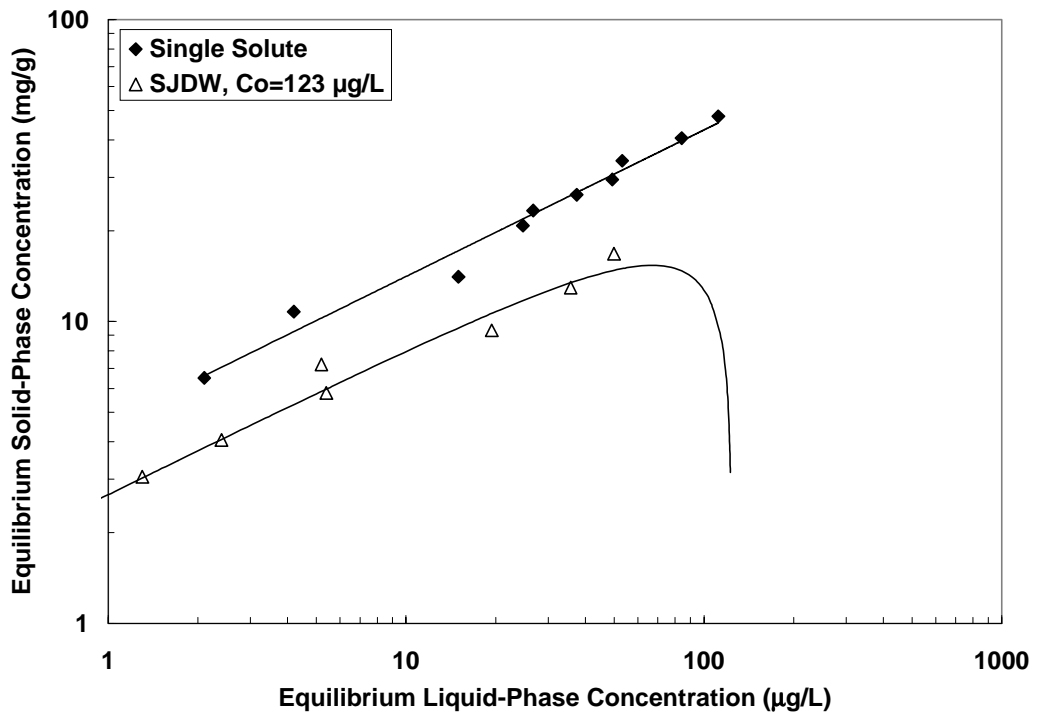


Figure B.20 Effect of NOM on TCE Adsorption by AAW10

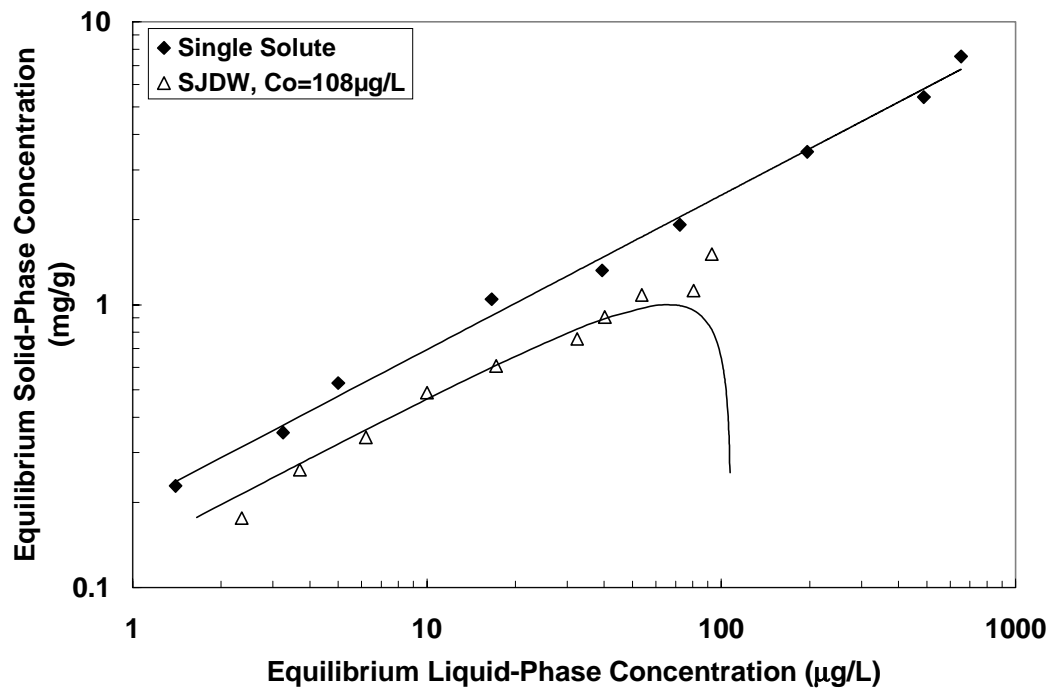


Figure B.21 Effect of NOM on MTBE Adsorption by AAW15

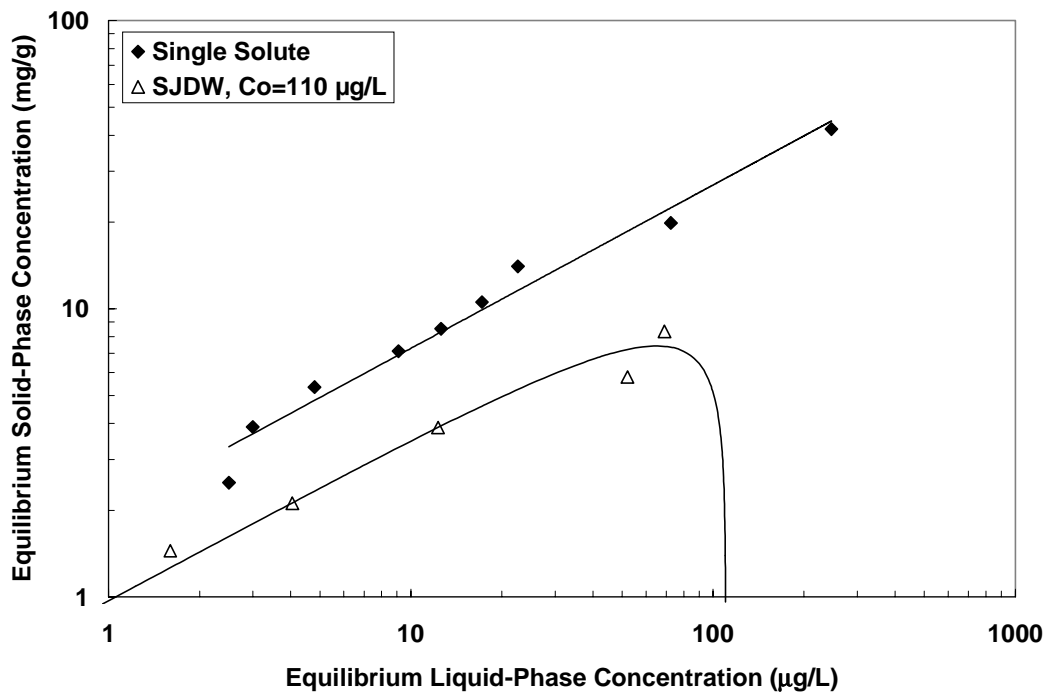


Figure B.22 Effect of NOM on TCE Adsorption by AAW15

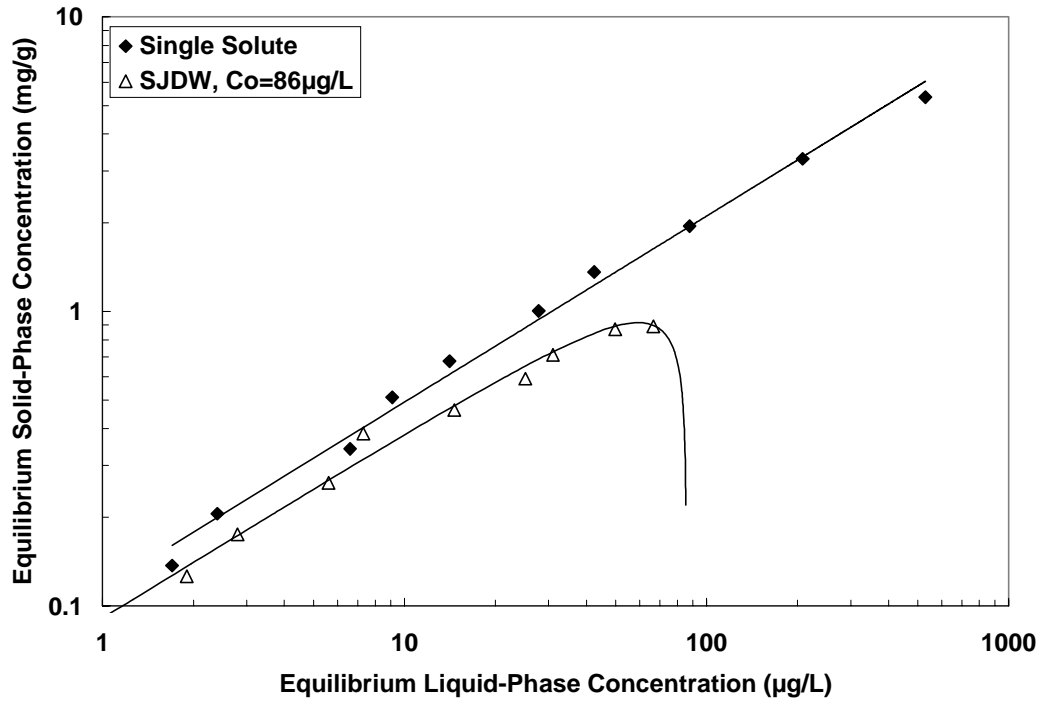


Figure B.23 Effect of NOM on MTBE Adsorption by AAW20

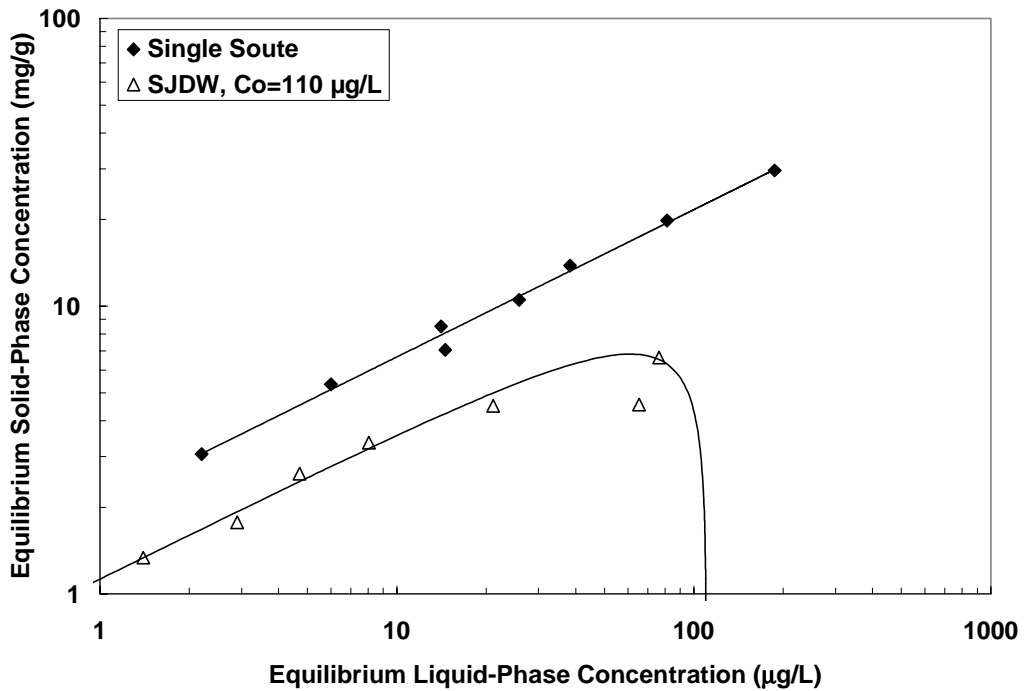


Figure B.24 Effect of NOM on TCE Adsorption by AAW20

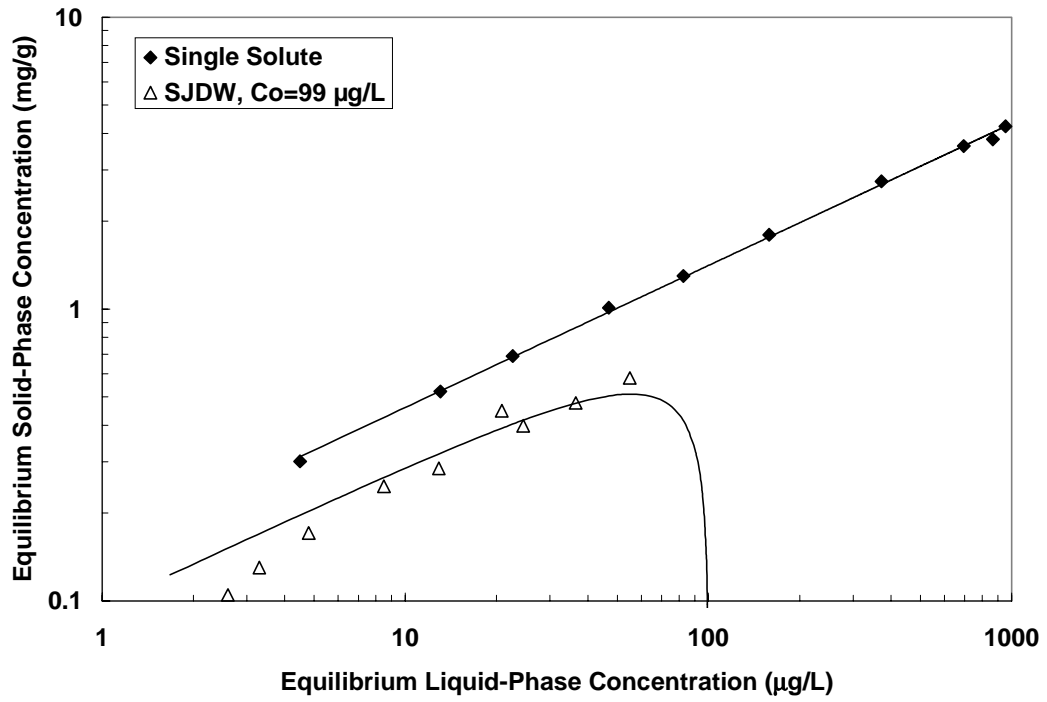


Figure B.25 Effect of NOM on MTBE Adsorption by F600

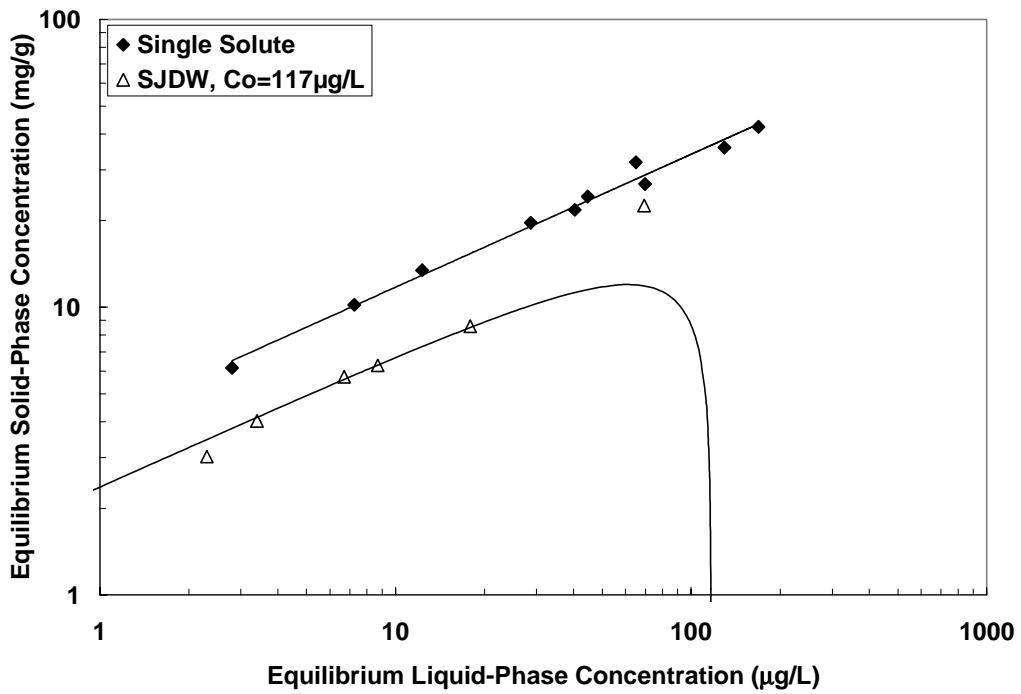


Figure B.26 Effect of NOM on TCE Adsorption by F600

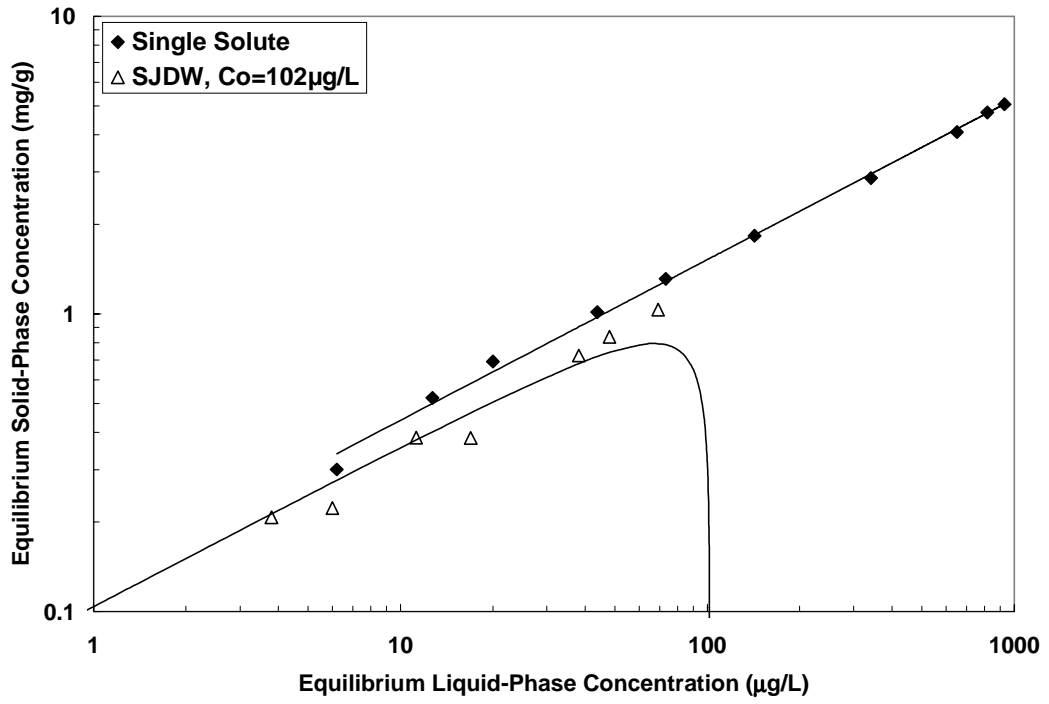


Figure B.27 Effect of NOM on MTBE Adsorption by G219

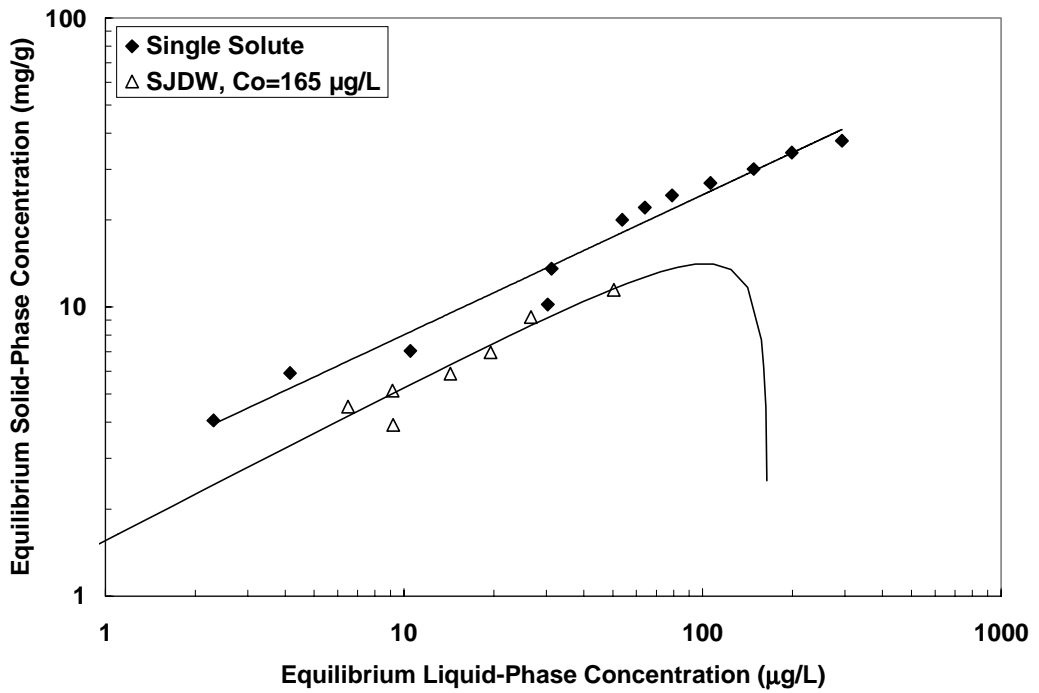


Figure B.28 Effect of NOM on TCE Adsorption by G219

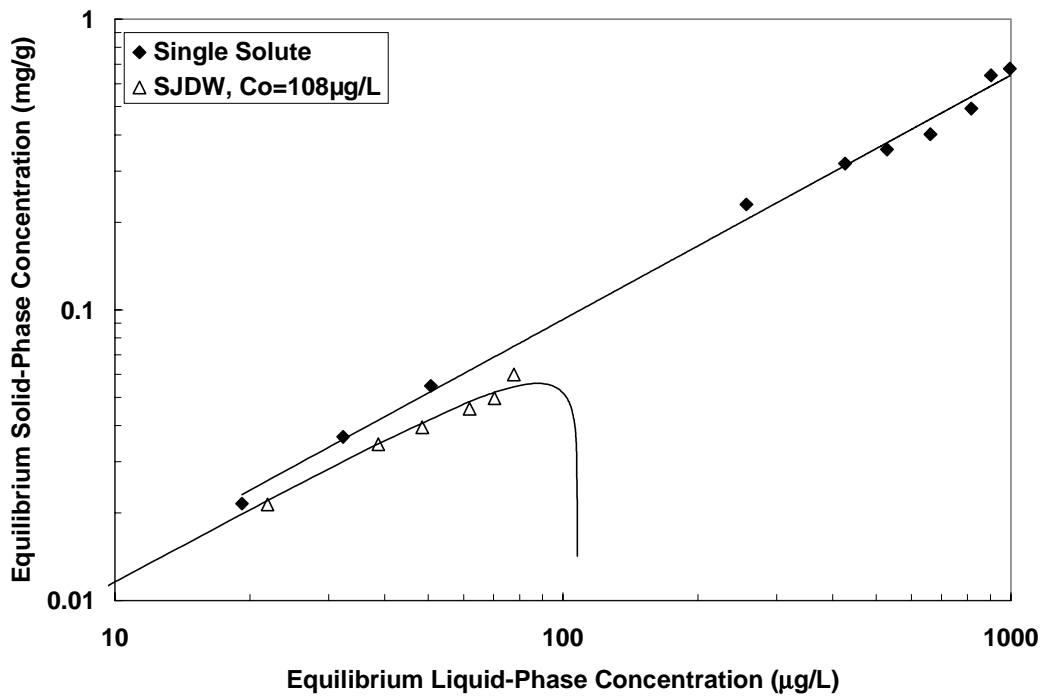


Figure B.29 Effect of NOM on MTBE Adsorption by Picazine

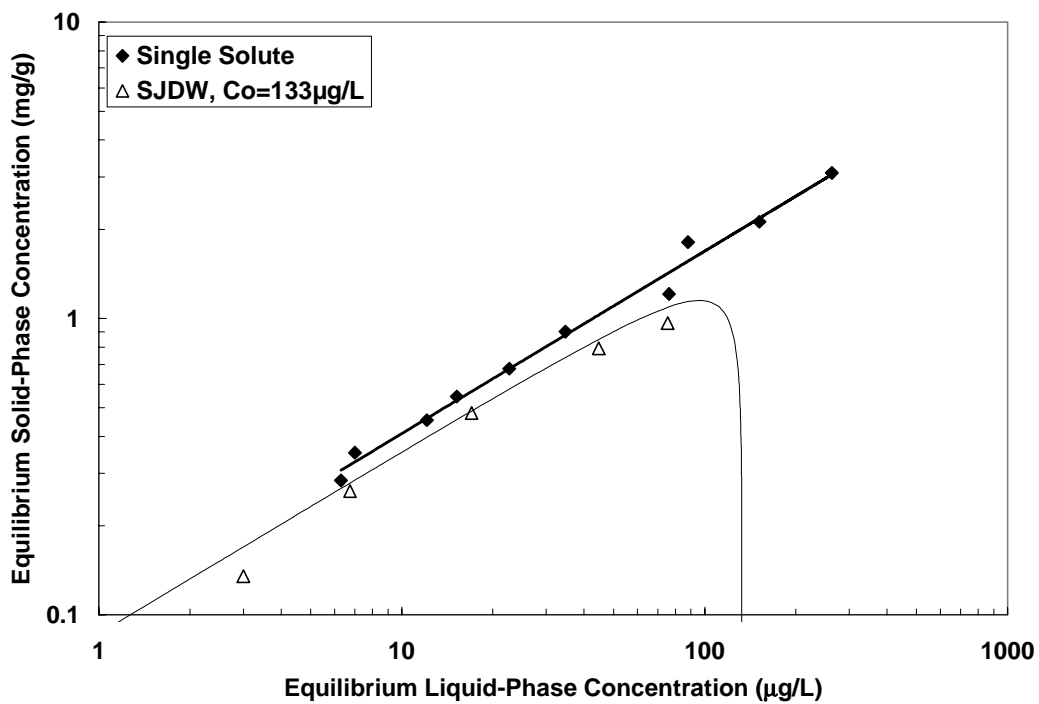


Figure B.30 Effect of NOM on TCE Adsorption by Picazine